RESOLFT nanoscopy with water-soluble synthetic fluorophores

Dissertation

for the award of the degree

"*Doctor rerum naturalium*"

of the Georg-August-Universität Göttingen

within the doctoral program
"Physics of Biological and Complex Systems"
of the Georg-August University School of Science (GAUSS)

submitted by

Philipp Johannes Alt

from Trier

Göttingen 2017

GEORG-AUGUST-UNIVERSITÄT
GÖTTINGEN

Max Planck Institute for
Biophysical Chemistry

Members of the Thesis Committee

Prof. Dr. Stefan W. Hell (Referee)

Department of NanoBiophotonics,
Max Planck Institute for Biophysical Chemistry, Göttingen

Prof. Dr. Hans-Jürgen Troe (2nd Referee)

Institute of Physical Chemistry, Georg-August-Universität Göttingen

Dr. Thomas P. Burg

Research Group of Biological Micro- and Nanotechnology
Max Planck Institute for Biophysical Chemistry, Göttingen

Further members of the Examination Board

Dr. Melina Schuh

Department of Meiosis,
Max Planck Institute for Biophysical Chemistry, Göttingen

PD Dr. Alexander Egner

Department of Optical Nanoscopy,
Laser-Laboratorium Göttingen e.V.

Prof. Dr. Tim Salditt

Research Group for Structure, Dynamics, Assembly and Interaction of Biological Macromolecules,
Institute for X-Ray Physics, Georg-August-Universität Göttingen

Date of oral examination: 15.12.2017

Abstract

Fluorescence microscopy is an important and widely used tool in the life sciences due to its unique ability to observe cellular processes in living specimens with target-specific image contrast. The development of high resolution methods in the far-field has increased its importance further by enabling the visualization of structures featuring sizes below the diffraction limit of light. In particular, RESOLFT (reversible saturable optical linear fluorescence transitions) nanoscopy using low light intensities has become a method of choice for live-cell high-resolution fluorescence imaging.

RESOLFT nanoscopy requires labels with specialized properties which, to date, have only been observed in reversibly photoswitchable fluorescent proteins (RSFPs). Attempts to extend the palette of RESOLFT labels using synthetic organic fluorophores have been limited to proof of concept studies, mostly owing to their insolubility in water. However, organic fluorophores bear the potential for higher brightness, broader emission and excitation wavelength range as well as higher photostability than RSFPs.

In this work the first demonstration of RESOLFT nanoscopy with photoswitchable diarylethene-based fluorophores in aqueous environments is presented. The photophysical behavior of these novel fluorophores was characterized and compared to RSFPs commonly used for RESOLFT. Furthermore, the fluorophores were successfully applied to label biological structures in fixed mammalian cells. Imaging based on the RESOLFT concept with these fluorophores yielded two- to threefold improved spatial resolution compared with confocal imaging. The fluorophores presented in this work thus lay the foundation for the further development of synthetic fluorophores for RESOLFT nanoscopy in living specimens.

Contents

List of Abbreviations

AOM	Acousto-optic modulator
AOTF	Acousto-optic tunable filter
APD	Avalanche photo-diode
BSA	Bovine serum albumin
CCD	Charge-coupled device
CF	"Closed" form isomer
DAE	Diarylethene
DBS	Directional beam splitter
DIC	Differential interference contrast
DOL	Degree of labeling
DOPC	1,2-dioleoyl-sn-glycero-3-phosphocholine
EBT	1,2-bis(2-ethyl-6-phenyl-1-benzothiophen-1,1-dioxide-3-yl)-perfluorocyclopentene
F(PALM)	(Fluorescence) photoactivated localization microscopy
FWHM	Full width at half maximum
GFP	Green fluorescent protein
GSD	Ground state depletion
IC	Internal conversion
ISC	Intersystem crossing
IRF	Instrument response function
LED	Light emitting diode
***me*DAE**	Methylated diarylethene
***m*IDAE**	*Myo*-inositol substituted diarylethene
MMF	Multi-mode fiber
NA	Numerical aperture
NHS	*N*-hydroxysuccinimide
NI-DAQ	National Instruments Data Acquisition (Device)
Ni-NTA	Nickel-nitrilotriacetic acid

|	
OF	"Open" form isomer
PAA	polyacrylamide
PBS	Phosphate buffered saline
PFA	Paraformaldehyde
PMT	Photomultiplier tube
PSF	Point spread function
RESOLFT	Reversible saturable optical linear fluorescence transitions
RET	Resonance energy transfer
RSFP	Reversibly switchable fluorescent protein
SBR	Signal-to-background ratio
SLM	Spatial light modulator
SMF	Polarization-maintaining single-mode fiber
SMLM	Single molecule localization microscopy
SPAD	Single-photon avalanche diode
STED	Stimulated emission depletion
STORM	Stochastic optical reconstruction microscopy
TCSPC	Time-correlated single photon counting
TIRF	Total internal reflection fluorescence
TTL	Transistor–transistor logic
UV	Ultraviolet

1 Introduction

The investigation of processes involved in the evolution of biological life and its functions has been pursued for hundreds of years. The development of magnifying optical elements facilitated the exploration of processes which are invisible to the human eye. Although the invention of the microscope itself can be assigned to different individuals in history, it is known that the utilization of these instruments revealed the existence of tiny building blocks of life such as blood cells and spermatozoa already in the late 17th century [1].

The detailed optical examination of many biological specimen is hampered without special methods because the structures of interest are translucent, containing small features showing little contrast. It is therefore necessary to increase the contrast between different sample features. On the one hand, the microscope can be tailored to maximize the contrast due to small changes in the local refractive index, e.g. by dark-field illumination, phase contrast or differential interference contrast (DIC) microscopy [2]. On the other hand, the preparation of the specimen remains essential and allows the staining of specific features. For classical transmission microscopy, the image contrast can be enhanced by staining various structures in cells with highly absorptive dyes of different colors. Most recently, the use of fluorophores became one of the most important methods to stain biological samples, because fluorescence and matched color filters provide excellent contrast which allows to detect the signal against an otherwise nearly black background. The possibility to specifically label structures of interest using immunofluorescence or genetically expressed markers in the late 20th century has elevated fluorescence microscopy to an essential tool in the life sciences. Moreover, since light microscopy is not limited to the observation of surfaces, it allows noninvasive imaging of structures and processes inside of living cells and tissues.

The basic concepts of fluorescence, fluorescence microscopes, the resolution limit of optical microscopes and the concepts to overcome it will be described in the following.

1.1 Fluorescence

Fluorescence was already described in the late 16th century, while it appears in nature since millions of years in different forms[3]. Fluorescent molecules, or fluorophores, emit light of a different color shortly after absorption of electromagnetic radiation.
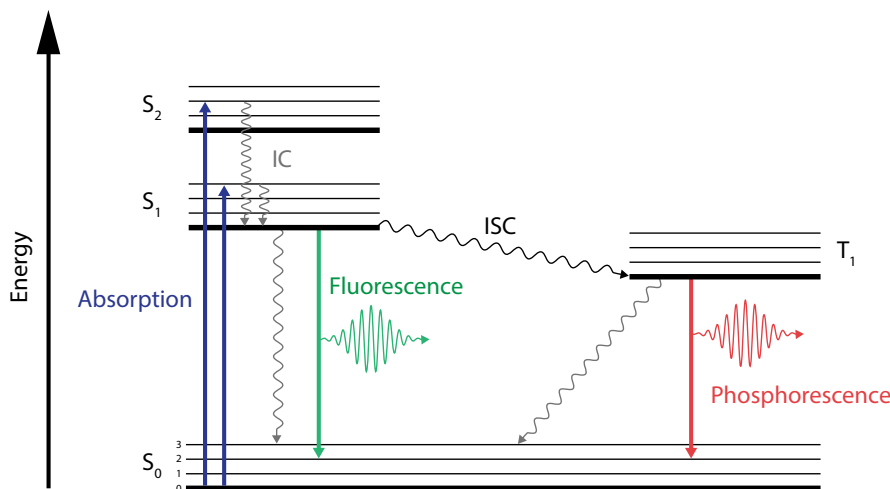
Figure 1.1: Jablonski diagram showing the different energy levels of a fluorescent molecule with the singlet states S_i and triplet state T_1. The different arrows show the possible transitions between these states (IC: internal conversion, ISC: intersystem crossing).

Fluorophores possess discrete and quantized energy levels including electronic states and vibrational and rotational sublevels, which can be described with a Jablonski diagram as shown in Figure 1.1. Fluorophores in thermal equilibrium usually reside in their singlet ground state, the electronic state with the lowest energy. In singlet states all electron spins are paired, resulting in an angular momentum of zero. The absorption of light of specific wavelengths, depending on the molecule's electron configuration, brings the molecules to higher vibrational levels of the exited singlet state with the lowest energy S_1. Within picoseconds, the molecules thermally relax to the vibrational ground state of S_1. The return to S_0 occurs either by the spontaneous emission of a photon or via internal conversion (IC) and thermal relaxation. Relaxation from the excited state can also occur through interactions with other molecules, for example through resonance energy transfer (RET) or electron transfer[4,5]. The characteristic residence time in the excited state S_1 is called fluorescence lifetime τ and is typically in the range of nanoseconds. The emitted photon

has lower energy than the absorbed photon because of energy losses due to vibrational relaxations and solvent interactions. This causes a red-shift of the emission spectrum compared to the absorption spectrum, known as Stokes shift [6].

The ratio of emitted to absorbed photons is defined as the fluorescence quantum yield ϕ ($0 < \phi < 1$) of a fluorophore. In combination with the molar extinction coefficient ε at a given wavelength, the brightness ($B = \phi \times \varepsilon$) of the molecule upon excitation with this wavelength can be determined.

Instead of returning to the ground state S_0, a non-radiative transition from the lowest excited singlet state S_1 to the lowest excited triplet state T_1 can also occur. This transition is denoted intersystem crossing (ISC) and involves an electron spin flip. In triplet states two electrons have identical spin, making the $S_1 \rightarrow T_1$ transition formally forbidden. Nevertheless, it occurs with a small probability due to mechanical interactions of the fluorophore with its environment and due to spin–orbit coupling. Hence, the relaxation to the ground state S_0 is also forbidden, resulting in a long lifetime (µs to ms) of the triplet state compared to that of S_1. From T_1, the molecules reach the ground state non-radiatively or by photon emission termed phosphorescence.

1.2 Fluorescence microscopes

The primary optical components of an epi-fluorescence microscope are a light source, wavelength-selective filters and mirrors, an objective lens, a tube lens and a detector. The sample is illuminated through the objective lens with the excitation light. The induced fluorescence from the sample is collected by the same objective lens and separated from the excitation light by a dichroic mirror, reflecting light of wavelengths below a specific threshold and transmitting all wavelengths above, utilizing the fluorophore's Stokes shift. Signals originating from the focal plane are collimated by the objective lens and imaged on the detector by the tube lens. An additional fluorescence filter only transmits light in a wavelength band of the anticipated fluorescence to block any background light. Fluorescence microscopes differ in the way of sample illumination and signal detection, as depicted in Figure 1.2.

In a typical widefield microscope, the whole sample is evenly illuminated by the excitation light and the fluorescence is imaged onto a camera. In this approach, the light emitted from all sample features is collected simultaneously, which results in a blurred background signal caused by the emission from the out-of-focus planes.
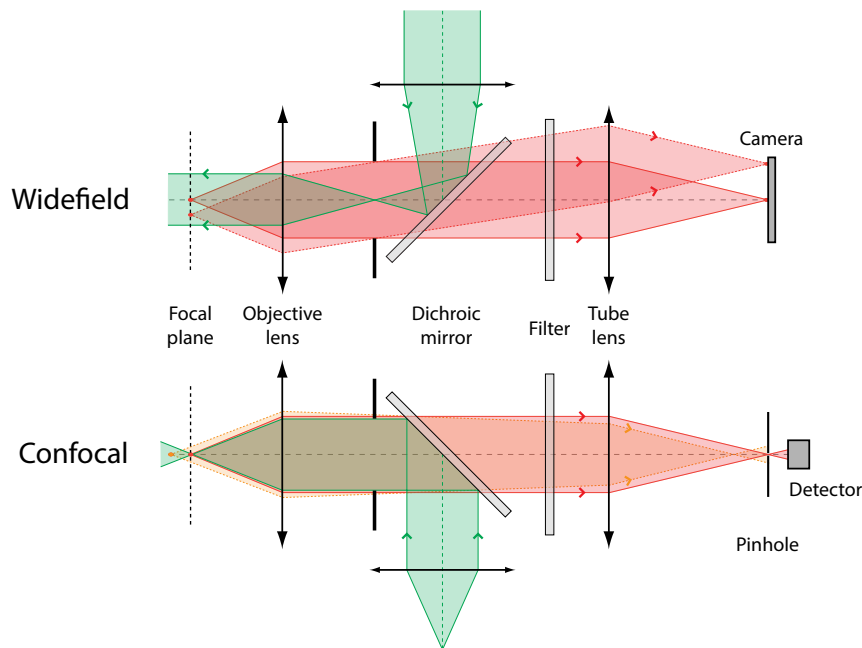
Figure 1.2: Schematic illustration of a widefield and a confocal microscope with their essential elements. Excitation light is shown in green. Fluorescence from the focal plane is shown in red and from out-of-focus in orange.

This causes reduced image contrast when imaging thick samples.

A method to exclude this undesired background is confocal microscopy[7], whose development marked a milestone in the field. Instead of illuminating the whole sample simultaneously, only a restricted volume is illuminated. The excitation light is tightly focused to a small spot into the sample by the objective lens. The application of lasers as coherent light sources allows for diffraction-limited spot sizes. The emitted fluorescence is focused to a spot, whereby a pinhole in an optically conjugate focal plane in front of the detector blocks the undesired out-of-focus light. This increases the signal-to-background ratio and allows axial sectioning of thick samples. By scanning the focused excitation beam over the sample and simultaneous detection of the emitted fluorescence, the image is recorded point-by-point as intensity values at each position.

1.3 Diffraction limit in far-field light microscopy

Technical advancements in the utilized optical elements and better sample preparations improved the imaging quality in optical microscopy. However, Ernst Abbe already described in 1873 that the achievable optical resolution is ultimately limited

by the diffraction of light [8]. A radiating point source like a single fluorophore will be imaged by an optical system as a spatial intensity distribution, called the point spread function (PSF) of the system. The PSF of an ideal optical imaging system with a circular aperture is a pattern consisting of a central maximum encircled by concentric minima and maxima. The spot formed by uniform illumination of a circular aperture and focused at small angles is called Airy pattern, its central maximum the Airy disk [9]. A measure for the resolving power of a microscope is given by the Rayleigh criterion [10]. It states that two point emitters can still be distinguished if the maximum image intensity of the first emitter falls into the first minimum image intensity of the second emitter. Thus, the minimal distance Δr at which two point emitters can be separated laterally is described by the radius of the Airy disk given as

$$\Delta r \cong 0.61 \frac{\lambda}{n \sin \alpha} \cong 0.61 \frac{\lambda}{\text{NA}} \tag{1.1}$$

with the wavelength λ of the light forming the image. The refractive index of the medium n and the maximum half angle α of light entering the imaging lens defines the numerical aperture NA of the imaging system. An analogous expression for the axial distance Δz is given by

$$\Delta z \cong 2.00 \frac{n\lambda}{\text{NA}^2}. \tag{1.2}$$

An alternative measure for the resolution is represented by the full width at half maximum (FWHM) of the PSF. The FWHM is convenient since a diffraction-limited PSF is often approximated by a Gaussian profile.

Following Equations 1.1 and 1.2, the spatial resolution can be increased by using shorter wavelengths or higher NA objective lenses. However, both factors are limited: visible light ranges from 400 to 700 nm and the maximal NA of an oil-immersion objective lens is typically < 1.5. This limits the lateral resolving power of a light microscope to ~ 180 nm, preventing the distinction of cellular structures with mutual distances smaller than the resolution limit.

Different methods were developed to push the diffraction limit to its boundaries. Total internal reflection fluorescence (TIRF) microscopy [11] uses an evanescent wave of the excitation light to illuminate the sample in a restricted depth of about 100 nm. This results in sub-diffraction axial resolution, but limits the method to observations only at the glass-medium interface. In 4-Pi microscopy, two opposing objective lenses are used to increase the effective numerical aperture of the system [12]. In

combination with deconvolution algorithms, this allowed spatially uniform resolution of down to $100\,\mathrm{nm}$ [13].

In all conventional light microscopy methods, the resolution is restricted by the diffraction-limit, which impedes the observation of structures with sizes smaller than this limit.

1.4 Diffraction-unlimited microscopy

The concept to overcome the diffraction limit by utilizing discernible states of fluorescent molecules was first proposed in 1994 by Hell and Wichmann [14]. Assuming that fluorophores or other markers can be completely transferred repeatedly between different and distinguishable states, switching between these states allows to theoretically reach unlimited spatial resolution. This opened up a new field of super-resolution light microscopy methods, denoted as nanoscopy. Applied to fluorophores, optical nanoscopy methods commonly utilize a fluorescent on-state and at least one non-fluorescent off-state. One of the transitions between the on- and off-state has to be light-driven. The fluorescent state of the molecules reports on their local population of states, whereas the populations are taken stochastically or prepared by specific illumination fields. In general, any transition between two distinguishable states can be employed, e.g. changes in the absorption cross-section. However, featuring excellent sensitivity and contrast, fluorescence has proved optimal suitability for optical nanoscopy [15].

All nanoscopy methods developed to date share the concept to separate neighboring fluorophores by state transitions and can be assigned in two different categories: coordinate-targeted and coordinate-stochastic methods.

1.4.1 Coordinate-targeted switching methods

Coordinate-targeted switching methods expose the sample to a light pattern featuring at least one zero-intensity area. The pattern shall transfer all molecules to a different state except the ones in the vicinity of the intensity zero. This allows the preparation of a sub-diffraction-limit sized area of molecules in a defined state. The strength of the transfer allows to tune the size of the region of non-transferred fluorophores and thus the spatial resolution.

Different methods employ different state transitions of molecules. The general method of targeted switching of molecules between a fluorescent on- and a non-

fluorescent off-state is named RESOLFT (REversible Saturable Optical Linear Fluorescence Transitions)[16–18]. It covers all possible reversible and saturable transitions between states. This includes the population of the ground state in stimulated emission depletion (STED)[14] and the population of the triplet state of the fluorophores as the non-fluorescent state in ground state depletion (GSD)[19,20]. However, throughout this thesis, the term RESOLFT specifically refers to targeted switching between metastable states of reversibly photoswitchable fluorescent proteins (RSFPs, section 1.6) and fluorophores (section 1.7).

The light-driven transition between an on- and off-state is characterized by its transition rate $k_{\mathrm{on}\to\mathrm{off}} = 1/\tau = \sigma \times I$. This rate depends on the photon cross-section σ and the applied light intensity I driving the transition. The saturation intensity I_{sat} is characteristic for each fluorophore and typically describes the intensity at which the number of molecules in the on-state is halved. Intensities $I \gg I_{\mathrm{sat}}$ transfer the fluorophores almost completely to the off-state.

In single beam scanning approaches, the commonly used off-switching beam is doughnut-shaped[21]. The combination of the Gaussian-shaped excitation beam and the parabola-shaped intensity zero of the off-switching beam effectively confines the detection area. The spontaneous fluorescence emission decreases exponentially with increasing off-switching intensity[22]. The size of this sub-diffraction-sized spot, the effective PSF, mainly depends on the light intensity I and can, related to Abbe's description, be written as[23]:

$$\Delta r \approx \frac{\lambda}{2\,\mathrm{NA}\,\sqrt{1 + I/I_{\mathrm{sat}}}} \tag{1.3}$$

Stimulated emission depletion was the first method to actually overcome the diffraction limit[14,24,25]. In STED, the fluorescent state is the excited state S_1 of the fluorophores and the dark state is the ground state S_0. After excitation to S_1 the fluorophores are returned to the ground state by stimulated emission. The process of stimulated emission describes the interaction of a photon with an excited molecular state, causing the transition to a lower energy level by emitting a photon. The emitted photon has the same wavelength, polarization and phase as the stimulating photon. Therefore this process is distinctly different from the spontaneous emission, where the emitted photons are polarized according to the orientation of the molecules' dipole moment and have no phase relation. The STED light has to match the energy gap between S_1 and S_0 of the fluorophore. To reduce re-excitation by the

STED light, the STED wavelength should be red-shifted as much as the emission spectrum of the fluorophores allows[25]. Typically the used STED wavelengths are in the range of 590 nm for green emitting to 780 nm for red emitting fluorophores[26]. With typical values of $\sigma = 10^{-17}\,\mathrm{cm^2}$ and $\tau = 1 - 4\,\mathrm{ns}$[27], saturation intensities I_sat of several $\mathrm{MW/cm^2}$ are required for stimulated emission[28].

It is possible to multiplex the process of stimulated emission depletion either by several single beams at different positions in the sample or by massive parallelization using standing wave patterns in a widefield approach[29,30].

1.4.2 Coordinate-stochastic switching methods

Coordinate-stochastic methods rely on the stochastic transfer of fluorophores between different states such that they can be imaged individually by temporal separation. During detection, only a subset of all fluorophores in the sample shall reside in their fluorescent state at random spatial coordinates. Here it is essential, that the detected fluorophores are further apart than the diffraction limit. The fluorescence signals of the single emitters are imaged on a camera and their positions are subsequently determined precisely by fitting the center positions of the emitters' image spots. This yields the positions of the individual emitters with sub-diffraction precision. The localization precision scales with the inverse square root of the number of detected photons[31]. This imaging scheme is repeated with multiple subsets of molecules to reconstruct an image from the extracted positions of the fluorophores.

The experimental implementation of single molecule localization microscopy (SMLM) was independently developed under the terms (fluorescence) photoactivated localization microscopy ((F)PALM)[31,32] and stochastic optical reconstruction microscopy (STORM)[33]. The two methods mainly differ in the labels used. (F)PALM uses photoactivatable fluorescent proteins and dyes, which are bleached after detection, whereas STORM relies on reversibly photoswitchable organic fluorophores. In STORM, special imaging buffers are needed to control the photo-physical and -chemical behavior of the used labels. Commonly employed buffers contain an oxygen-scavenging system, e.g. a glucose oxidase system, to reduce photobleaching and thiols to facilitate the photoswitching process by association with the fluorophore and to act as triplet quenchers[34].

The coordinate-stochastic methods underlie certain limitations. Mostly, the samples have to be fixed to avoid motion artifacts due to the time-displaced detection of the single emitters. Furthermore, detecting enough fluorophores for an image makes the

process time-consuming and the image reconstruction requires additional computation time. This hampers the application of these methods for live-cell imaging, although advances in this direction were recently made[35,36].

1.5 RESOLFT nanoscopy with photoswitchable labels

The principle of RESOLFT nanoscopy with switchable fluorescent labels was proposed in 2003 by Hell *et al.*[16]. Employing molecular states with long lifetimes (ms to s) allows for low light intensities to toggle between these states. The concept was demonstrated for the first time with a photoswitchable fluorescent protein, asFP595, on artificial structures[18]. Subsequently, the concept was also applied to living cells with different RSFP-variants[37,38].

Similar to other coordinate-targeted switching methods only one of the transitions has to be light driven. However, if both state transitions are light induced, as in RSFPs, the imaging process can be controlled more precisely. Transition to the fluorescent state is denoted as on-switching, whereas transition to the non-fluorescent form is named off-switching. Assuming a switchable label, which emits fluorescence during illumination with the off-switching wavelength, so called negative switching markers, a typical RESOLFT scheme consists of an on-switching step, an off-switching step with a doughnut-shaped beam and an excitation step to read out the residual fluorescence. This three-step process, shown in Figure 1.3, is repeated at every scanned position.

Compared to STED, where the state transition can be considered as instantaneous[25], RESOLFT with switchable labels suffers from the reduced imaging speed as the off-switching step takes μs to ms[37–40]. RESOLFT additionally requires very specialized labels, from which only few are available. Despite these constraints, the low light intensities in RESOLFT (W/cm^2 to kW/cm^2) render the method suitable for the observation of living specimen and long-term experiments causing low photodamage to the organism[41].

Like all high-resolution microscopy methods, RESOLFT strongly depends on the availability of suitable fluorescent labels[15]. The properties of the fluorescent molecules determine several important key parameters of the imaging process. This includes the time it takes to acquire a high-resolution image, the achievable spatial resolution and image contrast, the sample preparation protocol and the type of specimen that can be observed.
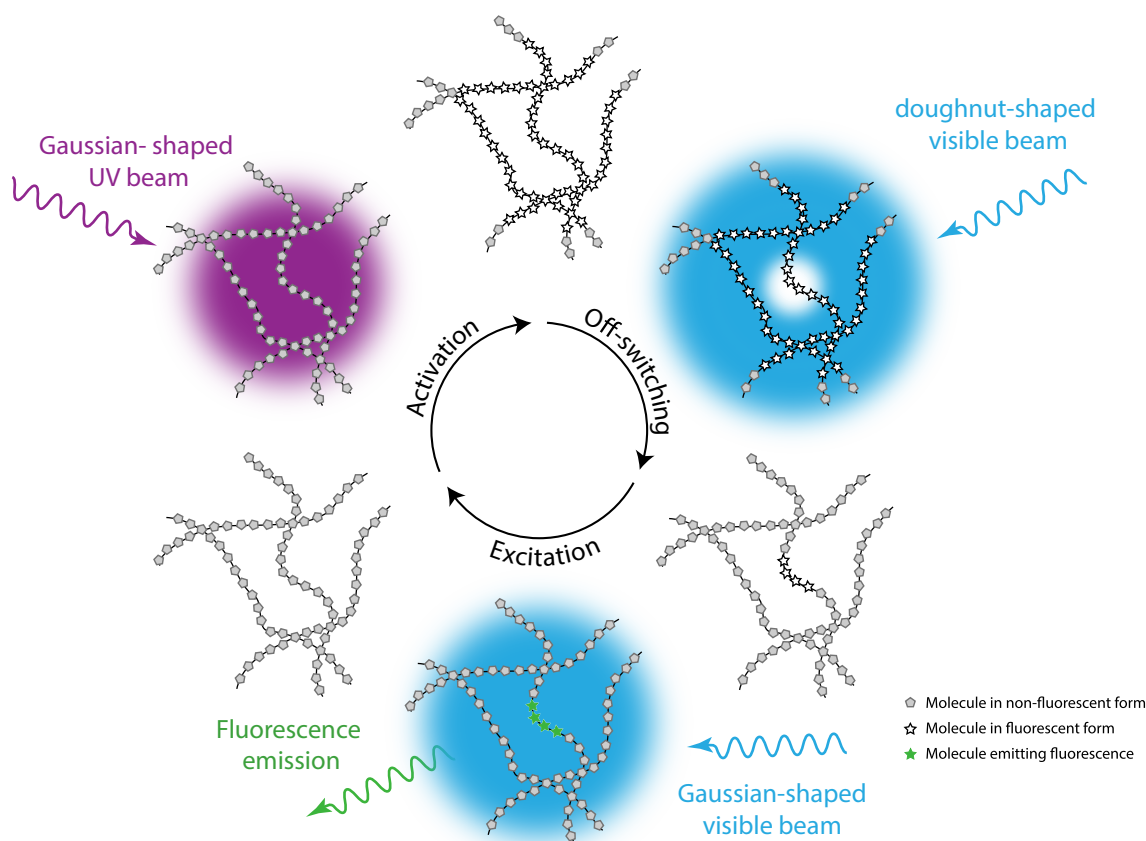
Figure 1.3: Schematic illustration of the steps required to acquire high resolution images with negative switching markers based on the RESOLFT concept. For imaging, the sequence of activation, off-switching and excitation is repeated at every scanned position in the sample.

Therefore the development of new labels is crucial for the advancement of RESOLFT nanoscopy and its application in the life sciences. This can either be accomplished by modifying existing fluorescent proteins via targeted or random mutagenesis to obtain photoswitchable variants with improved properties or by designing synthetic photochromic and fluorescent molecules[42,43]. The most common method so far is to mutate fluorescent proteins because they are applicable in live-cell imaging as genetically encoded tags. A wide range of fluorescent photoswitchable proteins have been described since the first application of asFP595 for RESOLFT nanoscopy[44], but only few of the recently developed fluorescent proteins proved to be highly suitable for optical nanoscopy[15,42]. Although these candidates showed their high capability in several applications, fully synthetic photoswitchable labels for RESOLFT nanoscopy contain the potential for a wider spectral range, higher photostability and higher brightness[43].

1.5.1 Requirements for labels used in RESOLFT nanoscopy

RESOLFT nanoscopy imposes special requirements on the used labels. Ideally, two different states of the molecule are addressable separately. In this regard, thermally stable but photochemically reversible photochromic compounds are advantageous because the transformation between two isomers, accompanied by a change in the absorption spectrum, can be induced with light of different wavelengths. The spatial resolution obtainable in RESOLFT is limited by several factors, in particular the number of switching cycles before photo-bleaching, the switching contrast and the fluorescence signal[42].

The number of possible switching cycles before the label is photobleached or loses its switching capability, denoted as switching fatigue, is a crucial factor for the achievable resolution increase. Higher spatial resolutions require smaller scanning steps (pixels) where at each step all labels in the diffraction limited area undergo a switching cycle. Therefore the number of cycles a label has to undergo depends on the FWHM of the activation spot r_{act} and the estimated FWHM of the effective PSF r_{eff}. Assuming that the sampling step equals half the FWHM diameter of the estimated effective PSF, the number of performed switching cycles when acquiring a RESOLFT image in two dimensions can be written as[42]

$$\text{Number of cycles} = \left(\frac{r_{\mathrm{act}}}{r_{\mathrm{eff}}/2} \right)^2 . \tag{1.4}$$

It follows that a confocal image in the focal plane already requires four switching cycles and that an m-fold resolution improvement in two dimensions requires $4 \times m^2$ switching cycles[16]. To avoid excessive photo-bleaching, the fluorophores should withstand at least this number of cycles.

Many photoswitchable fluorophores show fluorescence even after they are switched to the off-state. The origin of this fluorescence is not definitely determined yet. It can either originate from weak fluorescence in the off-state, a spontaneous return to the on-state[42] or referred to ensemble measurements from a proportion of fluorophores that can not be switched off[45]. The ratio of residual fluorescence after off-switching and the initial fluorescence in the on-state, denoted as γ, also impacts the achievable resolution increase[43,46]. It causes a background signal during the read-out of the region confined by the doughnut-shaped off-switching beam. This leads to a reduced signal-to-background ratio. The intensity of this background signal is strongly de-

pendent on the particular label and the type of sample. Additionally, samples with sparse structures cause lower background than dense samples.

In two dimensions, the signal originates from the confined effective area A_{eff}, whereas the background signal originates from the area illuminated by the focused excitation beam $A_{\text{CF}} \gg A_{\text{eff}}$ with the FWHM r_{CF}. The signal-to-background ratio (SBR) can then be written as

$$\text{SBR} = \frac{I_{\text{signal}}}{I_{\text{background}}} \approx \frac{A_{\text{eff}}}{A_{\text{CF}} \cdot \gamma} = \frac{1}{m^2 \gamma} \tag{1.5}$$

where m denotes the resolution improvement $r_{\text{CF}}/r_{\text{eff}}$. Presupposing that the signal can only be reliably detected at SBR $\gtrsim 1$, the resolution increase for two-dimensional RESOLFT imaging can be estimated by $m \lesssim \sqrt{1/\gamma}$.

Along with this, another import key parameter for a RESOLFT label is its molecular brightness. Bright labels ensure reliable detection against noise caused by the system and the specimen like shot noise and autofluorescence.

Long imaging times render the experiment susceptible to disturbances like vibrations and hamper the observation of dynamic processes. In general, one of the switching processes represents the time-consuming step during the imaging[37,39]. Therefore high switching rates of the involved switching processes are desired. Furthermore, longer wavelength are preferred for photoswitching to reduce phototoxicity and the overall photon energy the samples are exposed to[41].

All artificial markers need to be somehow attached to the target structure. Fluorescent proteins have the advantage to be genetically encodable, provided that their expression does not impede the natural functions of the organism. Organic fluorophores are well implemented in immunostaining protocols, although their application in living specimen requires membrane permeability, water-solubility and a functionalization to label biomolecules[47].

1.6 Photoswitchable fluorescent proteins

The discovery of the green fluorescent protein (GFP) and its first application as genetically encoded tag for proteins in living organisms marked a major breakthrough for cell biology[48–50]. GFP-like proteins have different oligomerization states in nature and consist of about 240 amino acids. They form a barrel-like structure consisting of 11 β-sheets, spanned by an α-helix. Inside the α-helix, the chromophore is formed autocatalytically from three partially conserved amino acids. The chro-

mophore maturation is only possible under the presence of molecular oxygen. The fluorescence is strongly dependent on the environment of the chromophore provided by the protein barrel[51]. The originally described wild type avGFP was further improved by mutations and subsequently applied in fluorescence microscopy[52]. In the following years, mutagenesis and isolation from different organisms yielded proteins with yellow and red emission wavelengths and the first photoactivatable and photoconvertible GFPs were discovered[53–55].

Photoactivatable proteins are initially non-fluorescent. Illumination with UV-light induces a structural change of the chromophore resulting in fluorescence of the protein. Photoconvertible proteins show specific absorption and emission spectra which are typically red-shifted upon illumination with a certain wavelength. In most cases these structural changes can only be performed once[56].

In contrast to this, reversibly photoswitchable fluorescent proteins (RSFPs) can be switched between an on- and an off-state state reversibly. The transitions between the states are driven by light of different wavelengths. Thereby a distinction is made between positive- and negative-switching RSFPs. Illumination with the excitation wavelength converts positive-switching RSFPs to their fluorescent state, whereas negative-switching RSFPs are switched to the non-fluorescent state. Accordingly, illumination with the excitation wavelength in negative switchers causes two concurrent processes: fluorescence emission and off-switching. The molecular switching mechanism of most RSFPs was revealed by crystallographic studies to be a cis-trans-isomerization of the chromophore[57,58]. The repositioning of the chromophore's imidazole ring by the isomerization increases the probability for a change of its protonation. The protonation induces a blue-shift of the protein's absorption maximum. Therefore the different states can be addressed separately to switch between them. In the trans-position, the chromophore is less stabilized by the β-barrel causing a substantial drop of the fluorescence quantum yield[58]. As a result, the cis-isomer is typically fluorescent and the trans-isomer is non-fluorescent. One exception of the cis/trans isomerization based photoswitching is the RSFP Dreiklang with a decoupled switching and excitation process. In Dreiklang the photochromic process is enabled by reversible covalent water addition to the chromophore[38].

The discovery of the first photoswitchable GFP-like protein, the positive-switching asFP595[59], revealed the potential of these labels for nanoscopy[16,18]. However, its tetrameric structure impeded the application as genetically encoded marker. The first monomeric RSFP Dronpa was used to reveal cellular signaling pathways[60] and for RESOLFT imaging of artificial structures[40]. Albeit, pronounced switching fa-

tigue and slow switching rates of these proteins hampered biological high-resolution imaging [40,61]. Protein mutagenesis and screening later yielded new variants with shorter switching halftimes, higher quantum yields, faster maturation times or different spectral properties [44]. Particularly noteworthy are rsEGFP and Dreiklang which enabled the first demonstrations of live-cell RESOLFT imaging [37,38]. The successor of rsEGFP, namely rsEGFP2, proved particular suitability in this context, due to its high photostability and fast switching kinetics [39,62–65].

1.7 Photoswitchable synthetic fluorophores

Synthetic organic fluorophores were used to label structures of interest using immunofluorescence already before proteins were established as fluorescent tags [66]. Typically, organic fluorophores of various origin are conjugated to an antibody, which binds to a specific target structure. The organic fluorophores are optimized for brightness, photostability, excitation and emission wavelengths and fluorescence lifetime. These properties render them applicable in all branches of fluorescence microscopy, especially for high resolution methods [67]. Different bioorthogonal labeling strategies (SNAP-tag, CLIP-tag, HaloTag [68–70]) furthermore enabled their wide applicability in live-cell imaging [71].

The RESOLFT concept has been demonstrated as a proof-of-principle only with few switchable organic fluorophores on test structures like stained grooves in a glass surface or silica beads [72,73]. More recently, RESOLFT was performed with a reporter-activator pair of two covalently linked fluorophores used to stain cellular structures in mammalian cells [74]. The switching process requires the reversible formation of a non-fluorescent state upon thiol addition to the fluorophore, comparable to the photoblinking process frequently exploited in SMLM [34]. This requires the application of blinking-enhancing and stabilizing buffers (see subsection 1.4.2) that precludes or hampers the application in living cells.

Diarylethenes represent a majority among the synthetic photochromic molecules. The first diarylethenes were presented three decades ago [76]. They offer higher fatigue resistances and thermal stability [77] compared to other photochromic compounds like azobenzenes or spiropyrans [78,79]. Diarylethenes have two thermally stable forms, open- and closed-ring isomers. Their core structure and electronic states, derived from theoretical studies and ultrafast pump-probe spectroscopy [80–82], are depicted in Figure 1.4. The thermal stability originates from a relatively high en-
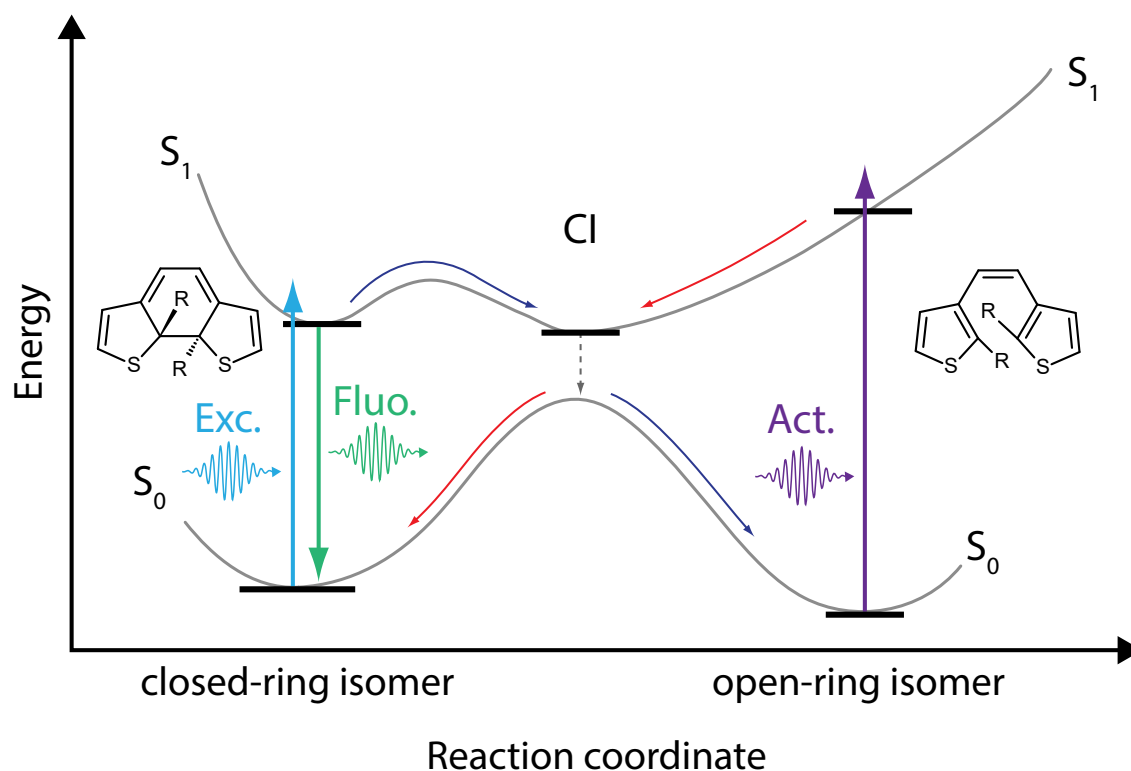
Figure 1.4: Jablonski diagram for diarylethene derivatives including conventional adiabatic potential energy curves (solid light gray), adapted from Irie *et al.* [75]. The excitation (Exc.) of the closed-ring isomer from the ground state S_0 to the first excited state S_1 is depicted in light blue and the excitation (Act.) of the open-ring isomer from its S_0 state to S_1 in dark purple. The fluorescence (Fluo.) emission is depicted in green. The red and dark blue arrows show the pathways of isomerization from the closed-ring to the open-ring and from the open-ring to the closed-ring isomer, respectively. The dotted light gray arrow indicates the transition from S_1 to S_0 at the conical intersection (CI).

ergy barrier of $\sim 192\,\mathrm{kJ/mol}$ on the potential energy surface of S_0 [80]. The open-ring isomer is formed by excitation to the S_1 state with visible light and subsequent relaxation to S_0. The chromophore can be returned to the closed-ring form (CF) by illumination with UV light. In the open-ring isomer, the π-conjugation involves the thiophene rings or benzothiophene fragments. The ring closure causes a delocalization of the π-conjugation over the molecule inducing a substantial ($\geq 150\,\mathrm{nm}$) red-shift in the absorption spectrum [75]. In solution diarylethenes exhibit two different conformations in their open form (OF). According to the Woodward-Hoffmann rules, the photoinduced cyclization reaction is only possible conrotatory [83], resulting in a photo-inactive parallel and a photo-active antiparallel conformation depicted in Figure 1.5. In thermal equilibrium of the two conformers, only the molecules

in the antiparallel form can undergo the ring-closure reaction upon absorption of a UV photon. Thus, the quantum yield for ring closure cannot exceed 50%[84]. However, due to rapid interconversion between parallel and antiparallel conformers, full reaction to the closed form is possible. The introduction of diarylperfluorcyclopentens enabled fatigue resistances comprising above 10000 switching cycles and high thermal stability over several months in organic solvents or in a solid state[85].
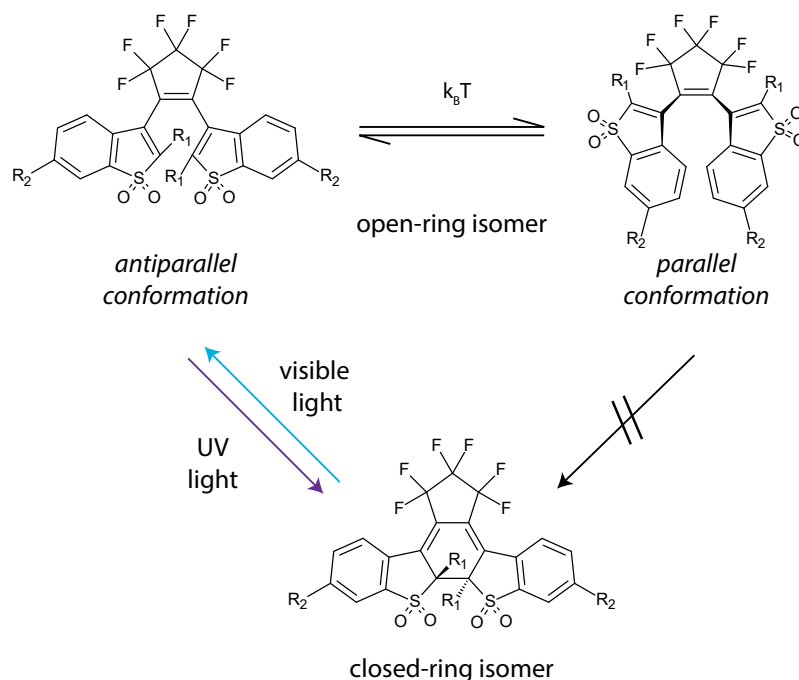
Figure 1.5: Antiparallel and parallel conformation of the open form of diarylethenes and possible transitions to the closed form.

A majority of diarylethenes is non-fluorescent in both open- and closed ring-forms, but oxidated benzothiophene derivatives, as depicted in Figure 1.5, exhibit strong fluorescence in the closed form[86,87]. Non-fluorescent diarylethenes were incorporated into bichromophoric compounds with a photochromic and a fluorescent unit to prepare photoswitchable fluorophores. In these compounds, the fluorescence is quenched either by resonant energy transfer or electron-transfer from the fluorescent unit to the closed form of the diarylethene[88–92]. Unfortunately, these compounds are not water-soluble, require light of 375 nm or below for cyclization and often show very low switching rates and rapid photodecomposition in water. Nevertheless, using target-specific fluorescent units, certain compounds of this type were used for staining cellular structures and biological imaging by exploiting hydrophobic subcompartments[93,94].

A viable and straightforward approach to confer water solubility to diarylethenes is to attach hydrophilic residues to the core structure. Photochromic properties in polar solvents were reported for derivatives decorated with acetyl[95] or inositol residues[96]. Compounds with sulfonic residues often require cyclodextrin as non-polar cavity[97]. Poly(ethyleneglycol) chains induce the formation of nanoaggregates[98,99], which were reported to show unspecific accumulation in the cytoplasm of living cells and could be switched between their fluorescent and non-fluorescent states in the timescale of minutes to hours using UV and visible light[100–102]. However, the aggregation of markers compromises labeling and resolving specific cellular structures. These restrictions hampered the application of photochromic diarylethenes in biological imaging.

All of the above mentioned demonstrations of fluorescent, photoswitchable diarylethenes show that they lack one or more of the key features required for RESOLFT nanoscopy. In particular, these compounds have limited water solubility, reduced photoswitching and fluorescence performance in water and often lack a reactive group required for bioconjugation[103,104]. As a result, no specific staining of cellular structures, neither in living nor in fixed cells, was reported for diarylethenes without fluorescent molecules attached to the core structure.

1.8 Aim of the study

RESOLFT nanoscopy requires labels with optimized features which to date are only provided by a limited number of RSFPs. The generation of new RSFPs demands extensive protein mutagenesis and screening. The utilization of organic fluorophores bears the potential to expand the palette of available RESOLFT labels based on rational design.

In this work the properties and perspectives of synthetic reversible switchable fluorophores for their application in high resolution microscopy based on the RESOLFT concept with low light energies is evaluated. The focus is on the characterization and implementation of new diarylethene-based fluorophores in aqueous solutions.

The findings shall provide a foundation to advance synthetic fluorophores for live-cell RESOLFT.

2 Experimental Methods

The investigation and application of fluorescent labels for high resolution microscopy requires different methods. In addition to measurements of the absorption and emission spectra in solution, it is also of significant interest how these labels perform under conditions present in confocal microscopy. For this purpose a confocal screening microscope was constructed giving the opportunity to apply different excitation wavelengths to the samples and to detect their specific fluorescence. The high-resolution RESOLFT image acquisitions were performed on a modified 1C RESOLFT QUAD Scanning microscope (Abberior Instruments, Göttingen, Germany).

2.1 Absorption and emission measurements in solution

The first characterizations of new synthetic fluorophores were performed using a standard absorption spectrophotometer (Cary 4000 UV-Vis, Agilent, Santa Clara, CA, USA) and a fluorescence spectrophotometer (Cary Eclipse, Agilent, Santa Clara, CA, USA) to acquire absorption and fluorescence spectra of the respective compounds in solution. These measurements were performed in quartz cuvettes with 10 mm path length.

The different absorption spectra of the two isomers present in the synthesized photochromic molecules were only detectable individually if nearly all molecules in the detection volume were present in one of the isomeric forms. Therefore the cuvette was placed in an optical setup (Figure 2.1a) providing collimated illumination by LEDs with blue light at 470 nm (M470L3, Thorlabs, Munich, Germany) and UV light at 365 nm (M365L2, Thorlabs, Munich, Germany). The illumination spot's diameter in the sample was ~ 3 mm. The sample was illuminated with light of the desired wavelength for a specific time period under continuous vigorous stirring to convert the molecules into one of the isomers by using computer-controlled shut-

ters. Typically illumination powers in the range of $10-20\,\mathrm{mW}$ were applied. The photoswitching experiments in solution were conducted by stepwise exposure of the sample with subsequent recording of the absorption and emission spectra after each illumination step.

The fluorescence lifetime of fluorophores in solution was determined using the optical setup depicted in Figure 2.1b. A picosecond-pulsed laser diode (LDH-P-C-470, Pico-Quant, pulse width $\sim 100\,\mathrm{ps}$) emitting light at $470\,\mathrm{nm}$ wavelength and pulsing at a rate of $40\,\mathrm{MHz}$ was used for the excitation. The emitted fluorescence was collected, transmitted through an emission band-pass filter (selected according to the emission spectrum of the corresponding fluorophore) and recorded by a single-photon avalanche diode (SPAD) detector (ID100-50, ID Quantique, Geneva, Switzerland) and a stand-alone time correlated single photon counting (TCSPC) module (Pico-Harp 300, PicoQuant, Berlin, Germany). The photon arrival times were determined using the sync signal provided by the laser driver. The count rates on the detector were adjusted to values below 10^3 cps (counts per second). The instrument response function (IRF) of the system was determined by using a dispersant under identical conditions as during the measurement of the sample, but without the emission filter. The characteristic lifetimes were obtained as described in section 2.5.
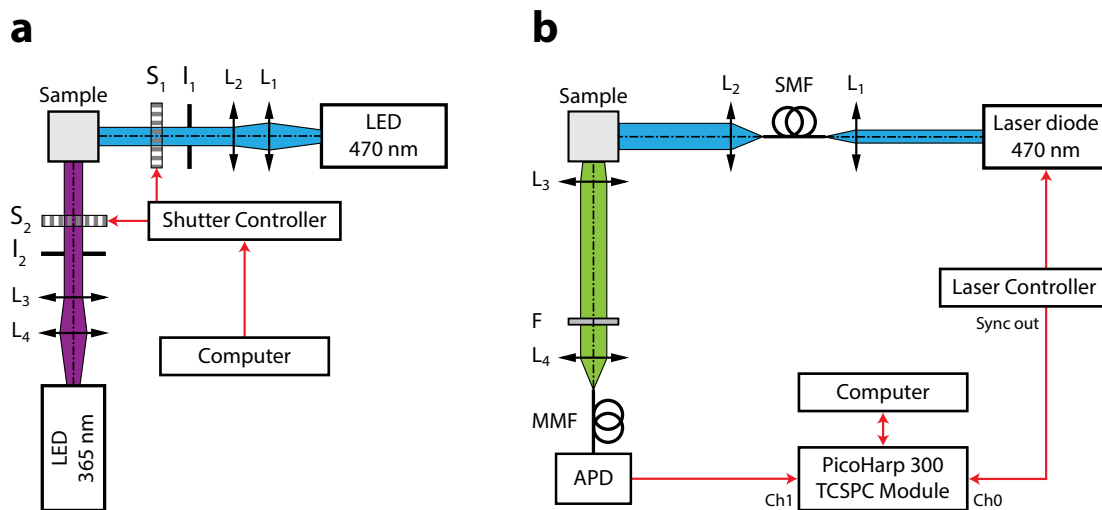
Figure 2.1: Schematic illustration of the described optical setups used for the investigation of fluorophore behavior in solution. **a:** Setup for photoswitching in solution: $L_{1,2}$ and $L_{3,4}$: collimating lens pair; S_1 and S_2: shutter; I_1 and I_2: iris; **b:** Setup for TCSPC measurements: L_1 and L_4: focusing lens; L_2 and L_3: collimating lens; F: emission filter; SMF: single-mode fiber; MMF: multi-mode fiber; APD: avalanche photo-diode; red lines and arrows indicate electrical signals between devices.

2.2 Confocal screening setup

The experiments to determine the potential of different fluorescent labels for high resolution imaging were performed on a custom-built confocal microscope as shown in Figure 2.2.

For the excitation of the investigated fluorescent labels, different laser sources were used. Pulsed excitation light (40 MHz repetition rate, ~ 100 ps pulse width) was provided by a broad-band supercontinuum laser (SuperK Extreme EXB-6, NKT Photonics, Birkerød, Denmark). Since the emission of the supercontinuum laser was not polarized, a polarizing beam splitter (PBS251, Thorlabs, Munich, Germany), provided the proper polarization for the following optical element. An acousto-optic tunable filter (AOTF) (AOTFnC-VIS TN head with MDS8C-B66-22-80.153 driver, AA OptoElectronic, Orsay, France) allowed the selection of a wavelength band from $450 - 700$ nm with ~ 3 nm FWHM bandwidth as well as the modulation of the excitation power. The rise time of the AOTF was limited to about 2 μs with a delay of 8 μs to the applied voltage. The spatial mode profile of the pulsed excitation light was cleaned up using a polarization-maintaining single-mode fiber (PM460-HP, Thorlabs, Munich, Germany). The excitation beam was collimated by an achromatic lens L_1 ($f_1 = 10$ mm, AC080-010-A, Thorlabs, Munich, Germany) to a beam diameter of about 2 mm. Due to the insufficient suppression of the supercontinuum spectrum by the acousto-optic tunable filter, a filter wheel F_1 with different bandpass filters was used to clean up the spectrum. The bandpass filters were selected according to the required wavelength.

A directional beam splitter (DBS)[105] consisting of two polarizing beam splitters (PBS251, Thorlabs, Munich, Germany), an achromatic half-wavelength retarder plate $\lambda/2$ (AHWP05M-600, Thorlabs, Munich, Germany) and a Faraday rotator (711A, Conoptics, Danbury, CT, USA; used without polarizers) was used for directional broad-band beam splitting of the excitation and fluorescence light[105]. The excitation light below 500 nm emitted by the supercontinuum source bypassed the DBS via two dichroic mirrors D_1 and D_3 (Z488RDC, Chroma, Bellows Falls, VT, USA) due to the low transmission ($\sim 2\%$) of the Faraday rotator at wavelengths below 500 nm. The bypassing beam path was used to include UV light for photo-switching. Therefore a UV laser diode (405 nm wavelength, 30 mW, BCL-30-405-S, CrystaLaser, Reno, NV, USA), whose spectrum was cleaned up by a bandpass filter F_2 (Z405/10x, Chroma, Bellows Falls, VT, USA), was power-modulated by an acousto-optic modulator (MT110-A1-VIS head with MODAA110-B4-3060 driver,
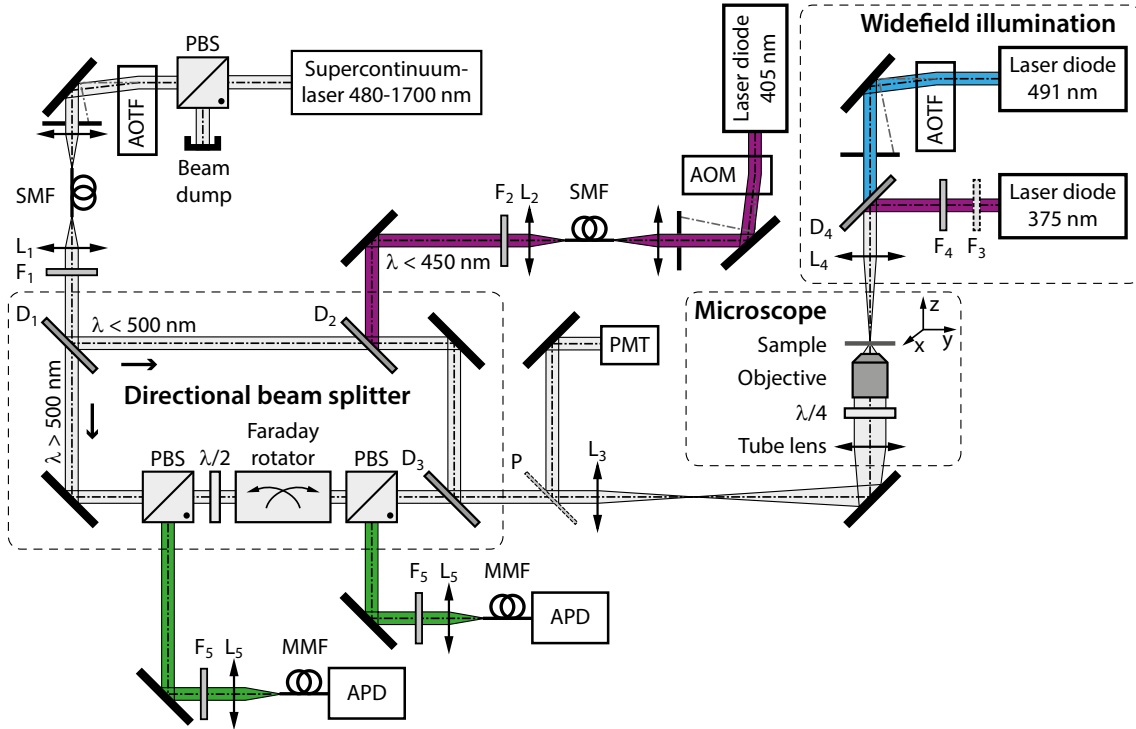
Figure 2.2: Schematic illustration of the described custom-built confocal screening setup including all relevant optical elements. PBS: polarizing beam splitter; AOTF: acousto-optic tunable filters; SMF: polarization-maintaining single-mode fiber; AOM: acousto-optic modulator; L: lens; F: filter; D: dichroic mirror; $\lambda/2$: half-wavelength retarder plate; $\lambda/4$: quarter-wavelength retarder plate; P: flippable pellicle beamsplitter; PMT: photomultiplier tube; MMF: multi-mode fiber; APD: avalanche photo-diode.

AA OptoElectronic, Orsay, France) and coupled into a polarization-maintaining single-mode fiber (P5-405BPM, Thorlabs, Munich, Germany). After the beam was collimated by an achromatic lens L_2 ($f_2 = 30$ mm, AC254-030-A, Thorlabs, Munich, Germany), the illumination beams were combined by a dichroic mirror D_2 (Z405RDC, Chroma, Bellows Falls, VT, USA). All illumination beams were then magnified four times by the combination of the achromatic lens L_3 ($f_3 = 50$ mm, AC254-050-A, Thorlabs, Munich, Germany) and the microscope tube lens ($f_t = 200$ mm) of a commercial microscope stand (DM IRBE, Leica Microsystems, Wetzlar, Germany). The illumination beams were circularly polarized with a quarter-wave retarder plate $\lambda/4$ (AQWP05M-630, Thorlabs, Munich, Germany). A $100\times$ oil-immersion objective lens with 1.4 NA (HCX PL APO $100\times/1.4 - 0.7$ Oil CS, Leica Microsystems, Wetzlar, Germany) then focused the light into the sample. All experiments were performed using Leica Type F immersion oil (Leica Microsystems, Wetzlar, Germany).

The fluorescence emission was split by the DBS into two orthogonally polarized beams and selected by band-pass filters F_5 according to the emission spectrum of the investigated fluorophore. The fluorescence light was focused with achromatic lenses L_5 ($f_5 = 30\,\text{mm}$, AC254-030-A, Thorlabs, Munich, Germany) into step-index multimode fibers (core-diameter: $25\,\mu\text{m}$, M67L01, Thorlabs, Munich, Germany) functioning as the confocal pinhole and detected by two avalanche photo-diodes (PD-050-CTD-FC, MicroPhotonDevices, Bolzano, Italy). The core diameter of the multimode fibers corresponded to a diameter of 0.91 Airy units for emissions centered at 525 nm. The detected photon events were recorded as photon streams with a TimeHarp260 PICO board (PicoQuant, Berlin, Germany) and analyzed for fluorescence lifetime. Simultaneously, a hardware correlator (Flex02-08D/C, correlator.com, Bridgewater, NJ, USA) was used for real-time monitoring of the detection count rates and for fluorescence correlation spectroscopy of fluorophore solutions, which proved useful for aligning the setup.

Precise positioning and scanning of the sample was provided by an xy-translation stage (P-733K034 stage driven by an E-633 LVPZT-Amplifier, Physik Instrumente, Karlsruhe, Germany) and a separate z-translation stage for the objective lens (MI-POS 100 focus positioner driven by NV120 1CLE, Piezosystem Jena, Jena, Germany).

The IRF of the system was determined through the reflection of the excitation beam on gold nanoparticles ($\varnothing 150\,\text{nm}$, BBI Solutions, Cardiff, UK) for all used excitation and emission filters. For this purpose, the signal was integrated until at least 10^5 photons per channel were detected. The characteristic lifetimes were obtained as described in section 2.5.

In addition to the confocal point illumination, a second illumination path was implemented to achieve homogenous illumination over an area larger than the spatial extent of the confocal detection PSF. It was not possible to incorporate light with wavelengths below 400 nm through the base port of the microscope because the tube lens showed very low transmission for these wavelengths ($\sim 0.1\,\%$). Hence, for widefield photoswitching, two laser beams, one at 491 nm (50 mW cw, Calypso 50, Cobolt, Solna, Sweden) and the other at 375 nm (20 mW cw, directly modulatable up to 100 kHz, FBB-375-020-FS-E-1-0, RGBLase LLC, Fremont, CA, USA) were implemented in a trans-illumination configuration. An AOTF (AOTFnC-TN head with MOD4C-VIS driver, AA OptoElectronic, Orsay, France) was used to modulate the power of the 491 nm light. The spectrum of the 375 nm laser beam was cleaned
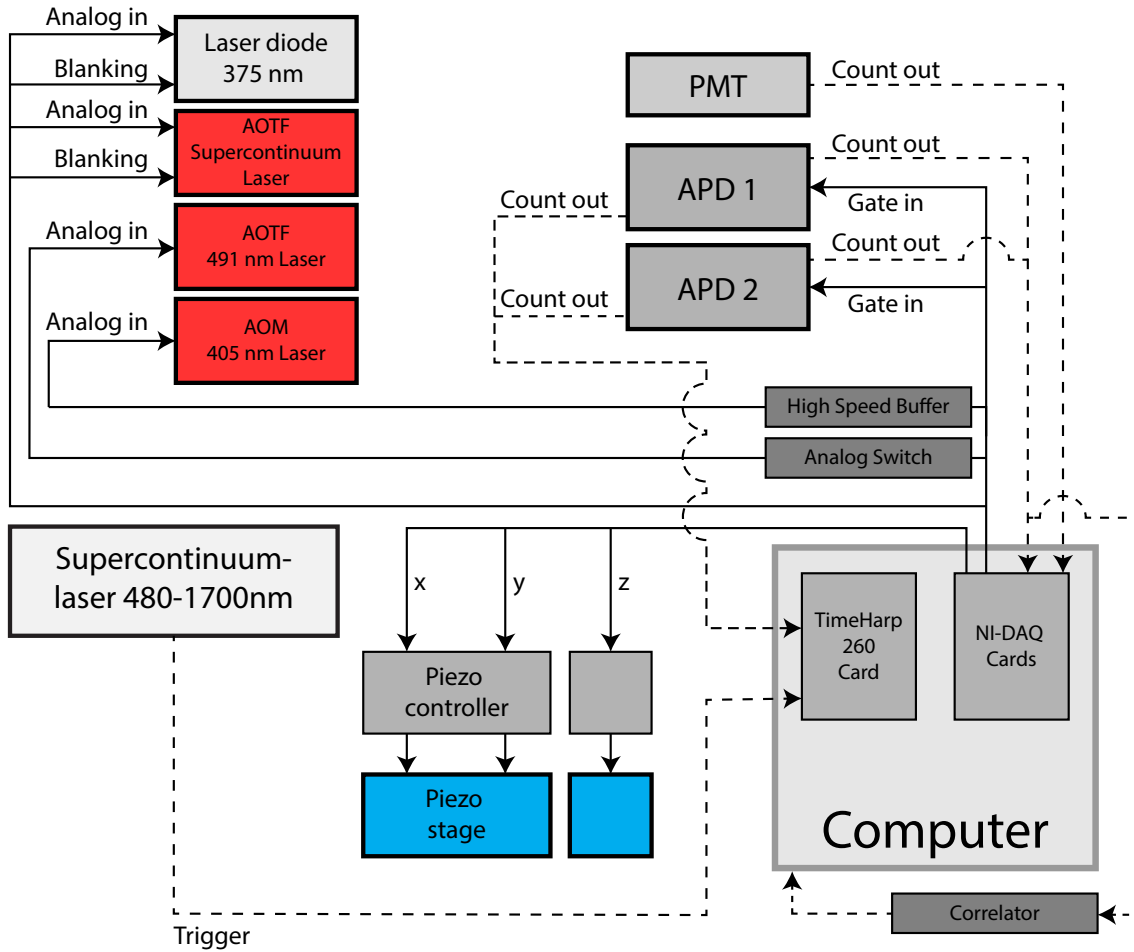
Figure 2.3: Schematic illustration of the electrical setup of the confocal screening setup shown in Figure 2.2. Electrical signals generated by the NI-DAQ cards are depicted as solid arrows. Signals generated by other devices in the experimental setup that were acquired using different hardware are depicted as dashed arrows.

up by a band-pass filter F_4 (Z375/10x, Chroma, Bellows Falls, VT, USA) and the power was adjusted by different neutral density filters F_3. The laser beams were combined by a dichroic mirror D_4 (Z375RDC, Chroma, Bellows Falls, VT, USA). By focusing the beams into the sample with an achromatic lens L_4 ($f_4 = 45\,\mathrm{mm}$, AC254-045-A, Thorlabs, Munich, Germany), an illumination field of $15-20\,\mu\mathrm{m}$ diameter was obtained.

For the examination of the excitation PSFs of the different laser sources, a pellicle beamsplitter (BP108, Thorlabs, Munich, Germany) could be inserted into the beam path between D_3 and L_3 directing the reflected light from the sample onto a non-confocal detector (photomultiplier tube) (H10723-01, Hamamatsu Photonics, Hamamatsu, Japan). The widefield illumination could be adjusted and examined by

a CCD camera (mvBlueFOX-223G, Matrix Vision GmbH, Oppenweiler, Germany) mounted onto the camera port of the microscope stand.

All above described components were controlled by two multifunction data acquisition cards (NI PCI-6731, National Instruments, Austin, TX, USA) capable of generating analog voltages and digital TTL outputs. These cards were also used to acquire the signals generated by the detectors. The high speed buffer was used to adapt current-limited signals ($<5\,\mathrm{mA}$) from the NI-DAQ cards to $50\,\Omega$ inputs at $180\,\mathrm{MHz}$ bandwidth. The analog switch enabled to switch between $0\,\mathrm{V}$ and the analog voltage outputs generated by the NI-DAQ cards via a TTL signal. Figure 2.3 shows a schematic illustration of the wiring. Experimental control and data acquisition was performed with custom-written routines for MATLAB (The MathWorks, Natick, MA, USA) and software supplied with the TimeHarp260 NANO board (PicoQuant, Berlin, Germany).

The measurement of the excitation power of the focused illuminations from the different laser sources was accomplished by placing the sensor of a power meter (PM100A with S120VC sensor, Thorlabs, Munich, Germany) in front of the objective lens and the use of an iris adjusted to the diameter of the back focal plane of the objective lens ($\varnothing 5.6\,\mathrm{mm}$). The transmission of the objective lens was specified to $\sim 80\,\%$ in the range from $400 - 700\,\mathrm{nm}$. The specified power values were corrected according to this transmission coefficient. The excitation power of the widefield illumination was measured by placing the sensor of a power meter after the lens L_4.

2.3 Confocal and high resolution imaging

Confocal and high resolution imaging was performed on a 1C RESOLFT QUAD Scanning microscope (Abberior Instruments, Göttingen, Germany) modified for additional point illumination with a $355\,\mathrm{nm}$ laser line. The microscope featured an IX83 microscope stand (Olympus Deutschland GmbH, Hamburg, Germany), wide field illumination with halogen lamps, beam scanning by four galvanometer-driven mirrors (QUAD scanner), focused excitation with laser lines at $355\,\mathrm{nm}$, $405\,\mathrm{nm}$ and $488\,\mathrm{nm}$ wavelengths, generation of a doughnut-shaped beam at $488\,\mathrm{nm}$ wavelength using a spatial light modulator (SLM), examination of the excitation PSFs with a PMT and fluorescence detection with an avalanche photo-diode. Experimental control and data acquisition was performed by the supplied software Inspector. All

measurements were performed using a $100\times$ oil-immersion objective lens with 1.4 NA (UPLSAPO 100XO, Olympus Deutschland GmbH, Hamburg, Germany) and a confocal pinhole with a diameter of one Airy unit.

Line profiles on the acquired images were performed with the Fiji software package (http://imagej.net/Fiji)[106]. The obtained intensity profiles were transferred to the software Origin (OriginLab, Northhampton, MA, USA) and the data was subsequently fitted with the built-in Lorentzian peak function.

2.4 Specification of light intensities

It is assumed that focusing a collimated beam produces a spot with a Gaussian intensity distribution given by

$$I(r) = I_0 \exp\left(-4\ln(2)\left(\frac{r}{\text{FWHM}}\right)^2\right) \tag{2.1}$$

with the FWHM of the Gaussian profile of the spot and the peak intensity in the center of the spot I_0 given by

$$I_0 = \frac{4}{\pi}\ln(2)\frac{P}{\text{FWHM}^2}. \tag{2.2}$$

Here, P indicates the measured power of the incident light. All light intensities given in this thesis refer to a calculated equivalent intensity of a Gaussian beam profile $I_{\text{equi,Gauss}}$. For the equivalent intensity it was assumed that the total incident power gets uniformly distributed in an area where the intensity is at least half of the peak intensity I_0, termed equivalent area. The FWHMs of the PSFs generated by the different light sources were determined experimentally by utilizing the reflection of gold nanoparticles (see section 2.2) for the focused excitations and the emission of a thin fluorescent layer (see subsection 2.6.1) for the widefield excitations. The equivalent intensities were then calculated according to

$$I_{\text{equi,Gauss}} = \frac{P}{\pi\,\text{FWHM}^2/4} = \frac{I_0}{\ln(2)}. \tag{2.3}$$

In case of the doughnut-shaped off-switching beam of the 1C RESOLFT QUAD Scanning microscope, the light intensities were estimated comparing the equivalent areas of a doughnut-shaped beam and a Gaussian-shaped beam generated by the same laser power. Due to the larger area of the doughnut-shaped beam, its equivalent intensity is given by:

$$I_{\text{equi,doughnut}} \approx \frac{P}{2.72 \cdot \pi \, \text{FWHM}^2/4} = \frac{I_{\text{equi,Gauss}}}{2.72} \tag{2.4}$$

2.5 Fluorescence lifetime analysis

The fluorescence lifetime data from the experimental setups described in sections 2.1 and 2.2 was analyzed to determine the characteristic lifetimes. The lifetimes were obtained by nonlinear least squares fitting of the fluorescence decay curve using custom-written routines for MATLAB (The MathWorks, Natick, MA, USA) based on the work of Enderlein and Erdmann[107]. This consisted of an initial estimation of decay times and subsequent fitting. The variable number of decay times were treated as free parameters, whereas the corresponding amplitudes were implicitly determined by linear least squares decomposition of the signal into the model functions (exponential decays) convoluted with the IRF.

To ensure a robust determination of the fluorescence lifetimes, five measurements per sample were performed and analyzed with the above described fitting routine, followed by averaging of the obtained values for the lifetimes and the amplitudes.

2.6 Sample preparation

Different types of photoswitchable fluorescent molecules were investigated using various types of sample preparations. The specific preparation methods were selected according to the respective molecule properties.

2.6.1 *E. coli* expressing fluorescent proteins

An appropriate method to investigate GFP-based photoswitchable fluorescent proteins is to express these proteins inside a culturable organism like *E. coli*. By introducing a plasmid, encoding the sequence for a specific protein cloned into the high-copy expression vector pQE31 (Qiagen, Hilden, Germany) into the cytosol of

these organisms, it is possible to obtain highly concentrated proteins in a cellular environment.

Direct observation of protein properties present inside the cytosol of *E. coli* was accomplished by immobilizing the bacteria in agarose gel (2 %) on standard coverslips (20 mm × 20 mm, #1.5) mounted to an object slide.

Alternatively, the expressed proteins could be purified by Ni-NTA (nickel-nitrilotriacetic acid) affinity chromatography (His SpinTrap, GE Healthcare, Freiburg, Germany), concentrated by ultrafiltration and taken up in 100 mM Tris-HCl, 150 mM NaCl, pH 7.5 buffer solution. The purified proteins were immobilized in thin PAA (polyacrylamide) gel layers on standard coverslips mounted to an object slide.

The preparation of *E. coli* cultures and the protein purification were kindly carried out by Sylvia Löbermann (Max Planck Institute for Biophysical Chemistry, Göttingen, Germany).

2.6.2 Preparation of liposomes

The examination of different hydrophobic, photochromic compounds under conditions present in a confocal microscope (excitation intensities $\geq 1\,\mathrm{kW/cm^2}$ and highly sensitive detection) was accomplished by preparing liposomes consisting of synthetic phospholipid derivatives. These spherical vesicles exhibit at least one lipid bilayer, offering a spatially restricted volume for lipophilic compounds, enclosing a volume of aqueous solution [108].

The synthetic phospholipid 1,2-dioleoyl-sn-glycero-3-phosphocholine (DOPC, Avanti Polar Lipids, Alabaster, AL, USA) was solved in 2:1 chloroform/methanol (v/v) to a lipid concentration of 10 mg/ml. The desired compound was solved in methanol $(1-5\,\mathrm{\mu M})$ and added to the lipid stock solution. Afterwards the solvent was evaporated under continuous nitrogen flow. The liposomes self-assemble after adding PBS (phosphate-buffered saline, pH 7.4) and mixing the solution for several minutes. This can be visually inspected since the solution becomes turbid during the process due to the dispersion of the newly formed liposomes. As the average diameter of these liposomes is many times larger than the spatial extent of a diffraction-limited PSF, their size needed to be reduced. Therefore the liposome solution was treated with a tip sonifier (450 Sonifier, Branson Ultrasonics, Danbury, CT, USA) leading to the rupture of large liposomes and formation of smaller liposomes with a diameter of 200 nm to several µm.

A volume of 10 µl of this liposome solution was placed under a standard coverslip

(20 mm × 20 mm, #1.5) on an object slide, both previously cleaned with ethanol and nitrogen flow, and sealed with addition-curing silicone (Picodent twinsil, Picodent, Wipperfuerth, Germany). After 30 minutes the majority of vesicles did not show movement any more due to adsorption to the glass surface.

2.6.3 Immunofluorescence labeling of cells

The following protocol was used to label specific structures of interest in cultured Vero cells. The stainings were prepared by Ellen Rothermel (Max Planck Institute for Biophysical Chemistry, Göttingen, Germany).

The cells were grown on standard cover slips (# 1.5) with 18 mm diameter in DMEM (Dulbecco's Modified Eagle Medium). To stain cytoskeletal proteins (Tubulin and Vimentin) the cells were fixed by placing them for five minutes in previously cooled (−20 °C) methanol. For the labeling of membrane associated proteins (NUP153), the fixation was performed by placing the cells in 8 % PFA (paraformaldehyde) at 37 °C for five minutes, followed by a permeabilization step in 0.5 % Triton X-100 (Sigma-Aldrich, St. Louis, Missouri, USA) for five minutes. Afterwards they were washed and unspecific binding cites were blocked by applying a 2 % BSA (Bovine serum albumin) in PBS solution (pH 7.4) three times for five minutes. Then 100 µl of the selected primary antibody, diluted 1:100 or 1:200 (depending on the antibody) in 2 % BSA in PBS was applied to each cover slip for one hour in a moist chamber followed by three washing steps with 2 % BSA in PBS. Then 100 µl of the selected secondary antibody, diluted depending on the concentration of the lot used, was also applied for one hour in a moist chamber. After one washing step of five minutes with 2 % BSA in PBS and two five-minutes washing steps with PBS, the cover slips were kept in PBS.

For imaging, the cover slips were placed on an object slide with cavity filled with 30 µl PBS and sealed with silicone.

Primary antibodies against α-Tubulin (T6074, Sigma-Aldrich, St. Louis, Missouri, USA), Vimentin (V6389, Sigma-Aldrich, St. Louis, Missouri, USA) and NUP153 (ab24700, Abcam, Cambridge, UK) were used.

3 Results

In this chapter, the results of this study are presented as follows: The reversibly photoswitchable fluorescent proteins rsEGFP and rsEGFP2 were investigated in detail concerning their photophysical properties, shown in section 3.1. Furthermore, new photoswitchable fluorophores based on diarylethenes were examined with respect to their potential utilization in high resolution microscopy as exhibited in section 3.2 while section 3.3 shows their successful application in RESOLFT nanoscopy with fixed immunostained mammalian cells in aqueous solution without any further additives.
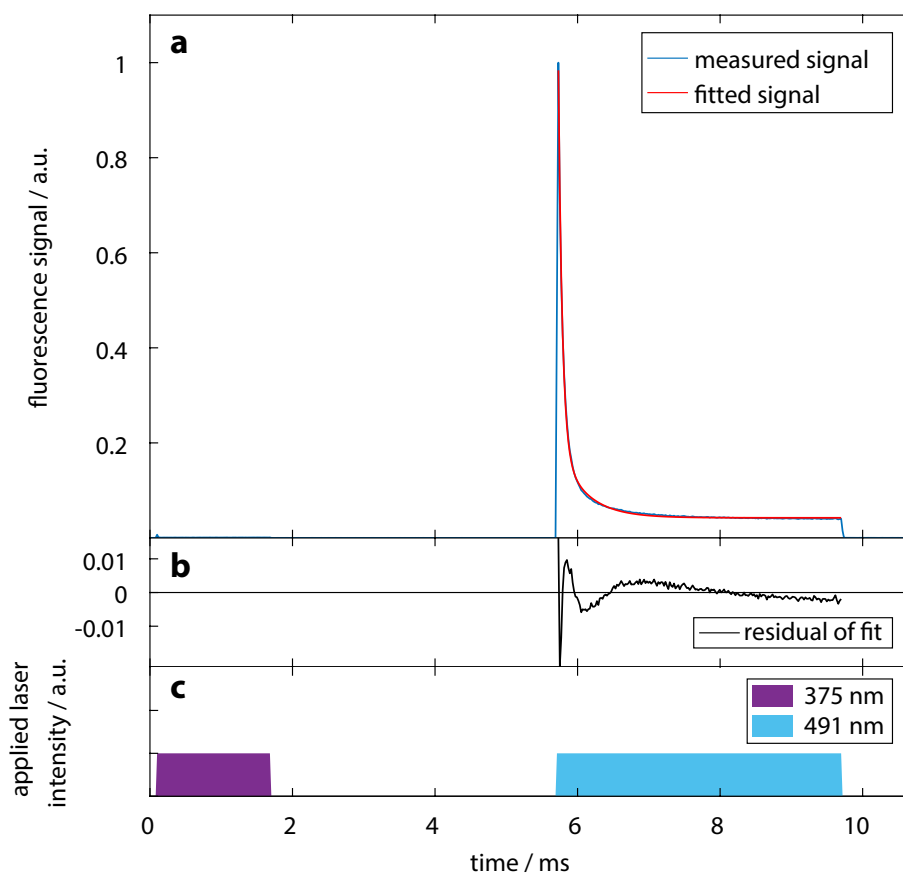
3.1 Reversibly photoswitchable fluorescent proteins

The confocal screening setup described in section 2.2 was used to examine the photophysical properties of the photoswitchable fluorescent proteins rsEGFP and rsEGFP2 to analyze its applicability for the characterization of photoswitchable labels. These two photoswitchable proteins were already successfully applied in high resolution imaging based on the RESOLFT concept. Their characteristics for RESOLFT are well documented and can therefore be used as a reference for comparison [37,39,62]. The typical characteristics for labels used in RESOLFT were investigated. According to the emission spectrum of the mentioned proteins (emission maxima at $510\,\mathrm{nm}$ and $503\,\mathrm{nm}$, respectively), BrightLine® 525/50 (Semrock, Rochester, NY, USA) filters were placed in front of the detectors (F_5, Figure 2.2).

3.1.1 Typical measurement scheme

The general approach to study the behavior of a photoswitchable fluorescent label upon photoexcitation is guided by the RESOLFT principle (see section 1.5). The preparation of a spatially distinct area which is smaller than the diffraction limit and capable of emitting fluorescence is the result of a two-step process of light-induced activation and deactivation. Accordingly, the typical characterization scheme for

Figure 3.1: Typical measurement scheme for a photoswitchable fluorescent label used in RESOLFT nanoscopy. **a:** Measured fluorescence signal (blue solid line) and a biexponential fit (red solid line) to the fluorescence decay caused by illumination with blue light (491 nm at $10\,\mathrm{kW/cm^2}$). **b:** Corresponding residual of the biexponential fit. **c:** Illustration of the illumination cycles with the different laser pulses. The data shows a measurement of rsEGFP2 in the cytosol of *E. coli* fixed on agarose as mean over 500 switching cycles.

RESOLFT labels consists of these two processes and optional pauses in between the light pulses as shown in Figure 3.1.

Prior to the actual measurement, the region of interest should be prepared such that all molecules are in a defined state, either non-fluorescent or fluorescent, to always achieve same initial parameters. In case of the examined RSFPs, the wavelength λ_{act} to convert the molecules to their fluorescent state is in the ultraviolet range. It exhibits a higher probability to photobleach the molecules than the excitation wavelength λ_{exc}. It is therefore advisable to prepare the molecules in their non-fluorescent form by illumination with the excitation light before the measurement to minimize the photobleaching. This initialization step is followed by a repeated pulse sequence pattern consisting of a UV pulse, an illumination break, an excitation/off-switching

pulse and another optional illumination break. A dark time interval in between the light pulses is required for the fluorophores that dwell in a transition state before complete isomerization to the fluorescent form. The chosen pulse pattern is applied consecutively to the observation area. Figure 3.1 exemplifies the resulting fluorescence signal as mean of 500 on/off-switching cycles. The molecules show no or only little fluorescence during the illumination with $\lambda_{\mathrm{act}} = 375\,\mathrm{nm}$ light (depending on the applied intensity I_{act}). The illumination with the excitation light at $\lambda_{\mathrm{exc}} = 491\,\mathrm{nm}$ causes the molecules to emit fluorescence and, concurrently, their isomerization to the non-fluorescent state evident from the decay of the fluorescence signal. Variations of the following parameters

(1) activation duration t_{act},

(2) activation intensity I_{act},

(3) duration of the illumination break t_{break},

(4) excitation duration t_{exc},

(5) excitation intensity I_{exc} and

(6) duration of the illumination break after excitation t_{wait}

can be used to reveal the switching characteristics of the molecules. The fluorescence decay during off-switching is modeled by a linear combination of several exponential decay functions:

$$I_{\mathrm{fl}}(t) = I_{\mathrm{fl,back}} + \sum_i A_i \exp(t/\tau_i) \tag{3.1}$$

with the fluorescence intensity $I_{\mathrm{fl}}(t)$ at time t, the residual fluorescence after off-switching $I_{\mathrm{fl,back}}$ and the characteristic decay times τ_i with their associated amplitudes of the total signal A_i. The fit provides information about the underlying molecular mechanisms, since it can further indicate the number of intermediate states involved in the off-switching, depending on the number of exponential decays needed to describe the off-switching curve properly. Direct evaluation of the fitted decay curve yields specific parameters of the studied fluorophore. These include the total characteristic decay time τ_{off} where the initial fluorescence value drops to $1/e$ and the relative residual fluorescence after off-switching (ratio of the fluorescence signal at the end of the illumination pulse and the initial fluorescence signal).

3.1.2 Different illumination methods

The ensemble switching kinetics of a fluorophore can depend on the applied light intensity distribution. Therefore, the two different illumination methods, confocal point illumination and detection, termed the confocal mode, and widefield illumination with point detection, termed the widefield mode, were compared using thin samples of the above mentioned proteins embedded in a polyacrylamide matrix (see subsection 2.6.1). These samples showed a layer thickness of about 700 nm. To achieve similar conditions, the measurements were performed at the same location in the sample for both illumination methods. To achieve this, the pulse pattern was modified such that one switching cycle consisted of four pulses: widefield activation, widefield off-switching, focused activation and focused off-switching including the aforementioned illumination breaks. The intensities and durations of the activation pulses were chosen such that all molecules in the observation area were switched to the fluorescent state. The on-switching illumination parameters were determined in a separate experiment previously. The intensities of the off-switching pulses were chosen such that the characteristic decay time τ_{off} (decay of the fluorescence to $1/e$ of the initial value) was identical for both illumination methods. The applied peak intensities were $I_{\mathrm{exc,WF}} \cong 1\,\mathrm{kW/cm^2}$ in the widefield mode and $I_{\mathrm{exc,CF}} \cong 2\,\mathrm{kW/cm^2}$ in the confocal mode.
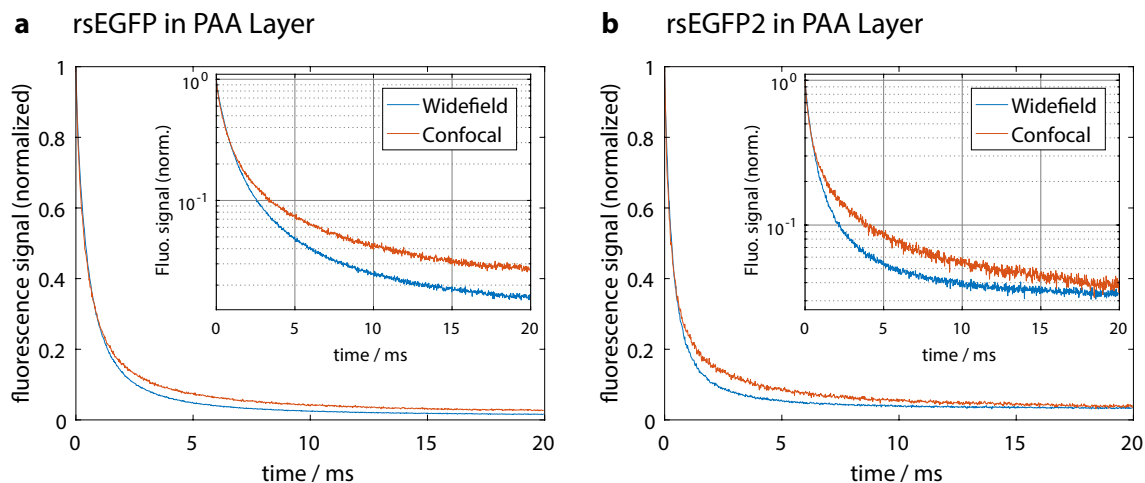
Figure 3.2: Normalized off-switching curves upon illumination with blue light (widefield mode: 491 nm, confocal mode: 488 nm) of the photoswitchable proteins rsEGFP (**a**) and rsEGFP2 (**b**) embedded in a thin layer of polyacrylamide (PAA) in widefield (blue) and confocal (orange) mode. The insets show the data on a logarithmic scale.

Using point illumination, the fluorophores contributing to the fluorescence signal are exposed to a range of illumination intensities, depending on their relative position to the focus. This leads to a superposition of varying off-switching rates as these rates scale with the local intensity. This alters the shape of the observed fluorescence decay, depending on the intensity distribution in the diffraction-limited spot and the local fluorophore density. This also affects the detectable background level because the outer part of the focused excitation volume exhibits a low intensity which leads to a significantly prolonged time to reach this level. Therefore, in the confocal mode, two times the peak intensity was needed to obtain the same characteristic decay time as in the widefield mode. Figure 3.2 compares both illumination methods for rsEGFP and rsEGFP2. It is clearly visible that for both fluorophores the decay curves for the confocal and widefield modes split after reaching about $1/e$ of the initial fluorescence value due to a slower decay in the periphery of the point illumination. At the illumination intensities and times used in this experiment, rsEGFP showed 60 % and rsEGFP2 11 % higher background level after 20 ms compared to the widefield illumination.

These findings show that the widefield illumination, by providing a homogeneous illumination of the complete detection volume, allows a distortion-free measurement of the switching kinetics. For this reason, all following measurements were carried out with the widefield illumination.

3.1.3 Switching fatigue

Different photobleaching mechanisms during the on- and off-switching steps cause a decrease of the detected photons during excitation. Accordingly, the switching fatigue of a fluorescent label is probably the most important factor regarding repeated observation of dynamic processes. Moreover, a minimal number of switching cycles is needed to achieve a notable resolution improvement (see subsection 1.5.1).

The number of photoswitching cycles a fluorescent label is able to perform can be determined by repeated illumination of an immobile molecule population with the measurement scheme outlined in subsection 3.1.1. Figure 3.3 shows the fluorescence decrease of rsEGFP and rsEGFP2 in the cytosol of *E. coli* upon repeated photoswitching. For both proteins the same illumination parameters were applied. Switching with $\lambda_{\mathrm{act}} = 375\,\mathrm{nm}$ for $1.5\,\mathrm{ms}$ at $0.1\,\mathrm{kW/cm^2}$ to the fluorescent state and, after a pause of $2\,\mathrm{ms}$, excitation/off-switching with $\lambda_{\mathrm{exc}} = 491\,\mathrm{nm}$ for $20\,\mathrm{ms}$ at $2\,\mathrm{kW/cm^2}$ to reliably reach the background level. The fluorescence is given as the
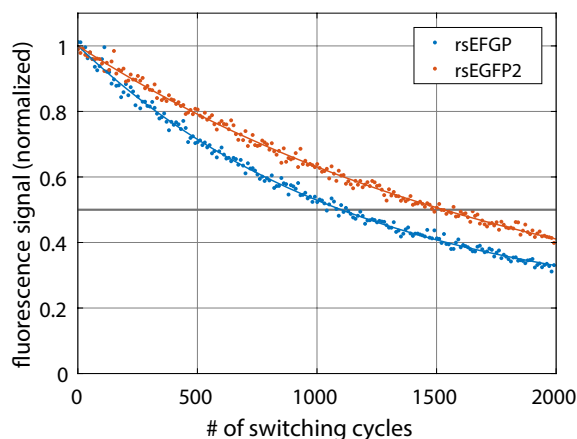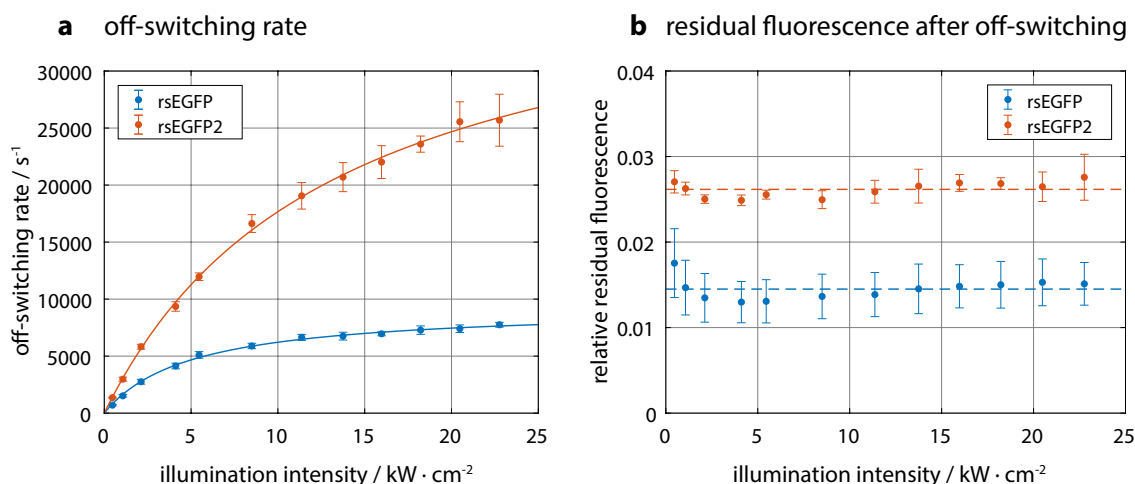
Figure 3.3: Switching fatigue of rsEGFP (blue) and rsEGFP2 (orange) present in the cytosol of *E. coli* fixed on agarose gel. Alternate illumination at $375\,\text{nm}$ $(0.1\,\text{kW/cm}^2$ for $1.5\,\text{ms})$ and $491\,\text{nm}$ $(2\,\text{kW/cm}^2$ for $20\,\text{ms})$ with the above described widefield excitations were used for the photoswitching. Data points (fluorescence during illumination with $491\,\text{nm}$ light as mean of 10 consecutive switching cycles) were fitted with monoexponential decays including an offset (solid lines).

integrated signal during the excitation pulse and normalized to the initial value of the first cycle. Fitting with a monoexponential decay with an offset revealed that under these conditions rsEGFP performed ~ 1100 and rsEGFP2 ~ 1550 cycles until half of the initial fluorophores were bleached.

3.1.4 Switching kinetics at different illumination intensities

The off-switching kinetic of a fluorophore is directly coupled to the applied light intensity. Careful investigation of this dependence allows to choose optimal conditions for photoswitching in RESOLFT nanoscopy.

To measure the off-switching kinetics, the measurement scheme was adjusted such that 12 excitation pulses with increasing intensities were applied after a corresponding activation pulse. This pulse pattern was repeated 20 times at 25 different positions in the sample for each protein. During the 20 repetitions of the pulse pattern no significant photobleaching was observed. The illumination times t_{exc} were chosen such that for all different excitation intensities the same light dose ($I_{\text{exc}} \times t_{\text{exc}}$) was applied to the sample. Consequently, the excitation times were extended for lower excitation intensities. The excitation pulse with the highest available intensity ($I_{\text{exc,max}} = 23\,\text{kW/cm}^2$) was set as the reference point. The illumination times t_{exc} for this pulse were set to $10\,\text{ms}$ for rsEGFP and $5\,\text{ms}$ for rsEGFP2. These times were chosen to ensure that the final background level of the respective fluorophore was

Figure 3.4: Intensity-dependent off-switching rate and relative residual fluorescence of rsEGFP and rsEGFP2. **a:** Off-switching rate of rsEGFP (blue) and rsEGFP2 (orange) as a function of illumination intensity. Solid lines show a fit to the data according to the model shown in Figure 3.5 and described in Equation 3.3. **b:** Residual fluorescence after off-switching of rsEGFP (blue) and rsEGFP2 (orange) as a function of illumination intensity. Dashed lines show the mean value of the residual fluorescence for different intensities. Illumination times were chosen such that the applied light dose was kept constant for different illumination intensities. All data were recorded in *E. coli* fixed on agarose gel expressing the respective protein in the cytosol. Error bars represent twice the standard deviation.

reached at all intensities. This resulted in light doses of $230\,\text{J/cm}^2$ per off-switching step for rsEGFP and $115\,\text{J/cm}^2$ for rsEGFP2.

Figure 3.4a shows the off-switching rates of rsEGFP and rsEGFP2 upon illumination with different intensities. The off-switching rate is defined as the reciprocal value of the total characteristic decay time τ_{off}. τ_{off} was extracted from the biexponential fits to the particular decay curves. The biexponential fit was chosen because a monoexponential fit did not describe the data properly. The applied intensities were varied from 0.5 to $23\,\text{kW/cm}^2$. Up to $2\,\text{kW/cm}^2$, the off-switching rate scales linearly with the intensity for both proteins. This behavior was verified in additional experiments with different intensities in the range from $40\,\text{W/cm}^2$ to $1.8\,\text{kW/cm}^2$ (Figure A.1). Above $5\,\text{kW/cm}^2$, rsEGFP switched off only slightly faster, reaching a maximal off-switching rate of about $7500/\text{s}$ ($\tau_{\text{off}} \cong 133\,\mu\text{s}$). rsEGFP2, however, exhibits a steeper increase up to a maximal rate of about $26\,000/\text{s}$ ($\tau_{\text{off}} \cong 39\,\mu\text{s}$).

As the maximal detected fluorescence in each excitation pulse increases linearly with the applied light intensity for both proteins (Figure A.2), the saturation of the off-switching rate cannot be explained by a single fluorescent state but indicates a
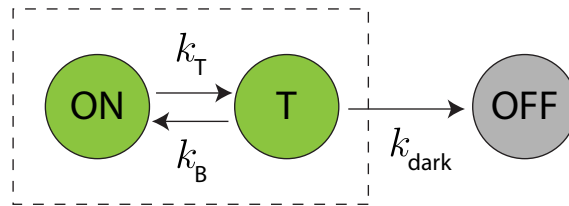
Figure 3.5: Three state model to describe the off-switching behavior of rsEGFP and rsEGFP2 upon illumination with increasing light intensities. The transition rate k_T is light driven, whereas k_B and k_{dark} are constant. The ON-state and the transient state T are fluorescent. The OFF-state is non-fluorescent. Possible transitions between the states are indicated by the arrows.

saturable transient fluorescent state before the proteins switch to the non-fluorescent state. A scheme of such a simple model is shown in Figure 3.5. This model is based on the assumption that the molecules in the fluorescent ON-state reach a fluorescent transition state T with a rate k_T linearly depending on the illumination intensity I_{exc} of the excitation light. This transition state shows a constant rate k_B back to the initial ON-state and a constant rate k_{dark} to the non-fluorescent OFF-state. Since no return rate from the OFF-state to the two fluorescent states is assumed, the model can be simplified to a two state system. The populations P in the ON- and T-state can then be described as

$$\dot{P}_{ON}(t) = -k_T P_{ON}(t) + k_B P_T(t)$$
$$\dot{P}_T(t) = k_T P_{ON}(t) + (-k_B - k_{dark}) P_T(t). \tag{3.2}$$

Solving this system of differential equations leads to the experimentally observable off-switching rate

$$k(I_{exc}) = \frac{I_{exc}/I_{1/2}}{1 + I_{exc}/I_{1/2}} \cdot k_{dark} \tag{3.3}$$

depending on the illumination intensity I_{exc}, the maximal possible off-switching rate k_{dark} and the intensity $I_{1/2}$ where k represents half of k_{dark}. The detailed derivation of this model is presented in section A.1. This description for the intensity-dependent off-switching rate k can be fitted with good agreement to the acquired data sets as shown in Figure 3.4a, resulting in $I_{1/2} \cong 5\,\text{kW/cm}^2$ for rsEGFP and $I_{1/2} \cong 13\,\text{kW/cm}^2$ for rsEGFP2.

Another interesting characteristic is the dependence of the background level of fluorescence after the off-switching process on the applied intensity. It is obvious that due to increasing off-switching rates at higher intensities, equal illumination times

t_{exc} would lead to different background levels. By keeping the light dose constant throughout the measurement, this factor was canceled out. Figure 3.4b shows the dependence of the residual fluorescence after off-switching on the illumination intensity. For both proteins, the residual fluorescence shows no significant changes and is around 1.5 % of the maximal signal per switching cycle for rsEGFP and 2.6 % for rsEGPF2. This reveals that for these proteins the achievable residual fluorescence only depends on the applied light dose but not on the illumination intensity.

3.1.5 Fluorescence lifetime

The fluorescence lifetime is a key property of a fluorophore and can give information about its chemical environment. In case of fluorescent proteins this mainly represents the direct neighborhood of the chromophore.
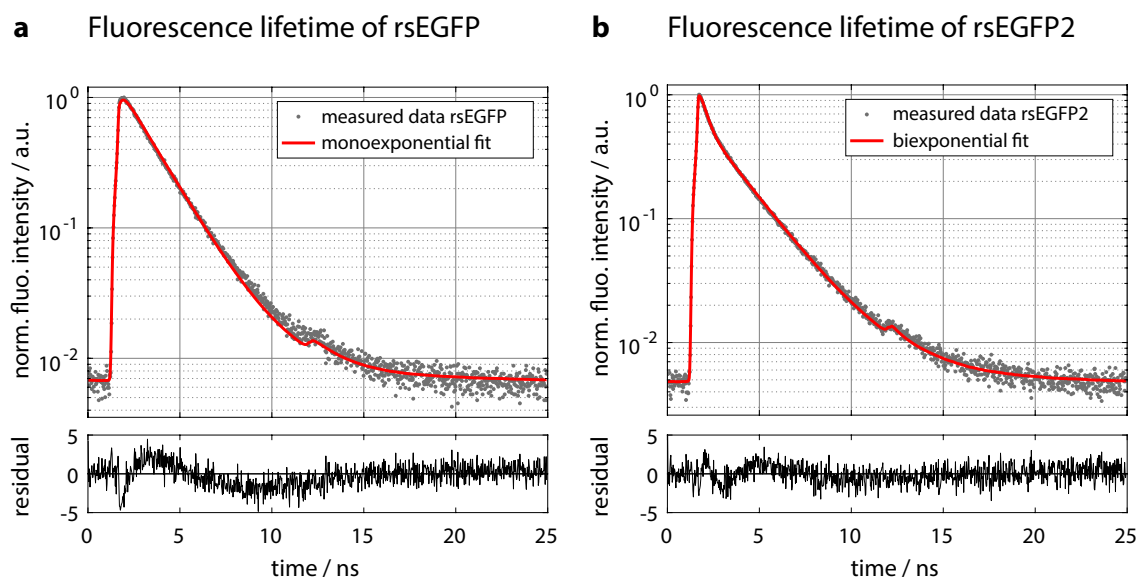
Figure 3.6: Fluorescence lifetime of rsEGFP (**a**) and rsEGFP2 (**b**) measured in *E. coli* fixed on agarose gel. Grey dots show the normalized measured data and red lines exponential fits. The monoexponential fit resulted in a fluorescence lifetime of $\tau = 1.8\,\mathrm{ns}$ for rsEGFP and the biexponential fit yielded the two fluorescence lifetimes $\tau_1 = 0.3\,\mathrm{ns}$ and $\tau_2 = 2.3\,\mathrm{ns}$ (amplitude ratios: $A_1 = 0.18$, $A_2 = 0.82$) for rsEGFP2. The minor peak in the data and in the fit at 12 ns originates from an additional peak in the IRF.

Figure 3.6 shows typical lifetime measurements of rsEGFP and rsEGFP2 in the cytosol of *E. coli*. The data was recorded using focused excitation at $\lambda_{\mathrm{exc}} = 488\,\mathrm{nm}$ with the supercontinuum source described in section 2.2 with 120 ps FWHM of the

IRF. The acquisition was performed on a fixed spot in the sample over an integration time of 30 seconds and adjusting the count rate per detector to $\sim 5 \times 10^5$ cps. The described fitting routine (see section 2.5) was applied to the data yielding a lifetime of $\tau = 1.8$ ns for rsEGFP and the lifetimes $\tau_1 = 0.3$ ns and $\tau_2 = 2.3$ ns with the amplitude ratios $A_1 = 0.18$ and $A_2 = 0.82$ for rsEGFP2. Control measurements of the organic fluorophores fluorescein, rhodamine B and *Alexa Fluor 488* (Thermo Fisher Scientific) in solution (PBS, pH 7.5) yielded previously reported values of 4 ns, 1.7 ns and 4 ns, respectively [27].

Summary

The microscope described in this work is capable of determining the key parameters of reversibly photoswitchable fluorescent labels. It was shown that a focused excitation alters the observable off-switching kinetic of a fluorophore ensemble. A homogeneous widefield illumination provided unbiased values and new insight on the intensity-dependent off-switching behavior of rsEGFP and rsEGFP2 was gained. A three-state model was presented to account for the observed saturation of the off-switching rate with increasing excitation intensity. This model can be applied to estimate the intensities used for the off-switching step in RESOLFT nanoscopy.

## 3.2 Synthetic photoswitchable fluorophores without linker

This section describes the investigation of the photophysical properties of diaryl-ethene-based reversibly photoswitchable fluorescent compounds under conditions present in a confocal microscope. The model fluorophores were hydrophobic and did not have any linker for coupling to a biomolecule/antibody. Therefore, a special sample preparation was required in order to prevent diffusion of the molecules out of the observation area while sustaining the ability to photoswitch and fluoresce. The latter prerequisite turned out to be a challenging task, as established methods to restrict diffusion, like embedding the fluorophores in thin layers of transparent polymers (e.g. polyvinyl alcohol)[109,110], did not sufficiently immobilize the fluorophores or suppressed their fluorescence. A successful approach was to prepare artificial liposomes that offered an environment in which the switching and fluorescence properties of the hydrophobic fluorophores were preserved. Liposomes were selected because the molecular switch of diarylethenes is inherently hydrophobic. The lipid membrane of liposomes offers a hydrophobic environment for the fluorophores to associate with.

3.2.1 Methylated diarylethene

The first reversibly photoswitchable synthetic fluorophore investigated in this work was a methylated diarylethene (*me*DAE), shown in Figure 3.7. The compound was synthesized and provided by Dr. Heydar Shojaei (Max Planck Institute for Biophysical Chemistry, Göttingen, Germany). The photoswitching unit of the fluorophore is an integral part of its chromophore. The symmetric diarylethene core structure 1,2-bis(2-methyl-1-benzothiophene-1,1-dioxide-3-yl)perfluorocyclopentene was decorated with a p-methoxyphenyl group at the C6 position and a methyl group at the C6′ position. The compound showed very low solubility in water, but was soluble in organic solvents. As described in section 1.7, the fluorescent closed form (CF) of *me*DAE is formed by a cyclization reaction induced by irradiation with UV light. The non-fluorescent open form (OF) is obtained by irradiating the closed form with visible light. Figure 3.8 shows the absorption spectra of the non-fluorescent open ring isomer, the fluorescent closed form and the emission spectra of the closed form dissolved in methanol. The absorption maximum of the open form is found at 312 nm and the absorption maximum of the closed form at 451 nm. The fluorescence
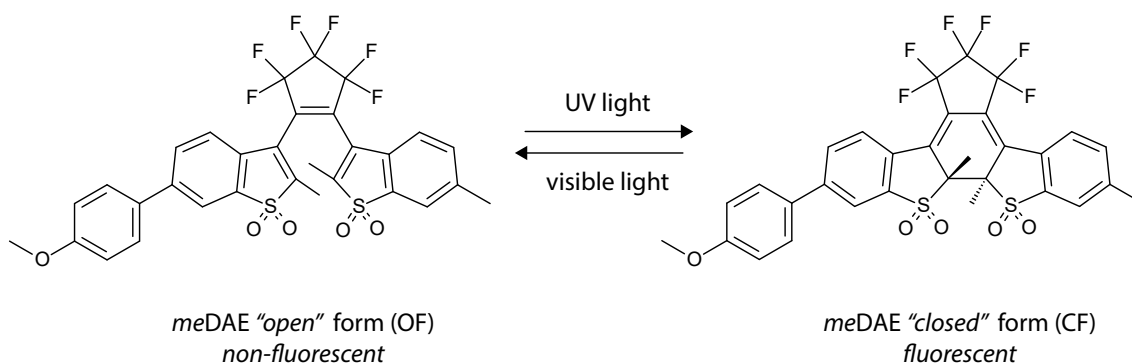
Figure 3.7: Structure of *me*DAE in its open (OF) and closed forms (CF). The open from is non-fluorescent and can be transformed to the closed fluorescent form by illumination with UV light. The closed form emits red fluorescence upon illumination with blue light and is transformed back to the open form with visible light. The fluorophore was synthesized and provided by Dr. Heydar Shojaei.
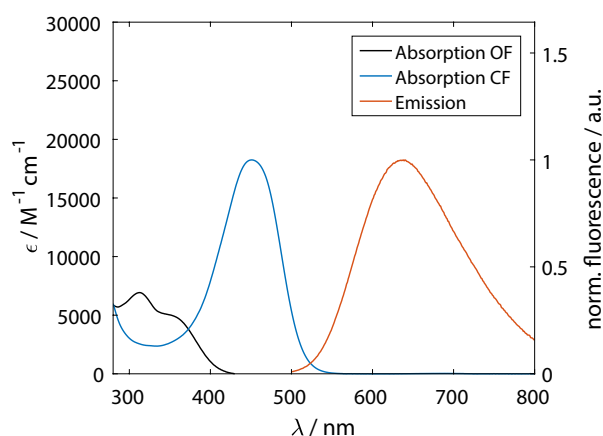
Figure 3.8: Absorption and emission spectra of *me*DAE in methanol. Absorption coefficients (ϵ) of the open (black line) and the closed (blue line) form are given on the left axis. Fluorescence of the closed form upon excitation with $\lambda_{\mathrm{exc}} = 450\,\mathrm{nm}$ (orange line) is given in arbitrary units on the right axis.

maximum was situated at $634\,\mathrm{nm}$, resulting in a large Stokes shift of $183\,\mathrm{nm}$. The filters F_5 (Figure 2.2) in front of the detectors were adjusted to BrightLine® 624/40 (Semrock, Rochester, NY, USA) to match the emission of the fluorophore. Samples were prepared as described in subsection 2.6.2. The liposomes were highly fluorescent and showed a large variation in diameter ranging from $200\,\mathrm{nm}$ up to several µm. Small single liposomes with a diameter below $250\,\mathrm{nm}$ were first selected in a coarse widefield search and then precisely positioned in the confocal detection volume in all three dimensions by maximizing the detected fluorescence signal. For

this purpose, a weak focused excitation with $\lambda_{\mathrm{exc}} = 488\,\mathrm{nm}$ at intensities around $30\,\mathrm{W/cm^2}$ was used. The wavelength of $\lambda_{\mathrm{exc}} = 488\,\mathrm{nm}$ was chosen for the excitation because most light sources for confocal and high resolution microscopy are in this spectral region. Although the maximum absorption of the closed isomer is at 451 nm, the absorption at 488 nm still reached 55 % of the maximal value.

Fluorescence pump-probe measurements

Following the approach described in subsection 3.1.1 to examine reversible photo-switchable labels, the liposomes were illuminated with alternating light pulses of UV (375 nm) and blue (491 nm) light by the widefield illuminations described in section 2.2.
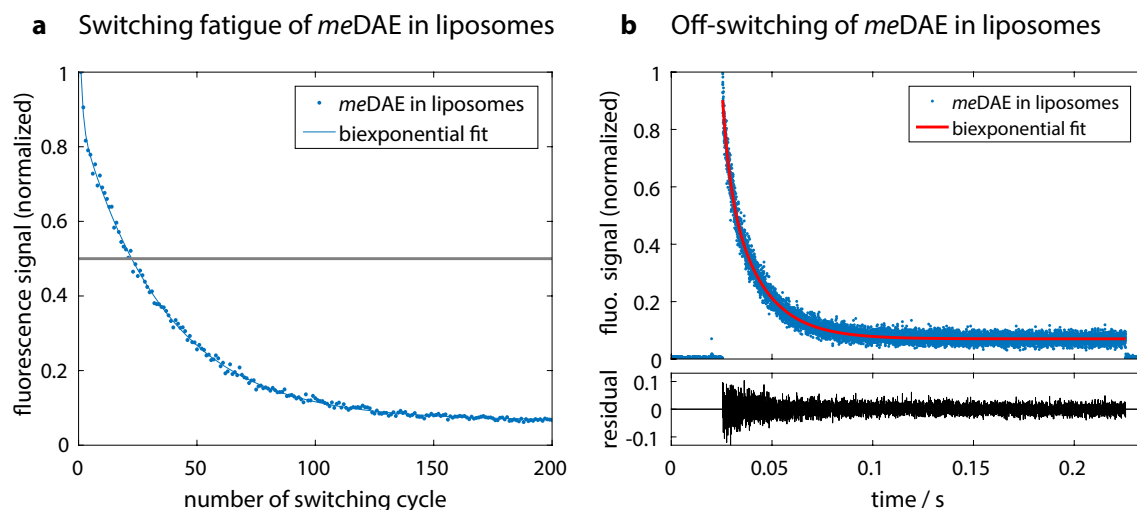

Figure 3.9: Switching fatigue and off-switching behavior of *me*DAE in liposomes. **a:** Switching fatigue of *me*DAE in liposomes. Alternate illumination at 375 nm and 491 nm with the widefield excitations described in section 2.2 were used for photo-switching. Data points (fluorescence during illumination with 491 nm light) were fitted with a biexponential decay (solid line). **b:** Fluorescence decay of *me*DAE in liposomes due to illumination with 491 nm light as mean of the first 30 switching cycles. A biexponential decay was fitted to the data (red solid line). The corresponding residual is shown in the lower graph.

Figure 3.9a shows the switching fatigue of *me*DAE upon repeated photoswitching. For the photoactivation, light intensities of $30\,\mathrm{W/cm^2}$ at 375 nm were applied for 0.5 ms. These parameters were determined in a preceding experiment and ensured that almost all molecules in the observation area were switched to the fluorescent form. Off-switching was achieved by illumination with 491 nm light for 200 ms at

$7\,\mathrm{kW/cm^2}$. To examine the bleaching behavior, the signal during illumination with the 491 nm light was integrated for each cycle and the resulting data was normalized to the first cycle. The fluorescence signal decreased to half of the initial value after about 22 cycles. A biexponential fit was used to describe the data. The short component was only used to fit the first few data points, indicating a different bleaching/fading process in the beginning of the experiment.

Figure 3.9b shows the corresponding fluorescence signal of the described illumination pattern as an average of the first 30 switching cycles. The data was fitted with a biexponential function with time constants $\tau_1 = 3.7\,\mathrm{ms}$ and $\tau_2 = 18.7\,\mathrm{ms}$ and amplitude ratios $A_1 = 35\,\%$ and $A_2 = 65\,\%$. The $1/e$ decay time was determined to be 12.4 ms. The residual fluorescence after off-switching was determined to be 6.8 % of the initial value.
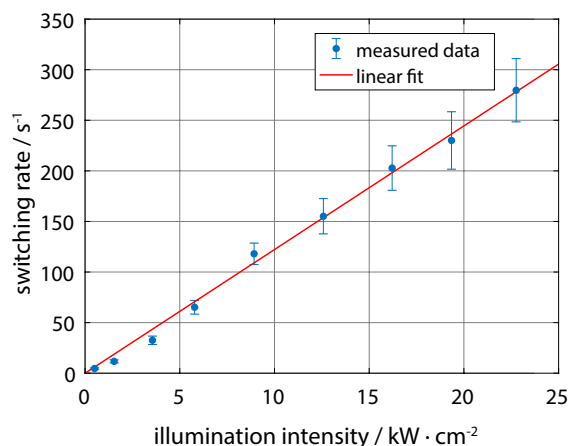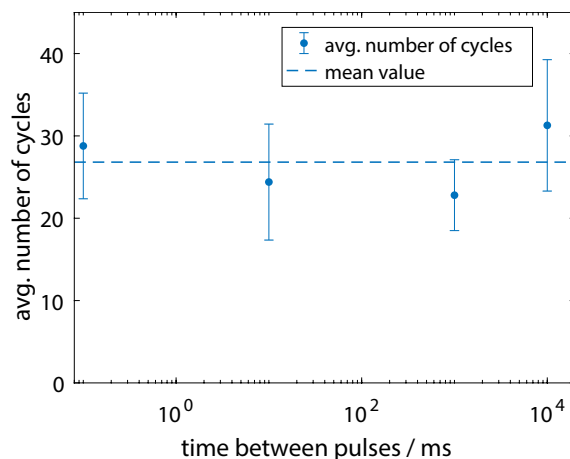

Figure 3.10: Off-switching rate of meDAE in liposomes as a function of illumination intensity. Solid red line shows a linear fit to the data. Error bars represent twice the standard deviation.

The rather low illumination intensity for the off-switching was chosen because the number of achievable switching cycles severely decreased for intensities above 10 $\mathrm{kW/cm^2}$. Regardless, the off-switching behavior depending on the illumination intensity was investigated. Figure 3.10 shows the off-switching rate of meDAE depending on the applied intensity. Due to the strong photobleaching at higher intensities, the measurements were not conducted using several excitation pulses with increasing intensity on single liposomes. Instead, every data point represents the mean value of 20 separate measurements with only 5 photoswitching cycles per measured liposome. The switching rates were extracted from exponential fits to the data. The off-switching rate scales linearly with the applied light intensity. The maximal

measured off-switching rate was 280/s ($\tau_{\text{off}} \cong 3.6\,\text{ms}$), which is 27 times slower than that for rsEGFP at similar illumination intensities (see subsection 3.1.4).

To exclude the possibility of fluorescence recovery by fluorophores that could be present in the surrounding media instead of being associated with the liposomes, the fluorescence of the surrounding media was examined. No increased fluorescence was observed compared to samples prepared without fluorophores. However, this could also arise from a significant reduction of the fluorescence quantum yield in aqueous solution. If there were still fluorophores present in the surrounding solution, they would tend to associate with the lipid bilayer. To rule out that additional fluorophores attach to the liposomes during a measurement via diffusion and thereby artificially increase the number of possible switching cycles, an illumination break was inserted after the off-switching pulse. This break was gradually increased to examine whether fluorescence recovery took place. For each value of this break, 40 individual measurements were averaged. As can be seen from Figure 3.11, increasing the illumination break up to 10 seconds did not significantly influence the measured number of possible switching cycles before photobleaching. In particular, no systematic increase with the duration of the pause was observed. This finding also indicates that no long-lived dark state exists in this time span from which the fluorophores could recover.


Figure 3.11: Number of photoswitching cycles of *me*DAE in liposomes where the fluorescence signal drops to half of its initial value depending on the delay between illumination pulses with excitation light. The dashed line shows the mean value of the data points. Error bars represent twice the standard deviation.

3.2.2 *Myo*-inositol substituted diarylethenes

In addition to the *me*DAE compound presented above, two *myo*-inositol substituted diarylethenes (*m*IDAEs) provided by Prof. Masahiro Irie (Rikkyo University, Tokyo, Japan) were investigated [111]. These symmetric compounds featured $2(2')$-ethyl and $6(6')$-phenyl groups. The phenyl groups at positions $C6(6')$ slightly shift the absorption and emission maxima to the red spectral region and increase the fluorescence quantum yield of the closed form, whereas the ethyl groups at positions $C2(2')$ are known to increase the fluorescence quantum yield in polar solvents [95,112]. The 1,2-bis(2-ethyl-6-phenyl-1-benzothiophen-1,1-dioxide-3-yl)perfluorocyclopentene core structure was decorated with two and four polar *myo*-inositol residues via carboxyl groups to obtain *(b)-m*IDAE and *(t)-m*IDAE, respectively. The structures are shown in Figure 3.12.
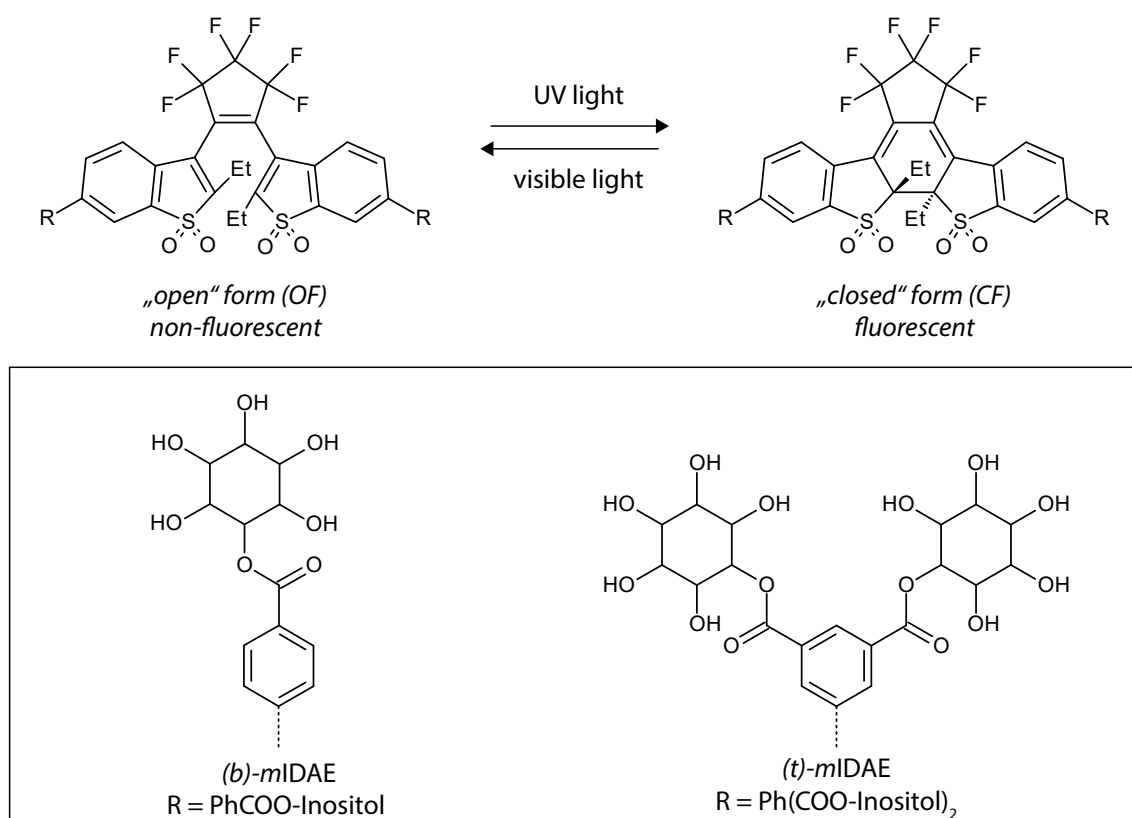
Figure 3.12: Structures of *m*IDAEs in their open (OF) and closed forms (CF). The open form is non-fluorescent and can be transformed to the closed fluorescent form by illumination with UV light. The closed form fluoresces upon illumination with blue light and is transformed back to the open form with visible light. *(b)-m*IDAE is decorated with two and *(t)-m*IDAE with four *myo*-inositol groups. Compounds were provided by Prof. Masahiro Irie (Rikkyo University, Tokyo, Japan) [111].
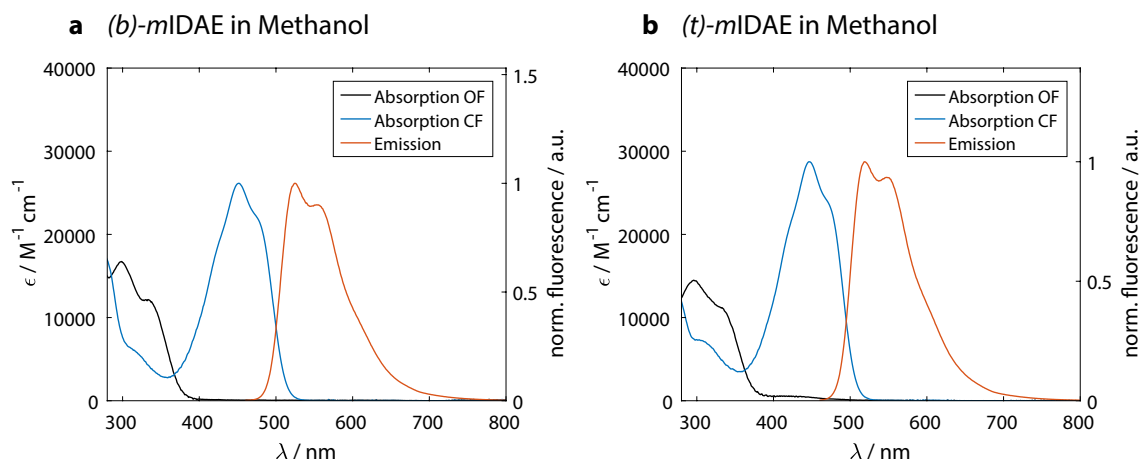
Figure 3.13: Absorption and emission spectra of *(b)-m*IDAE (**a**) and *(t)-m*IDAE (**b**) in methanol. Absorption coefficients (ϵ) of the open (black line) and the closed (blue line) form are given on the left axes. Fluorescence of the closed form (orange line) is given in arbitrary units on the right axes.

The introduction of inositol residues increased the water-solubility of the compounds due to the presence of multiple hydroxy groups. The emission of these compounds was significantly shifted to the green with the emission centered at around 550 nm (Figure 3.13). The emission filters F_5 (Figure 2.2) in front of the detectors were adjusted to BrightLine® 525/50 (Semrock, Rochester, NY, USA).

These compounds were used to prepare liposome samples as described before. Despite the increased water-solubility of the compounds, they showed high affinity to associate with the lipid membrane. Similar to the characterization of *me*DAE, the *myo*-inositol substituted diarylethenes were examined regarding their photophysical properties, summarized in Table 3.1. All displayed values, except the fluorescence lifetime, were acquired using widefield illuminations with $\lambda_{act} = 375$ nm and $\lambda_{exc} = 491$ nm and represent the arithmetic mean of the evaluation of 50 individual switching experiments. The activation light was applied for 1 ms at 120 W/cm², followed by the excitation for 200 ms at 8 kW/cm². Fluorescence lifetimes were obtained as described in subsection 3.1.5. The values are similar for both compounds, reflecting the fact that they share the same core structure and only differ in the number of water-solubilizing groups. The photostability is lower than that for *me*DAE, but the off-switching is about 12 times faster under similar conditions. The values for the residual fluorescence after off-switching and the fluorescence lifetime are similar for all three compounds.

Table 3.1: Photophysical properties of mIDAEs and meDAE in liposomes under similar illumination conditions. Off-switching was performed with a widefield illumination at 491nm for 200 ms with $8\,\text{kW/cm}^2$ for the mIDAEs and with $10\,\text{kW/cm}^2$ for meDAE.

	(b)-mIDAE	(t)-mIDAE	meDAE
number of cycles till half of initial fluorescence is bleached	8 ± 2	17 ± 5	22 ± 5
characteristic off-switching time τ_{off} $(1/e)$	$1.2 \pm 0.3\,\text{ms}$	$1.0 \pm 0.2\,\text{ms}$	$12.4 \pm 0.7\,\text{ms}$
residual fluorescence after off-switching	$6.5 \pm 2.3\,\%$	$4.8 \pm 1.9\,\%$	$6.8 \pm 0.8\,\%$
fluorescence lifetime	$\tau_1 = 0.5\,\text{ns}\,(9\,\%)$ $\tau_2 = 2.3\,\text{ns}\,(91\,\%)$	$\tau_1 = 0.7\,\text{ns}\,(8\,\%)$ $\tau_2 = 2.5\,\text{ns}\,(92\,\%)$	$\tau_1 = 0.6\,\text{ns}\,(6\,\%)$ $\tau_2 = 2.3\,\text{ns}\,(94\,\%)$

Summary

Although the preparation of liposomes allowed the examination of the hydrophobic fluorophores under conditions present in a confocal microscope, this type of sample entails some uncertainties. The fluorophores are not rigidly fixed to the liposome membrane and their relative orientation to the membrane remains unclear, in particular with regard to their photoswitching ability. A loose association to the outside-directed membrane could cause dissociation from the liposome and out of the observation area, especially in case of fluorophores with increased water-solubility. The observed off-switching time and the residual fluorescence after off-switching of the synthetic photoswitchable fluorophores presented in this section would generally allow their application in RESOLFT nanoscopy. However, the absence of a suitable linker to stain cellular structures and the low amount of possible switching cycles constrain this implementation.

3.3 Bioconjugateable photoswitchable synthetic fluorophores

This section describes the investigation and application of new reversibly photoswitchable diarylethene-based fluorophores with increased water-solubility and linkers for the conjugation to biomolecules. The new fluorophores were successfully used in confocal and high resolution RESOLFT imaging. The compounds were synthesized and provided by Dr. Benoît Roubinet and Dr. Heydar Shojaei (Max Planck Institute for Biophysical Chemistry, Göttingen, Germany)[113].
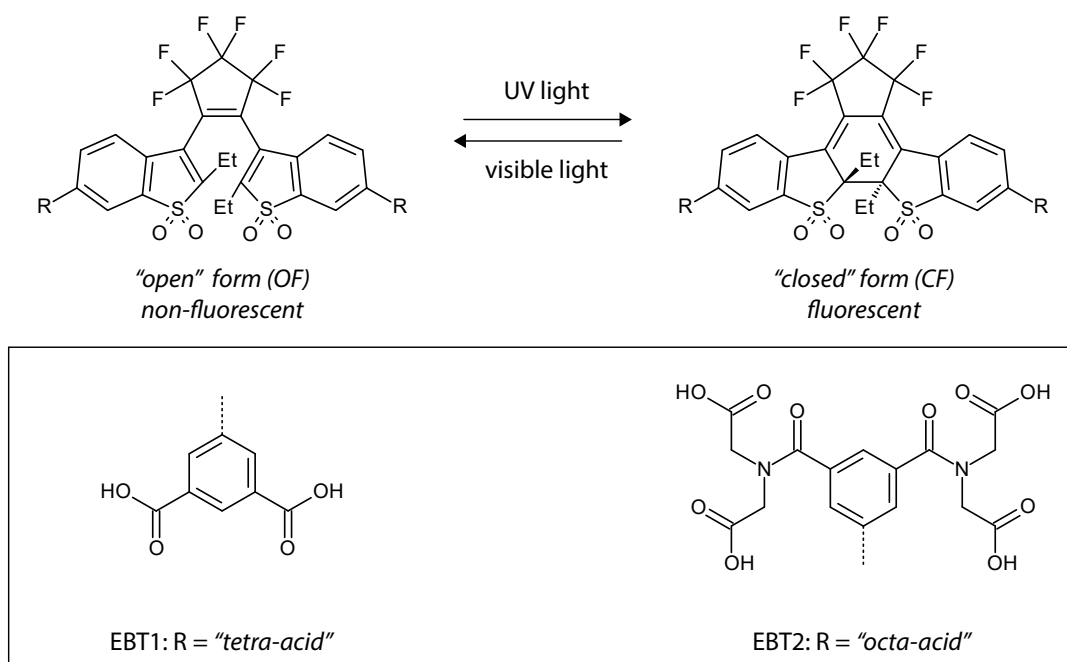
Figure 3.14: Structures of EBT1 and EBT2 in their open (OF) and closed form (CF). The open form is non-fluorescent and can be transformed to the fluorescent closed form by illumination with UV light. The closed form fluoresces upon illumination with blue light and is transformed back to the open form with visible light. EBT1 is decorated with four ("tetra-acid") and EBT2 with eight ("octa-acid") carboxylic groups. Compounds were synthesized and provided by Dr. Benoît Roubinet and Dr. Heydar Shojaei[113].

The highly symmetric core structure of 1,2-bis(2-ethyl-6-phenyl-1-benzothiophen-1,1-dioxide-3-yl)perfluorocyclopentene (EBT) was decorated with four carboxylic acid groups to obtain the "tetra-acid" EBT1 and eight carboxylic acid groups to obtain the "octa-acid" EBT2. The structures are shown in Figure 3.14. The carboxylic

acids are highly polar functional groups acting as hydrogen bond donors (carbonyl) and acceptors (hydroxyl). These properties conferred the desired water-solubility to the generally hydrophobic core. One or several carboxylic acid groups can be activated, e.g. by transformation to an NHS-ester (*N*-hydroxysuccinimide ester), giving the opportunity to conjugate the diarylethene to amino groups of proteins.

3.3.1 Photophysical properties in solution

Figures 3.15a and 3.15b show the emission and absorption spectra of the tetra-acid EBT1 and the octa-acid EBT2 in PBS. Their photophysical properties are summarized in Table 3.2. The data acquisition and antibody conjugation were kindly carried out by Dr. Mariano Bossi (Max Planck Institute for Biophysical Chemistry, Göttingen, Germany). The properties measured in aqueous solutions and in methanol show minor differences. The emission efficiencies and fluorescence lifetimes are reduced by 20 - 30 % in PBS, with stronger variations for EBT1. The ring-opening quantum yield is nearly unaltered for EBT2, whereas for EBT1 a 35 % reduction is observed in PBS. The quantum yields for the on-switching were affected the strongest, especially for EBT1.

EBT1 and EBT2 were conjugated to antibodies (AffiniPure Sheep Anti-Mouse IgG (H+L), Jackson ImmunoResearch Laboratories, Suffolk, UK) via NHS-ester crosslinking reaction [114]. The bioconjugates with EBT1 and EBT2 retain the photochromic and fluorescent properties of free fluorophores in solution. Figures 3.15c and 3.15d show the photoswitching of the bioconjugates in PBS. This was accomplished by first illuminating the sample with 470 nm light of 15 mW to reach maximal conversion to the non-fluorescent isomer. The illumination was applied till no change in the 450 nm-absorption band could be observed. Afterwards the sample was illuminated with 360 nm light of 10 mW to achieve conversion to the closed form. The first five illumination steps had a duration of 5 s, followed by a 10 s and a 15 s step and three 20 s steps. Absorption and emission spectra were recorded after each irradiation step, exhibiting a continuous increase at the absorption maximum of the closed isomer and the detected emission. Maximal conversion from the closed to the open form was confirmed upon examination of absorption and emission spectra.

The presence of the antibodies is evident from the absorption of their aromatic amino acids at 280 nm. The average number of fluorophores coupled to an antibody (degree of labeling, DOL) was calculated on the basis of the acquired absorption spectra of the free uncoupled fluorophores and the bioconjugates [114]. This gave a
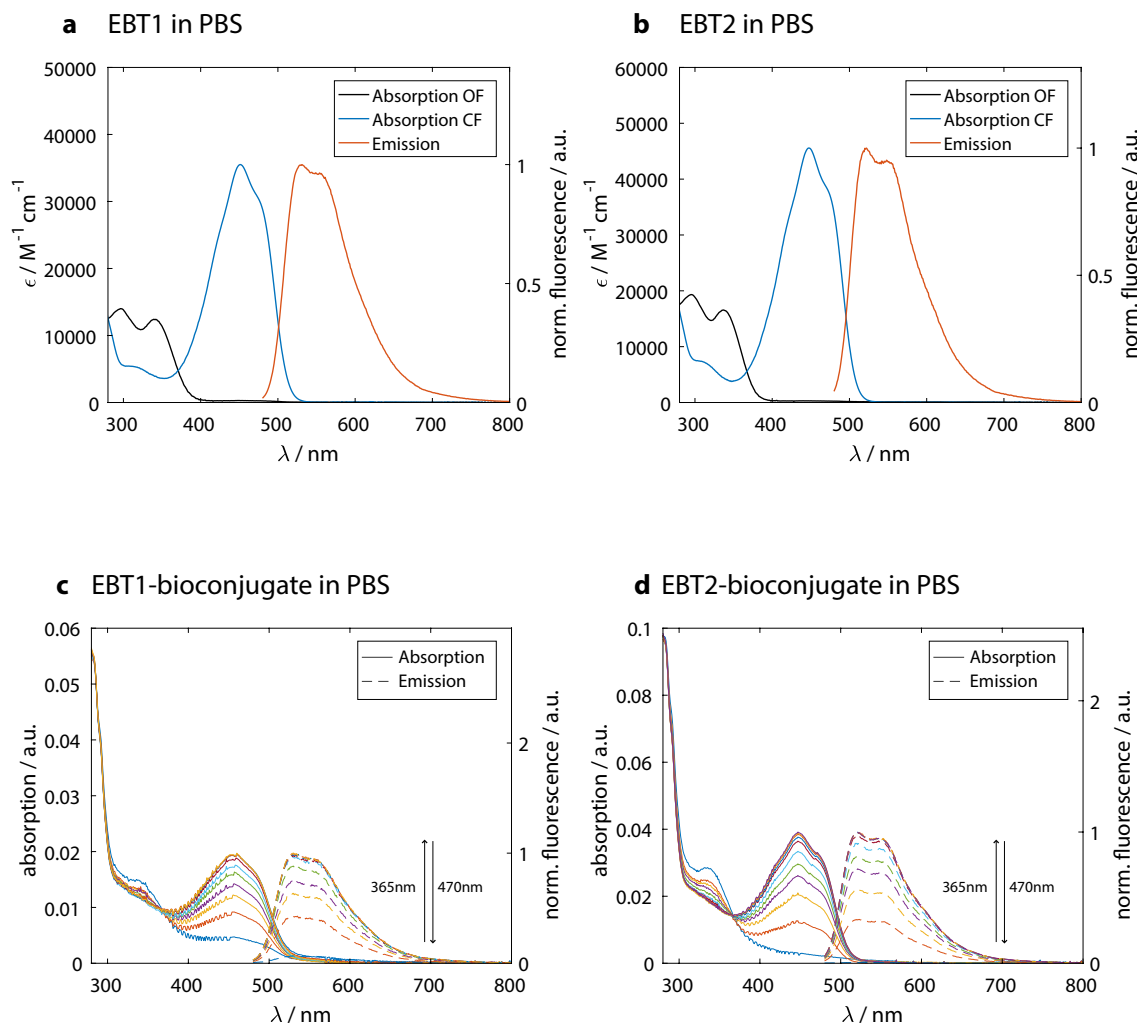
Figure 3.15: Absorption and emission spectra of EBT1 (**a**) and EBT2 (**b**) in PBS (pH 7.4). Absorption coefficients (ϵ) of the open (black line) and the closed (blue line) form are given on the left axes. Fluorescence of the closed form (orange line) is given in arbitrary units on the right axes. Absorption and emission spectra of diluted samples of EBT1 (**c**) and EBT2 (**d**) conjugated to an antibody in PBS (pH 7.4) with similar degree of labeling (DOL $\approx$ 5). Samples were first illuminated with 470 nm light to obtain only the non-fluorescent open isomer. Subsequent illumination with 365 nm light in several steps was performed. Absorption and emission spectra were recorded after each irradiation step. Data provided by Dr. Mariano Bossi.

Table 3.2: Photophysical properties of free EBT1 and EBT2 in aqueous solution (PBS, pH 7.4) and methanol. Data provided by Dr. Mariano Bossi.

		PBS		Methanol	
Parameter	State	EBT1	EBT2	EBT1	EBT2
$\lambda_{\text{max abs}} / \text{nm}$	OF	340	337	330	331
$\epsilon / \text{M}^{-1}\,\text{cm}^{-1}$	OF	12400	16500	12400	16000
$\lambda_{\text{max abs}} / \text{nm}$	CF	450	448	449	448
$\epsilon / \text{M}^{-1}\,\text{cm}^{-1}$	CF	35000	45000	35000	44500
$\lambda_{\text{max em}} / \text{nm}$	CF	534, 558	522, 550	525, 556	523, 552
Φ_{fl}	CF	0.48	0.57	0.69	0.70
$\tau_{\text{fl}} / \text{ns}$	CF	1.72 ± 0.05	2.04 ± 0.05	2.52 ± 0.05	2.54 ± 0.05
$\Phi_{\text{OF} \rightarrow \text{CF}}$	CF	0.19 ± 0.04	0.23 ± 0.04	0.29 ± 0.04	0.24 ± 0.04
$\Phi_{\text{CF} \rightarrow \text{OF}} / 10^{-3}$	CF	1.2 ± 0.3	2.0 ± 0.3	2.8 ± 0.3	2.6 ± 0.3

DOL of 5.1 and 4.8 for the EBT1- and the EBT2-conjugates, respectively. These values are in the range of the DOL of 2–5 which is considered as optimal[115]. As can be seen from Figure 3.15, attachment via NHS-ester to the secondary antibody did not change the spectral characteristics of the fluorophores.

3.3.2 Confocal imaging

The EBT-antibody conjugates with a DOL of ~ 5 were used to stain cellular structures of fixed Vero cells to further analyze their applicability for imaging. Figure 3.16 shows confocal images using a primary antibody against α-Tubulin. The filamentous structure was highly specifically stained by both secondary antibodies. The images were acquired using focused excitation at $\lambda_{\text{exc}} = 488\,\text{nm}$ with a preceding short widefield illumination at $355\,\text{nm}$ to switch all fluorophores to their fluorescent form. Repeated image acquisition of the same area led to a decrease in the fluorescence signal originating from the isomerization of the fluorophores to the non-fluorescent form. The signal could be restored by a short widefield illumination with $355\,\text{nm}$ prior to each frame. Simultaneous illumination with the excitation wavelength and the activation wavelength ($355\,\text{nm}$) during the image acquisition caused notable amount of photobleaching, recognizable by a decrease of the total fluorescence signal between the first and the second frame. This effect was heavily reduced by pixelwise sequential illumination with these two wavelengths. The EBT1-stained samples in general showed higher fluorescence intensities than their EBT2-stained counterparts. This is caused by the lower quantum yield for the ring-opening reac-

a Tubulin stained with EBT1
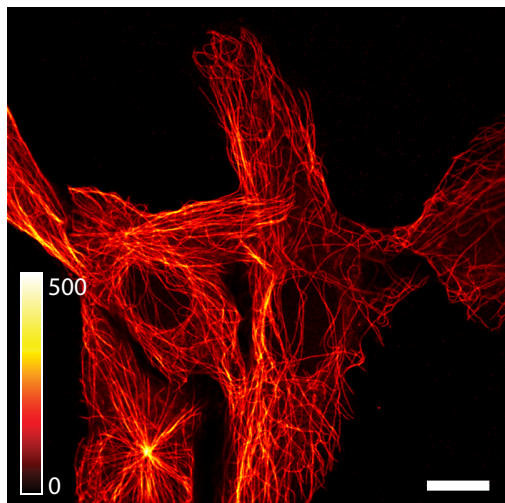
b Tubulin stained with EBT2
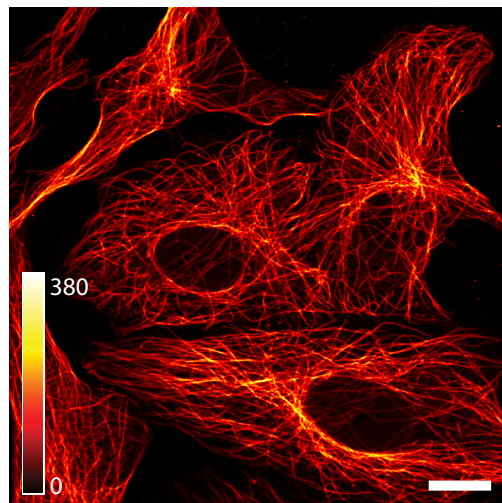
Figure 3.16: Confocal images of fixed Vero cells immunostained with primary antibodies against α-Tubulin. EBT1 (**a**) and EBT2 (**b**) were attached to the secondary antibodies. Scale bars: $10\,\mu m$. Excitation at $488\,nm$ with $10\,kW/cm^2$, $30\,\mu s$ dwell time and a pixelsize of $100\,nm$.

tion of EBT1 compared to EBT2. Therefore a larger amount of fluorophores reside in their fluorescent state during the excitation. The impact of this effect is decreased by the higher quantum yield of EBT2.

These samples were very well suited for subsequent investigation of their photophysical and photoswitching properties at illumination intensities used in confocal microscopy. Furthermore, the tubular structures offer a well-suited target structure for high resolution imaging based on the RESOLFT concept.

3.3.3 Fluorescence pump-probe measurements

The immunostained Vero cells were used to characterize the photophysical properties of the EBT-fluorophore-bioconjugates in the same samples as used for imaging. Samples were prepared as described in subsection 2.6.3 and examined with the described widefield illuminations. The emission filters F_5 (Figure 2.2) in front of the detectors were adjusted to BrightLine® 525/50 (Semrock, Rochester, NY, USA).

Switching to fluorescent on-state

First, the activation process was investigated to ensure that in the following experiments all fluorophores were switched to their fluorescent on-state. Both fluorophores

were activated completely with a 20 µs pulse of 375 nm light at 0.8 kW/cm². This was evaluated by increasing the illumination duration at this wavelength and sampling the resulting fluorescence signal with the excitation wavelength. Increasing the length of the UV illumination pulses did not increase the retrieved fluorescence further. However, using UV-illumination pulses longer than 20 µs caused a decrease in the number of possible switching cycles. Furthermore, the way how the activation light dose was applied was examined. The dose was kept at $t_{act} \times I_{act} = 16\,\text{mJ/cm}^2$. The fluorescence signal after the activation step did not change upon increasing the illumination time. Neither the number of switching cycles nor the off-switching kinetics were affected. To exclude the existence of a delayed ring-closure reaction after the UV-pulse, the waiting time between the activation and excitation pulses was gradually increased from 20 µs to 500 µs. This also did not influence the above mentioned characteristics of the fluorophores.

Since the way of applying the activation light dose to the sample did not influence its photophysical properties, the shortest illumination and waiting times of 20 µs were chosen for further experiments.

Off-switching kinetics

The off-switching behavior of the EBT-fluorophores was examined with the widefield switching scheme for negative switchers described in subsection 3.1.1. Figure 3.17 shows an exemplary switching experiment of EBT1 and EBT2 with activation at 375 nm and excitation/off-switching at 491 nm with 23 kW/cm². The off-switching duration was set to 10 ms, because after this time no change in the residual fluorescence after off-switching could be observed for both fluorophores. This ensured a precise determination of the minimal possible fluorescence signal in the off-state. The off-switching behavior is shown as mean of the first 30 switching cycles. For both fluorophores a biexponential fit was used to describe the data. In both cases the fast component describes about 80 % of the signal amplitude and is five times faster than the slow component. Compared in terms of the $1/e$-decay time, EBT2 switches of about 1.6 times faster than EBT1 at the same illumination intensity. Neither for EBT1 nor for EBT2, a single exponential decay could describe the observed off-switching curve. A second process is involved described by the slower decay of the biexponential fit.

a switching fatigue EBT1

b off-switching behaviour EBT1

c switching fatigue EBT2

d off-switching behaviour EBT2
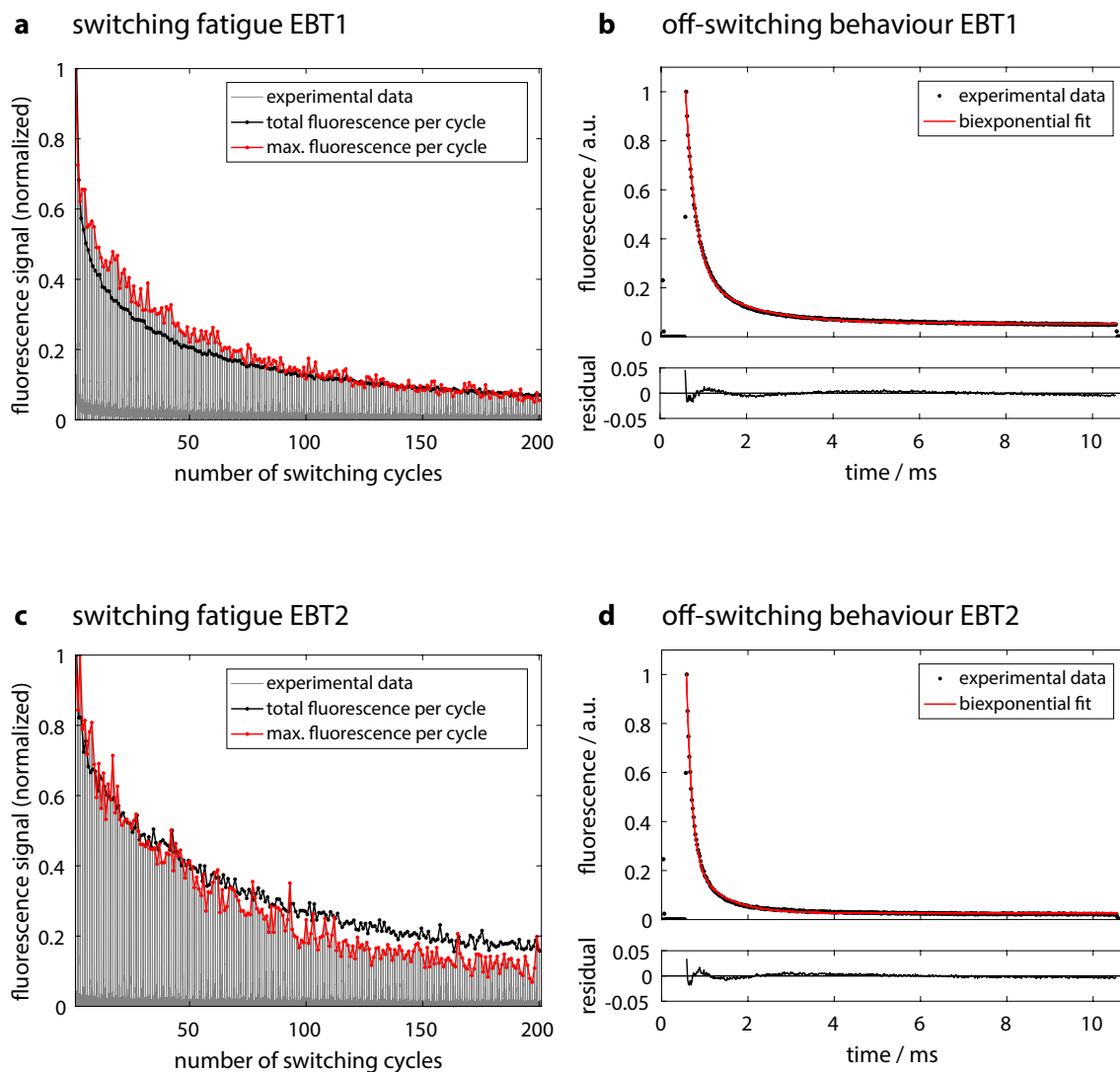
Figure 3.17: Fluorescence emission of cells immunolabeled with EBT1 (**a**) and EBT2 (**c**) showing the on-/off-switching cycles upon irradiation with the mentioned light pulse sequence (gray bursts). The red line indicates the maximum fluorescence signal detected within a switching cycle, while the black line displays the overall fluorescence gained per cycle, both normalized to the respective value of the first switching cycle. **b** and **d** show a single switching cycle as mean value of the first 30 cycles (black dots) of EBT1 and EBT2, respectively. The data point before the maximal signal in **b** and **d** is a result of the delayed response of the AOTF. This factor is integrated in the used fitting routine to obtain the correct values for the initial fluorescence. The biexponential fit used to determine the switching kinetics is shown as red solid line. Residuals of the fit are shown below. All plots were normalized to their maximum value. All measurements were taken with 20 µs bins.

Photobleaching

Under the same illumination conditions, EBT1 exhibits half the number of switching cycles compared to EBT2, till half of the initial fluorescence is bleached. It was consistently observed that EBT1 shows a faster decrease of fluorescence signal during the first cycles ($\sim 20 - 30\,\%$ during the first 3 cycles) and that the mean fluorescence signal during illumination with excitation light drops faster than the maximal fluorescence signal. After 200 cycles, only $10\,\%$ of the initial fluorescence is left for EBT1 and EBT2. The bleaching is more distinct for the detected peak intensity per switching cycle than for the residual fluorescence signal after off-switching. This causes a degradation of the peak-to-background ratio during a measurement. The residual fluorescence after off-switching increased from $5\,\%$ to $7\,\%$ for EBT1 and from $2\,\%$ to $3.5\,\%$ for EBT2 from the first to the last switching cycle. In contrast to that the $1/e$ decay times of the individual cycles remain the same throughout the measurement. Reducing the duration of illumination with the off-switching light five times to stop at a residual fluorescence after off-switching of twice the minimal possible values ($9.6\,\%$ for EBT1 and $3.8\,\%$ for EBT2, both reached after $2\,\mathrm{ms}$ at $23\,\mathrm{kW/cm^2}$) did not affect the number of possible switching cycles. Reducing the illumination times further revealed that the photobleaching scales linear with the applied light dose. No significant dependence was observed solely on the applied excitation intensity in the range from $0.8\,\mathrm{kW/cm^2}$ to $23\,\mathrm{kW/cm^2}$.

Table 3.3 summarizes the photophysical switching properties of both EBT fluorophores with $20\,\mathrm{\mu s}$ activation pulse of $375\,\mathrm{nm}$ light at $0.8\,\mathrm{kW/cm^2}$ and off-switching at $491\,\mathrm{nm}$ for $10\,\mathrm{ms}$ at $23\,\mathrm{kW/cm^2}$. The indicated values, except the fluorescence lifetime, represent the arithmetic mean of the evaluation of 50 individual switching experiments.

The fluorescence lifetime was acquired using pulsed focused excitation at $488\,\mathrm{nm}$. The lifetime is altered for both fluorophores compared to the values acquired in solution, exhibiting a biexponential decay. The major part of the decay ($> 80\,\%$ of the amplitude) is described by characteristic times being $0.5\,\mathrm{ns}$ longer than the monoexponential values of the measurements in solution.

Table 3.3: Photophysical switching properties of EBT1 and EBT2 in immunostained Vero cells in PBS (pH 7.4). Off-switching was performed with a widefield illumination at 491 nm with 23 kW/cm² for 10 ms.

	EBT1	EBT2
number of cycles till half of the initial fluorescence is bleached	11 ± 2	22 ± 2
characteristic time τ_1 (A_1)	$244 \pm 5\,\mu s\,(77\,\%)$	$148 \pm 4\,\mu s\,(76\,\%)$
characteristic time τ_2 (A_2)	$1324 \pm 37\,\mu s\,(23\,\%)$	$796 \pm 23\,\mu s\,(24\,\%)$
$1/e$-decay time τ_{off}	$323 \pm 6\,\mu s$	$202 \pm 5\,\mu s$
residual fluorescence after off-switching	$4.8 \pm 0.8\,\%$	$1.9 \pm 0.3\,\%$
fluorescence lifetime	$\tau_1 = 0.5\,ns\,(17\,\%)$ $\tau_2 = 2.2\,ns\,(83\,\%)$	$\tau_1 = 0.5\,ns\,(16\,\%)$ $\tau_2 = 2.4\,ns\,(84\,\%)$

Intensity-dependent off-switching kinetics

The intensity dependence of the off-switching rate was examined by a pattern of consecutive illumination pulses with increasing intensities. The displayed off-switching rates in Figure 3.18a depict the reciprocal value of the characteristic decay time τ_{off} extracted from biexponential fits to the decay curves. The light dose for off-switching was kept constant for all illumination intensities at 230 J/cm² for both fluorophores. The data shown in Figure 3.18 represent the mean over 30 individual measurements at different positions in the sample in which the pulse pattern was repeated five times.

For both EBT fluorophores, the off-switching rate increases linearly with the illumination intensity as can be seen by the linear fit in Figure 3.18a. Thus, the difference in the off-switching rate of EBT1 and EBT2 stays constant at a factor of 1.5 for the applied illumination intensities. In accordance to this, the two off-switching rates obtained from the biexponential fits show the same linear dependence and their amplitude ratio stays constant for all intensities for both fluorophores. These findings suggest that the off-switching processes of the EBT fluorophores occurs directly
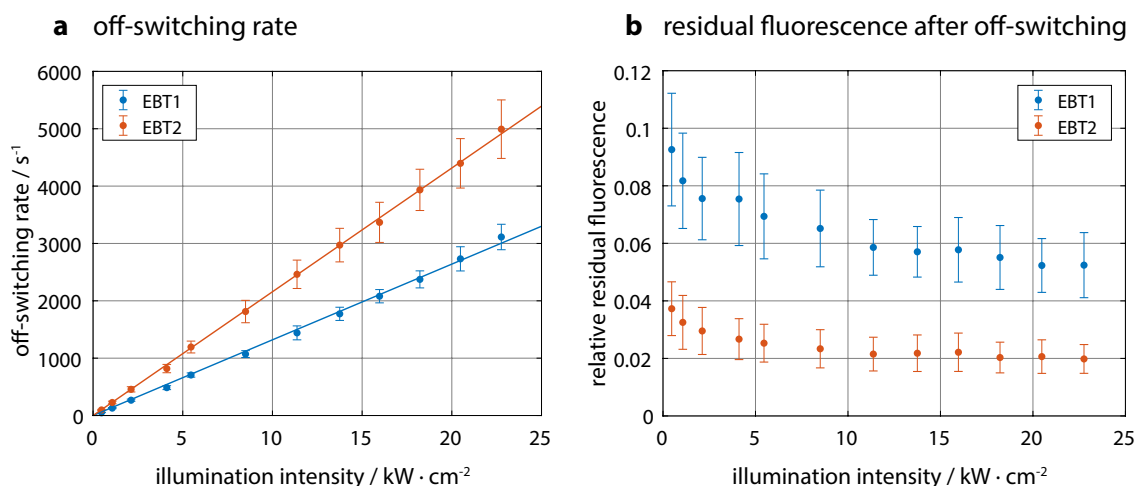
Figure 3.18: Intensity-dependent off-switching rate and relative residual fluorescence of EBT1 and EBT2. **a:** Off-switching rate of EBT1 (blue) and EBT2 (orange) as function of illumination intensity. Solid lines show a linear fit to the data. **b:** Residual fluorescence after off-switching of EBT1 (blue) and EBT2 (orange) as function of illumination intensity. Illumination times were chosen such that the applied light dose was kept constant for different illumination intensities. All data were recorded on immunostained Vero cells. Error bars represent twice the standard deviation.

from the S_1 state without further intermediate states at excitation intensities up to $23\,kW/cm^2$. The maximal observed off-switching rates of $3100/s$ ($\tau_{off} \cong 322\,\mu s$) for EBT1 and $5000/s$ ($\tau_{off} \cong 200\,\mu s$) for EBT2 at $23\,kW/cm^2$ are both lower than the off-switching rate of rsEGFP at this illumination intensity shown in Figure 3.4. The faster off-switching rate of EBT2 is in accordance with the higher quantum yield for the ring-opening reaction.

The residual fluorescence after off-switching decreases for both fluorophores at higher illumination intensities, starting at $9.3\,\%$ and $3.7\,\%$ for EBT1 and EBT2, respectively. As can be seen from Figure 3.18b, these values drop to approximately half at the maximal illumination intensity of $23\,kW/cm^2$ for both fluorophores. The decreasing relative residual fluorescence originates from the fact that the maximal fluorescence per cycle increases linearly with the applied intensity, whereas the fluorescence after off-switching shows a saturable behavior.

Slight deviations of the values shown in Figure 3.18 at illumination intensities of $23\,kW/cm^2$ compared to the values given in Table 3.3 are due to the different ways the measurements were performed. For the data given in Table 3.3, experiments were performed with the given intensity in repeated switching cycles. In contrast, for Figure 3.18, the different excitation intensities were consecutively applied to the

same area in the sample for better comparability. This can cause higher residual fluorescence after off-switching than in the single intensity experiments due to photobleaching. Nevertheless, higher residual fluorescence values at lower illumination intensities were also found in the single intensity experiments.

3.3.4 RESOLFT imaging

The antibody-coupled EBT-fluorophores successfully stained cellular structures of fixed mammalian cells and showed photophysical properties suitable for RESOLFT nanoscopy. The imaging was performed on immunostained Vero cells mounted in PBS. All presented images show raw data to demonstrate the capabilities of the EBT fluorophores without further post-processing image enhancement techniques like deconvolution algorithms.

For the RESOLFT imaging the following pixelwise scheme was deployed. The Gaussian-shaped activation beam (355 nm) was applied for 50 µs at $0.15\,\text{kW/cm}^2$, followed by a 10 µs illumination pause to ensure strict separation of the different illuminations. Subsequently, the doughnut-shaped off-switching beam (488 nm) was applied (duration and intensity where chosen depending on the respective sample) and after another 10 µs illumination pause, the Gaussian-shaped excitation beam (488 nm) was applied for 80 µs at $10\,\text{kW/cm}^2$ to read out the remaining fluorescence in the center of the focus. Comparison of the confocal and the RESOLFT images was achieved by consecutive recording of the same area following the described imaging scheme. For the confocal images the off-switching step with the doughnut-shaped beam was omitted. Due to the photobleaching of the fluorophores, the confocal images were recorded after the RESOLFT images. This assured higher fluorescence intensities in the RESOLFT images at the expense of reduced fluorescence in the confocal images. The overall bleaching caused by the RESOLFT and the corresponding confocal image was examined by confocal overviews before and after the imaging of the selected areas.

The RESOLFT images were obtained at off-switching intensities of $12\,\text{kW/cm}^2$ applied for 7 ms for EBT1-stained samples and $36\,\text{kW/cm}^2$ applied for 1.2 ms for EBT2. Remarkably, higher off-switching intensities for EBT1 did not improve the image quality, but instead caused higher photobleaching resulting in an inferior signal-to-noise ratio. These imaging parameters led to pixel dwell times of 7.15 ms for EBT1 and 1.35 ms for EBT2. The images were recorded with a pixel size of 30 nm because smaller pixel steps caused high photobleaching having negative effects on the image

quality. Accordingly, high resolution imaging of a $6\,\mu m \times 6\,\mu m$ area took ~ 5 minutes for EBT1 and ~ 1 minute for EBT2.

The tubular structures were considerably refined in the RESOLFT images. The attained resolution was quantified by measuring the FWHM of the EBT labeled microtubules. This was accomplished by averaging ten intensity profiles of adjacent pixels on single filaments. The averaging prevented the occurrence of inaccurate smaller resolution values arising from statistical outliers in the intensity of individual pixels. The FWHM of these line profiles were determined on Lorentzian functions fitted to the measured data. For a robust determination of the resolution in the images, individual line profiles of six different positions were averaged as exemplary shown for EBT2 in Figure A.5. From these line profiles the resolution was determined to be $86 \pm 1\,nm$ for EBT1 and $76 \pm 3\,nm$ for EBT2. As can be seen from the RESOLFT images and the corresponding line profiles (Figures 3.19 and 3.20), the enhanced resolution allowed to discern adjacent filaments where the confocal images only showed a single blurred fiber. The line profiles of the confocal images with EBT2 stained Tubulin show an FWHM of down to $175\,nm$ (Figure 3.20e).

EBT2 exhibited better characteristics concerning imaging speed and attainable resolution resulting from the higher fatigue resistance and lower residual fluorescence after off-switching. To show its applicability also for other cellular structures, the secondary EBT2-antibodies were further used to stain Vimentin filaments and the nuclear pore complex protein NUP153 of Vero cells (see Figures A.3 and A.4). The Vimentin stainings showed the same quality as the Tubulin stainings, whereas the NUP153 stainings showed unspecific signal outside the nucleus (Figure A.4). However, the nucleus itself could be imaged without any constraints. The described RESOLFT illumination pattern was also applied to these samples with the intensities for the off-switching step with the doughnut-shaped beam adjusted to $32\,kW/cm^2$ and $37\,kW/cm^2$ for Vimentin and NUP153, respectively. The attained resolution, determined as described above, was $80 \pm 5\,nm$ for the Vimentin and $88 \pm 6\,nm$ for NUP153 samples.

Due to photobleaching caused by the RESOLFT imaging, the acquisition of a second high-resolution image of the same area was not possible. Comparing the overall photon counts of the imaged area in the confocal overviews before and after the RESOLFT imaging yielded a decrease of $\sim 60\,\%$ after the imaging (Figures 3.19 and 3.20). The second RESOLFT images showed reduced signal-to-noise ratio, such that the cellular structures could not be clearly distinguished from the background.
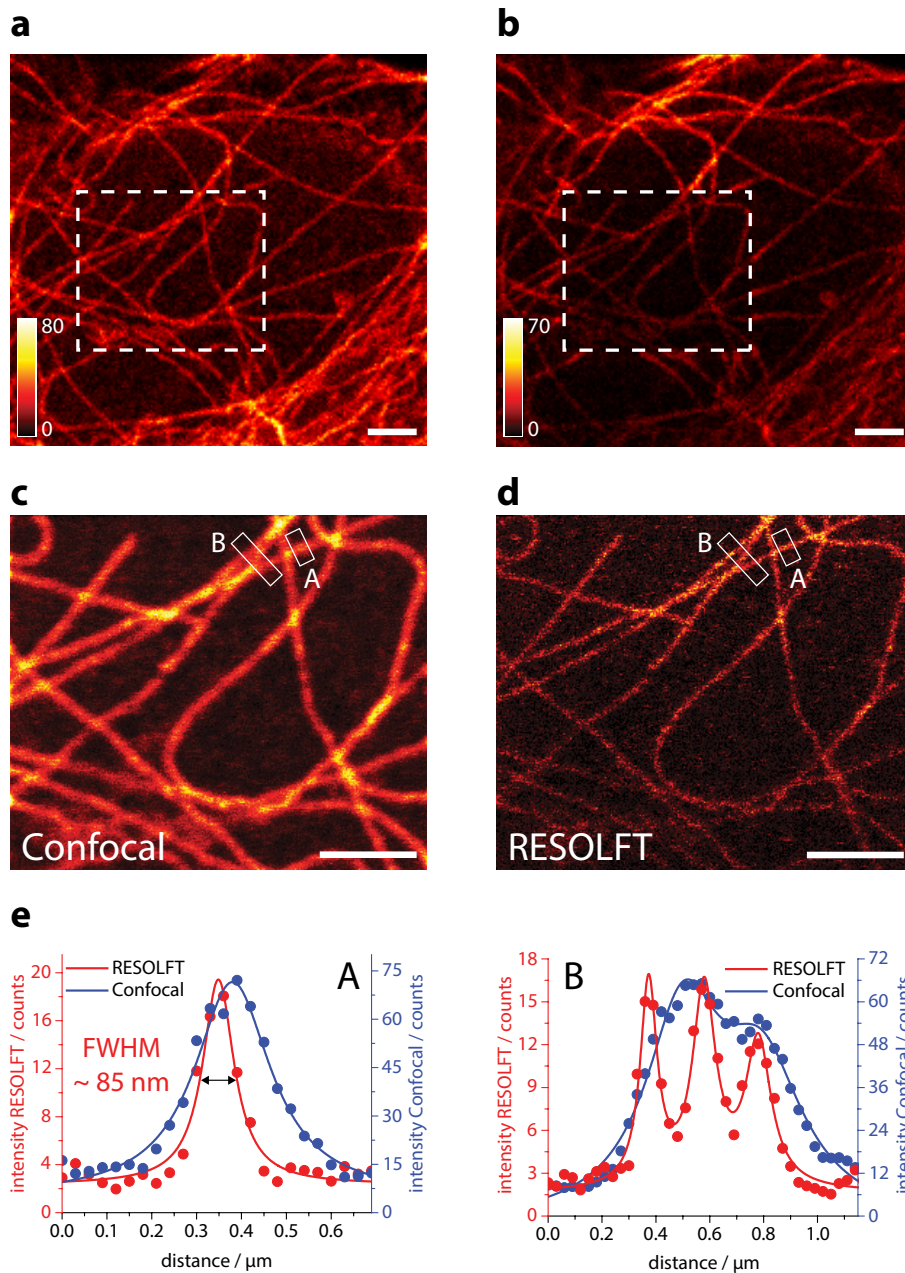
Figure 3.19: Confocal overview of fixed Vero cells immunostained with primary antibodies against α-Tubulin and with EBT1 attached to the secondary antibodies before (**a**) and after (**b**) the high resolution imaging. Confocal (**c**) and RESOLFT (**d**) image of the indicated areas in **a** and **b**. The RESOLFT images were recorded before confocal images. Scale bars: 2 µm. All images show raw data. **e:** Line profiles A-B (averaged over ten adjacent lines) display the regions indicated in **c** and **d**. The data (dots) was fitted with Lorentzian functions (solid line) for the RESOLFT (red) and the confocal (blue) image. The FWHM determined on fit A is indicated by the small black arrow.
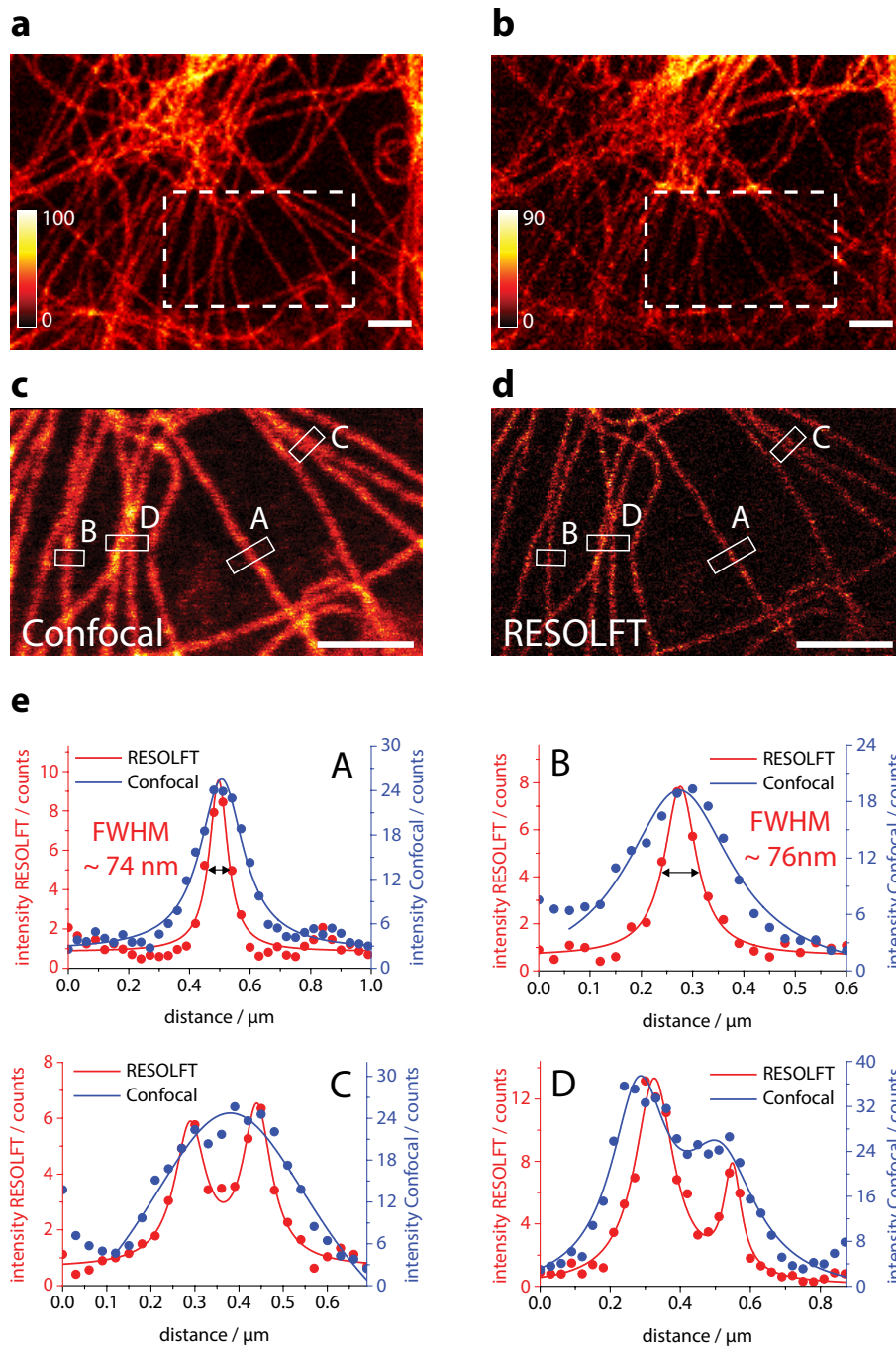
Figure 3.20: Confocal overview of fixed Vero cells immunostained with primary antibodies against α-Tubulin and with EBT2 attached to the secondary antibodies before (**a**) and after (**b**) the high resolution imaging. Confocal (**c**) and RESOLFT (**d**) image of the indicated areas in **a** and **b**. The RESOLFT images were recorded before confocal images. Scale bars: 2 μm. All images show raw data. **e:** Line profiles A-D (averaged over ten adjacent lines) display the regions indicated in **c** and **d**. The data (dots) was fitted with Lorentzian functions (solid line) for the RESOLFT (red) and the confocal (blue) image. The FWHMs determined on the fits A and B indicated are by the small black arrows.

60

Specificity of secondary antibodies

The secondary antibodies described in subsection 3.3.1 were used in standard immunostaining protocols for the first time and some stainings showed slight unspecific staining. To estimate to what extent this unspecificity arose from the binding of the secondary antibody to the cellular structures of the fixed cells, negative controls were conducted.
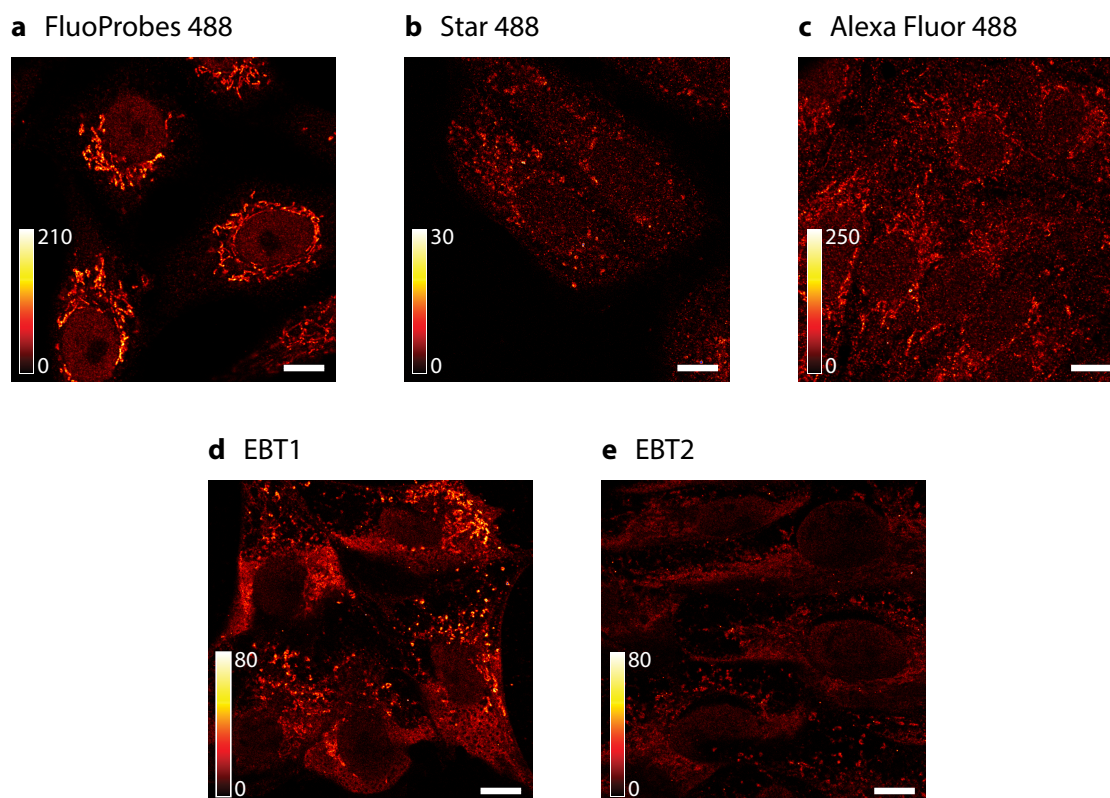
Figure 3.21: Confocal images of fixed Vero cells solely stained with secondary antibodies labeled with different fluorescent dyes: FluoProbes 488 (**a**), Star 488 (**b**), Alexa Fluor 488 (**c**), EBT1 (**d**) and EBT2 (**e**). Scale bars: 10 μm. Excitation at 488 nm with 10 kW/cm^2 and 30 μs dwell time.

The incubation with the primary antibody was omitted in the immunostaining protocol described in subsection 2.6.3. Thus only the secondary antibody was applied to the sample. This procedure was not only conducted with the antibodies conjugated with EBT1 and EBT2 but also with commercially available secondary antibodies commonly used in immunofluorescence. In particular, these antibodies were conjugated with the fluorophores *FluoProbes 488* (Interchim), *Star 488* (Abberior) and *Alexa Fluor 488* (Thermo Fisher Scientific).

The different samples were imaged under similar conditions (excitation at 488 nm with $10\,kW/cm^2$ and 30 µs dwell time). In case of samples with EBT1 and EBT2, it was ensured that all fluorophores were in their fluorescent form by a pixelwise illumination step with 355 nm ($130\,W/cm^2$ for 50 µs) prior to the excitation. All secondary antibodies showed a certain amount of unspecific labeling (see Figure 3.21). This demonstrates that the effect is not limited to the new compounds EBT1 and EBT2 and does not arise from the fluorophore properties.

Summary

The new reversibly photoswitchable EBT fluorophores were successfully used to label various structures in fixed mammalian cells. Based on the characterization of these new fluorophores, their first utilization for RESOLFT imaging could be demonstrated, featuring a $\sim$ 2.3-fold resolution increase. The enhanced water-solubility of the fluorophores allowed the use of aqueous buffers without further additives to enable their photoswitching behavior. This is a critical feature for future use in living samples.

4 Discussion and Outlook

Since the first demonstration of RESOLFT with an RSFP[18], the method was applied in living cells and even whole organisms[37–39,65]. In addition to RSFPs, synthetic photoswitchable labels were employed for RESOLFT, whereby their application was limited to artificial structures[72,73]. In the present study the possibilities to label and image biological structures with diarylethene-based reversibly photoswitchable fluorophores in purely aqueous solutions were evaluated and demonstrated for the first time. Furthermore, the photophysical properties of these fluorophores were compared with two RSFPs frequently applied in RESOLFT nanoscopy.

4.1 Reversibly photoswitchable fluorescent proteins

The photophysical ensemble switching properties of the two RSFPs rsEGFP[37] and rsEGFP2[39] were characterized. The results of this characterization shall be discussed in the following.

The precise determination of the fluorescence background after off-switching and the switching kinetics of a photoswitchable label is necessary for quantitative analysis of high-resolution RESOLFT images. This knowledge may even allow to determine the number of emitters involved in the imaging process[116].

It was shown that the observable off-switching kinetics and the residual fluorescence after off-switching of an ensemble of rsEGFP and rsEGFP2 are altered depending on the used illumination method (Figure 3.2). This originates from the location-dependent intensity profile in case of the illumination with a diffraction-limited PSF causing a superposition of different local off-switching kinetics. This is particularly pronounced in thick samples since the observed properties would be altered significantly due to the axial decrease of intensity in the PSF of a focused illumination.

These effects are prevented in case of an illumination with an uniform intensity profile. Therefore it is of advantage to use a spatially uniform illumination and thin samples (i.e. a thin layer) if the purpose of the study is to analyze the switching kinetics and the fluorescence background after off-switching of the labels.

The number of on/off-cycles a photoswitchable label can undergo before it is transferred to a permanent dark state influences the achievable optical resolution in RESOLFT imaging as well as the possibility for long term observations. For rsEGFP and rsEGFP2, the number of switching cycles till half of the initial fluorophores were bleached was measured to be 1100 and 1550 cycles, respectively (Figure 3.3). The reported numbers are ~ 1000 for rsEGFP and ~ 2000 for rsEGPF2[37,39]. The difference to the data presented in this thesis are likely related to differences in sample preparation and experimental conditions, as already noted by Grotjohann et al.[39]. The data in this study was acquired using light at $\lambda_{\mathrm{act}} = 375\,\mathrm{nm}$ to photoswitch the non-fluorescent form to the fluorescent form. The non-fluorescent form of rsEGFP features an absorption maximum at $\lambda_{\mathrm{abs}} = 396\,\mathrm{nm}$, whereas the absorption maximum of the non-fluorescent form of rsEGFP2 is located at $\lambda_{\mathrm{abs}} = 408\,\mathrm{nm}$. This leads to larger required illumination intensities or longer illumination times of rsEGFP2 using $375\,\mathrm{nm}$ UV light to fully populate the fluorescent form. Thus, compared to the $405\,\mathrm{nm}$ light used previously, the higher energy of the $375\,\mathrm{nm}$ light may cause a higher probability for photobleaching in case of rsEGFP2.

The switching-kinetics of a photoswitchable label are particularly interesting in terms of image acquisition time, as commonly one of the switching steps represents the speed limiting factor. The off-switching kinetics of rsEGFP and rsEGFP2 were modeled by a biexponential decay since a monoexponential curve did not fit the data properly (Figure 3.1). This is in accordance with previous reports on different RSFPs, assigning this behavior to two different emissive states with different switching kinetics[117,118].

Both RSFPs exhibited an intensity-dependent switching to the non-fluorescent state. Grotjohann et al. showed that the difference in off-switching half time of rsEGFP and rsEGFP2 decreases with higher illumination intensities, indicating a rate limiting process such as the conformational change that the protein performs upon switching. The experiments by Grotjohann et al. were performed using focused illumination with intensities up to $400\,\mathrm{kW/cm^2}$ on living cells expressing Vimentin labeled with the respective protein[39]. In the current study, the convergence of the off-switching rates at increasing illumination intensities could not be reproduced on E. coli expressing the proteins in the cytosol. This could either be an effect caused by the differing sample preparation, the lower illumination intensities used in this work or the different illumination methods. As mentioned above, focused illumination causes different observable off-switching kinetics than uniform illumination, which could contribute to the measured differences.

The off-switching rates of rsEGFP and rsEGFP2 showed a saturation with rising intensities. This behavior could be well described by a three-state model with a transient fluorescent state T that gets populated before the off-switching (Figure 3.5). The proposed model requires a high rate from state T back to the initial fluorescent on-state of the proteins. With regard to the complexity of factors influencing the fluorescence behavior of the proteins[45], the transition state T is most likely a superposition of several different states corresponding to minimal displacements of amino acids in direct proximity to the chromophore.

The saturation of the off-switching rate is an essential factor in terms of imaging. On the one hand, increasing the power of the depletion beam would cause higher photobleaching without shortening the overall imaging time. On the other hand, the fluorescence signal before switching off increases with the illumination intensity, which can be useful to increase the signal during the excitation. For future screening approaches it should be kept in mind that there is a limit for the switching speed of RSFPs. Concerning the phototoxicity for the specimen, it is desired to screen for protein variants with high off-switching rates in the intensity range where the response to the intensity is still linear.

For both RSFPs the residual fluorescence after off-switching depends only on the applied light dose independently of the applied intensity (Figure 3.4). This indicates that in the intensity range of up to $23\,\mathrm{kW/cm^2}$ no molecular states are populated or generated which would cause additional non-switchable background.

As one of the most important characteristic of a fluorophore, the fluorescence lifetime (Figure 3.6) of rsEGFP is consistent with previously reported values ($\tau = 1.7\,\mathrm{ns}$). In contrast, the value for rsEGFP2 is substantially different, as the decay was previously described as being monoexponential with $\tau = 1.6\,\mathrm{ns}$[62]. However, a monoexponential decay did not fit the measurements in this study. In this context, it should be noted that the fluorescence lifetime of a fluorophore can be altered by a range of factors like pH or viscosity of the surrounding medium[27,119]. Hence, the fluorescence lifetime of rsEGFP2 may be altered due to attachment to a cellular structure compared to unbound protein in the cytosol of *E. coli*. Furthermore, the amplitude of the very short decay time of rsEGFP2 represents only $18\,\%$ of the total signal. At low photon count rates, this could be easily covered by noise.

In summary, the photophysical characterization of ensembles of rsEGFP and rsEGFP2 with a uniform illumination profile revealed the dependence of the observable off-switching kinetics on the type of illumination and the saturation of

the off-switching rate already at comparatively low intensities. Recently presented RSFPs suitable for RESOLFT nanoscopy like rsFolder [120] and rsGreens [121] should also be evaluated for this potential behavior.

4.2 Fluorescent diarylethenes without linker

The fluorescent diarylethenes *me*DAE and *m*IDAEs represent reversibly photoswitchable fluorescent molecules without a specialized linker to label structures of interest. Therefore, the photophysical properties of these diarylethenes were examined in artificial liposomes to spatially restricted their motion during the measurements.

*me*DAE showed a linear dependence of the off-switching rate and illumination intensity (Figure 3.10). This supports the energy surface model of diarylethenes outlined in Figure 1.4, indicating that the decay from the closed to the open form occurs directly from the S_1 state without intermediate states.

In general *me*DAE and the *m*IDAEs showed similar photoswitching characteristics (Table 3.1), apart from the off-switching rate, which is ten times faster for the *m*IDAEs compared to *me*DAE. It has to be noted that the liposomes, although allowing photoswitching of the diarylethenes under microscopy conditions, present a heterogeneous environment to the fluorophores. This can have effects on the photokinetics that are difficult to estimate. Hence, whether the faster switching of the mIDAEs originates from the ethyl groups in position C2(2′) or the added myo-inositols remains uncertain. The water-soluble myo-inositols may allow for effective photoswitching if the fluorophores are exposed to the solvent rather than being associated with the lipids. This could lead to a higher off-switching rate of the observed ensemble kinetic.

A reliable detection of the photophysics in aqueous solution under conditions present in a confocal microscope could not be performed due to the low water-solubility in case of *me*DAE and the lack of a method to spatially fix these fluorophores.

4.3 Bioconjugateable fluorescent diarylethenes

The low water solubility of diarylethenes so far prevented their use in aqueous solution and thus also their use as markers for cellular structures. The diarylethenes EBT1 and EBT2 presented in this work allow this possibility due to their enhanced

water solubility and the availability of an NHS-ester to bind to biomolecules. The properties of EBT1 and EBT2 (Table 3.2) were significantly improved in aqueous solution compared to other fluorescent diarylethenes. In general, reports on fluorescent water-soluble diarylethene derivatives are rare, whereby in these studies the fluorescence emerged only in nanoaggregates of the particular compounds[100,122] or was very weak[123,124]. Previous studies mainly report on measurements in non-polar solvents like 1,4-dioxane[95,112] or in ethyl acetate[86,87,125]. In these solvents high fluorescent quantum yields of up to 85 % were described[95]. Beside the fluorescence quantum yield, the quantum yields for the cyclization (on-switching) and the cycloreversion (off-switching) are of importance as they stipulate the amount of light that has to be applied to induce the respective reaction. With regard to the application in microscopy, a negative switching label, where off-switching and fluorescence emission are two concurrent processes, the quantum yield for the off-switching should ideally be in the range of 0.1 to 1 % of the fluorescence quantum yield to allow a sufficient number of photon emissions per cycle. Taking into account that the fluorescence detection efficiency of a confocal microscope is limited to about 10 %,[†] about 10 to 100 photons can be detected per fluorophore before it switches to the non-fluorescent state. However, if the number of emitted photons before off-switching exceeds 10^3, unnecessarily high illumination doses are required to achieve the cycloreversion.

For fluorescent diarylethenes in non-polar solvents, cycloreversion quantum yields below 10^{-3} have been reported[95,112], whereas non-fluorescent diarylethenes showed quantum yields from 10^{-4} to 0.4 for the cycloreversion in aqueous solution.[96,103,126].

In the present study, the EBT fluorophores showed cyclization yields $\gtrsim 0.25$, cycloreversion yields $\gtrsim 2.6 \times 10^{-3}$ and fluorescence quantum yields of ~ 70 % in methanol which were largely retained in aqueous solution due to the attached carboxyl groups. The quantum yields for the cyclization and cycloreversion were reduced less in PBS compared to methanol for EBT2 than for EBT1. Apparently, the additional water-soluble groups of EBT2 provide better shielding against the impacts of the polar solvent[112,127].

The brightness of the EBT-fluorophores upon excitation with 488 nm light was calculated as the product of the molar extinction coefficient ϵ at the excitation wavelength

---

[†]The maximal detection efficiency of a confocal microscope of ~ 10 % is estimated from the collection efficiency of a 1.4 NA oil immersion objective lens of ~ 30 %, the detection efficiency of single-photon detectors of ~ 50 % and additional losses caused by transmission through optical elements like dichroic mirrors, lenses and filters.

and the determined quantum yield. EBT2 is 26 % brighter than EBT1, similar to the fluorescent proteins rsEGFP and rsEGFP2 that are 44 % and 41 % brighter than EBT1, respectively [37,39].

The EBT fluorophores were successfully coupled to antibodies and used in immunostaining protocols to label different cellular structures in Vero cells (Figures 3.16, A.3 and A.4). The cytoskeletal proteins α-Tubulin and Vimentin were highly specifically stained. Hence, the attachment of the fluorophores to the antibodies did not impair the antibodies' selectivity. However, staining a protein of the nuclear pore complex (NUP153) caused a certain amount of unspecific background in the samples. This could originate from the fact that staining of this protein requires the cell membranes to mostly stay intact. Apparently, the EBT2 fluorophores interact with cellular membranes (Figure A.4), which was also reported for several commercial fluorophores, like Atto550, Alex647N and Cy3 [128].

The complete on-switching of the EBT fluorophores can be performed in $\sim 20\,\mu s$ with 375 nm light at an intensity of $0.8\,kW/cm^2$. This is five times faster compared to rsEGFP, which needs $100\,\mu s$ at comparable intensities [37], and in the range of rsEGFP2 [39]. It was shown that for the fluorophores no additional time is needed to perform the ring-closure reaction after illumination with the UV light. It can therefore be assumed that in this time-regime no intermediate transition state exists, unlike described for certain RSFPs [42,129].

The off-switching curve of both EBTs required a description by biexponential decays (Figure 3.17). Concerning the rather simple structure of the EBT fluorophores, it may be assumed that the off-switching process can be described by a single rate. The application of uniform illumination within the whole detection volume assured that the experimentally observable decay was not influenced by the superposition of different light intensities. A possible explanation for the biexponential decay could be a metastable dark state that gets populated by the excitation light out of the closed-form isomer. A delayed recovery from that state followed by its off-switching attenuates the overall kinetic and could explain the second characteristic time in the exponential decay. The fit suggests that $\sim 20\,\%$ of the fluorophores are transferred to this assumed dark state and populating this state and subsequent off-switching takes five times longer than the direct off-switching to the non-fluorescent form (Table 3.3). This dark state could be a long lived triplet state of the diarylethenes, many times larger than triplet state lifetimes of organic fluorophores that are in the range of several microseconds [130].

The photostability of a fluorescent marker is a crucial property for imaging. In case of a reversibly photoswitchable fluorophore, the photostability refers primarily to the number of on-/off-cycles that the molecule can withstand. The presented EBT fluorophores exhibit about 10 to 20 full switching cycles till half of the initial fluorescence is bleached. The photobleaching was not reduced when the illumination was reduced to light doses where the residual fluorescence after off-switching had decayed to a value twice as high as the minimal possible value. This indicates that the reduced absorption cross section of the fluorophores in their non-fluorescent form efficiently prevents from photobleaching. The photobleaching scaled linearly with the applied light dose, but no dependence was identified solely on the light intensity. This indicates that in the tested intensity regime, the primary path for photobleaching of the EBT-fluorophores with the excitation light occurs during the ring-opening reaction, rather than from higher exited states.

The number of possible switching cycles of the EBT fluorophores is far below the reported values of diarylethenes showing 10000 cycles with minor loss in fluorescence in non-polar solvents and solids[85]. In the present study, the measurements were performed in aqueous solution which sets considerably differently requirements on the fluorophores. In general, the process of solvent-dependent photobleaching is still insufficiently understood. Common theories state that photobleaching is predominantly induced by molecular oxygen through direct interaction with the fluorophore and generation of free radicals in solution[131]. In addition to dissolved molecular oxygen, reactive oxygen species are produced by irradiation[132], causing a higher probability for photobleaching upon interaction with fluorophores. Moreover, photobleaching can also occur from higher exited states through two photon absorption[133,134]. In case of photoswitchable fluorophores, the observable loss of fluorescence can furthermore be assigned to two different reactions: bleaching from the fluorescent on-state and modification of the fluorophore in such a way that it can not be switched to the fluorescent state any more. The dominant mechanism for the photobleaching of the EBT fluorophores in aqueous solutions, either a perturbation of the photochromism of the molecules or their fluorescence capability or a combination of both, could not be identified within the scope of this thesis.

Both EBT fluorophores showed a linear dependence of the off-switching rate and the applied intensity (Figure 3.18), which as in the case of *me*DAE supports the energy surface model of diarylethenes (Figure 1.4). Due to the simple molecular structure of the molecules, it can be assumed that this linear correlation persists

for intensities above $25\,\mathrm{kW/cm^2}$, at least if the population of short-lived dark states does not grow over-proportional.

The residual fluorescence after off-switching decreased for both EBT fluorophores with increasing illumination intensity. A possible explanation could be the population of a dark state. As the applied light dose was kept constant, the duration for the illuminations was reduced with increasing intensity. During the extended time the molecules could return more often from such a dark state resulting in a higher residual fluorescence after off-switching. It is also conceivable that higher intensities cause a more efficient switching to the off-state by absorption of a second photon in the excited state. However, this behavior has so far only been described for picosecond-pulsed lasers with high peak intensities of $7 \times 10^6\,\mathrm{kW/cm^2}$ [135,136] and is rather unlikely at the intensities used in this work. Further experiments are needed to elucidate which one of the two hypotheses is more probable.

RESOLFT imaging

The EBT fluorophores were successfully used for RESOLFT nanoscopy of different biological structures in fixed mammalian cells (Figures 3.19, 3.20, A.3 and A.4). The short on-switching times of about $20\,\mu\mathrm{s}$ and the off-switching times to $1/e$ of the initial fluorescence of less than $350\,\mu\mathrm{s}$ allowed imaging in the timescale of previously reported implementations of RESOLFT [37,39].

Based on the mentioned requirements for a RESOLFT label (see subsection 1.5.1), the performance in high resolution imaging of the EBT fluorophores can be estimated. With 11 and 22 full switching cycles till half of the initial fluorescence is bleached for EBT1 and EBT2, respectively, a maximal 1.7- to 2.3-fold improvement of the lateral resolution can be expected according to Equation 1.4, whereas the values of the relative residual fluorescence after off-switching of 0.05 for EBT1 and 0.02 for EBT2 would allow to improve the lateral spatial resolution 4.5 to 7.0 times (Equation 1.5). The resolution increase achieved in the RESOLFT measurements of 2.3-fold was therefore close to the estimated performance and mainly limited by photobleaching. Here it should be noted that the visible size of the imaged structures was increased due to the applied staining method. In case of Tubulin, the spatial extent of the antibodies can lead to an extension of the structure size from $25\,\mathrm{nm}$ to approximately $55\,\mathrm{nm}$ [‡].

[‡]A more detailed description of the molecule sizes in fluorescence microscopy can be found in section A.4.

To date, the only other demonstration of RESOLFT nanoscopy with synthetic fluorophores on biological structures used a 'reporter'-'activator' dye pair of Cy3 and Alexa647 in immunostained mammalian cells[74]. This dye-pair needed 1 % v/v of primary thiol (β-mercaptoethylamine) and potassium iodide added to the buffer to control the photoswitching between its fluorescent and non-fluorescent states. These conditions allowed a residual fluorescence of ∼5 % and an off-switching time during imaging of 15 ms at 4 kW/cm² with 658 nm light. A resolution of about 75 nm was shown on nuclear pore complexes with labeled NUP153. Although stating that 20 % of the fluorophores were bleached during the pump-probe-measurements, no comments were made about the photobleaching during the imaging process. The used illumination intensities were comparably low but caused long off-switching times. The disadvantages of using a 'reporter'-'activator' pair is that optimal conditions have to be set for two different fluorophores and the exploited dark states are metastable. Additionally, this type of fluorophore pair is unlikely to be applicable in live-cell imaging as the required thiols are highly cytotoxic[137].

The EBT fluorophores presented in this work feature clear advantages such as higher imaging speeds, stability of the fluorescent and non-fluorescent form, photochromism and functionality in purely aqueous buffers. The extensive photobleaching encountered prevented repeated imaging of the same region of interest. The acquisition times for a RESOLFT image were in the range of 1 to 5 minutes for a 6 μm × 6 μm area using 30 nm pixels with the EBT fluorophores. Assuming the same conditions, this is significantly faster than the first demonstrations of RESOLFT with Dreiklang (> 30 minutes)[38], rsEGFP (∼ 7 to 15 minutes)[37] or the dye pair of Cy3 and Alexa647 (∼ 10 minutes)[74], but slower than for rsEGFP2 (∼ 5 to 20 seconds)[39], rsFolder (∼ 30 seconds)[120] or rsGreen (∼ 20 seconds)[121].

The high resolution in the confocal comparison images (Figures 3.19c and 3.20c), can be explained by the two-step imaging process. Every position was sampled by the activation with a 355 nm beam and the excitation with the 488 nm beam. Therefore the confocal resolution was not determined by the excitation beam alone but also by the spatial extent of the on-switched area, defined by the size of the activation beam. In total, the observable resolution is the product of the PSFs of activation, excitation and detection resulting in an effective PSF. Assuming ideal diffraction-limited PSFs and a confocal pinhole size of one Airy unit, this would result in a 120 nm FWHM of the effective PSF for the given laser lines and a detection centered at 525 nm. However, this value is strongly dependent on the size of the

activation 355 nm PSF. Standard optics are not optimized for wavelengths below 400 nm causing the 355 nm PSF to be significantly larger (FWHM = 180 nm) than the theoretically possible value. This results in a realistic effective confocal PSF with a FWHM of about 145 nm. The confocal images were further blurred because the fluorophores were not completely switched to the non-fluorescent form during the excitation step.

Altogether, EBT2 exhibited superior performance compared to EBT1 in all examined aspects in aqueous solution. Obviously, the additional water-solubilizing groups facilitated better preservation of the photochromic and fluorescence properties in the polar environment.

RSFPs compared to EBT fluorophores

The currently used RSFPs in RESOLFT nanoscopy offer more than 1000 switching cycles and can be genetically encoded to label structures of interest. The advantage of the RSFPs is that their chromophore is encased by a barrel of amino acids which shields it from direct interactions with solvent molecules and confers water solubility. This feature enabled resolutions of down to 45 nm in living cells[39] and 49 nm in living specimens[65] with rsEGFP2. Opposed to that, organic fluorophores are directly exposed to the solvent and the contained reactive species, apparently rendering them more prone to photobleaching. However, the brightness of the EBT fluorophores is comparable to or even higher than for most RSFPs[45], whereby the total number of emitted photons per molecule is restricted by their photostability. The diarylethene-based EBTs have clear advantages over RSFPs in terms of photo-switching background and long term stability of the fluorescent and non-fluorescent forms, as in the case of proteins, one of the two states is typically the equilibrium state[42].

Due to their switching fatigue, the presented EBT fluorophores are still inferior to RSFPs but give rise to the expectation that future developments will put forth synthetic fluorophores that can compete with or outperform RSFPs.

4.4 Outlook

The properties of the investigated EBT fluorophores give rise to a range of possible applications and implementations.

The imaging speed of negative switching labels for RESOLFT nanoscopy is mainly dominated by the illumination step with the doughnut shaped beam, which consumes 80 to 95 % of the acquisition time. Effective shortening of this speed limiting step could dramatically increase the imaging speed. It was reported that a stepwise two-photon excitation can dramatically increase the cycloreversion reaction rate of different diarylethene derivatives [135,136]. The cycloreversion quantum yield using two-photon excitation was reported to be around 50 % [136]. Compared to the values for the cycloreversion yield presented in this work, these values are three orders of magnitude higher. This could lead to a massively reduced off-switching time down to the range of μs. Albeit, the reported values were acquired in a non-polar solvent (n-hexane) and it is not possible to anticipate how the presented EBT fluorophores would react to two-photon excitation in aqueous environments, especially concerning photobleaching from higher excited states [133].

Another possibility to speed up the image acquisition is the massive parallelization of the illumination steps, which was up to now only shown for RSFPs [63,138]. The EBT fluorophores presented in this study and possible successors are suitable for massively parallelized RESOLFT nanoscopy giving the chance to speed up the imaging process by several orders of magnitude [138].

A further approach to improve the acquisition speed and additionally the attainable spatial resolution lies in the combination of multiple off state transitions as in protected STED [139]. In this approach the fluorophores are protected from the STED light by prior transition to a state that shows minor absorption for the depletion wavelength. Possibly, the EBT fluorophores are more resistant to the STED light than RSFPs. However, the low number of possible switching cycles of EBTs would considerably reduce the protecting effect.

Diarylethenes can not only be used for high resolution imaging based on coordinate-targeted switching. The applicability of diarylethene derivatives for coordinate-stochastic nanoscopy methods was demonstrated on artificial nanostructures in different polymers [140,141]. Beyond these proofs of concept, it was shown recently that variants of the EBT fluorophores presented in this work can be successfully used in STORM on fixed mammalian cells using only aqueous solutions as buffer. These molecules were modified with a methoxy group and showed spontaneous on-switching

under illumination with blue light [142]. This observation could lead to targeted modifications of fluorophores for different high resolution microscopy methods.

One of the greatest strengths of fluorescence microscopy is the non-invasive observation of processes in living specimen. For this purpose, the fluorophores used have to be compatible with live-cell imaging. The possibilities of bioorthogonal reactions like used with SNAP, CLIP or Halo-tag [68–70] fusion proteins should be evaluated for fluorescent diarylethenes. However, this would require a cell-permeable fluorophore with a corresponding linker. In this context, different functional groups which increase the water-solubility of the compounds should be evaluated. Most recently, Takagi *et al.* [143] reported on the prosperous use of sodium sulfonate groups. Currently, the wavelength needed for the cyclization reaction of the EBT fluorophores is in the range of 350 nm. In case of live-cell imaging, this could cause photostress to the cells. It could be of advantage if the whole absorption spectrum of the fluorophores, of the open-form as well as the closed-form isomer, was red-shifted to avoid illuminations with wavelengths in the near UV.

In conclusion, RESOLFT with man-made photoswitchable fluorescent labels in aqueous solution on mammalian cells was demonstrated for the first time. The findings gained in this thesis can be used to further improve synthetic fluorophores and to optimize them for the use in living cells.

A Appendix

A.1 Three-state model for RSFPs

The model shown in Figure 3.5 depicts three states. It can be simplified to a two-state model, as no rate back to the ON- or T-state from the OFF-state is assumed. The rate equations of the simplified model can be written in their matrix form

$$\begin{pmatrix} \dot{P}_{\mathrm{ON}}(t) \\ \dot{P}_{\mathrm{T}}(t) \end{pmatrix} = \underbrace{\begin{pmatrix} -k_{\mathrm{T}} & k_{\mathrm{B}} \\ k_{\mathrm{T}} & -k_{\mathrm{B}} - k_{\mathrm{dark}} \end{pmatrix}}_{Q} \underbrace{\begin{pmatrix} P_{\mathrm{ON}}(t) \\ P_{\mathrm{T}}(t) \end{pmatrix}}_{P(t)} \tag{A.1}$$

with the probability P of residing in a certain state after the time interval t, the rate $k_{\mathrm{T}} = \alpha I_{\mathrm{exc}}$ from the ON- to the T-state linearly depending on the excitation intensity I_{exc}, the constant return rate from the T- to the ON-state k_{B} and the constant rate from the T- to the OFF-state k_{dark}.

A solution to this system of differential equations can be derived from the matrix exponential of the transition matrix Q:

$$P(t) = \exp(Qt) \cdot P(0) = \begin{pmatrix} \dfrac{B+C}{2} + D & k_{\mathrm{B}} \cdot \dfrac{B-C}{A} \\ k_{\mathrm{T}} \cdot \dfrac{B-C}{A} & \dfrac{B+C}{2} - D \end{pmatrix} \cdot P(0) \tag{A.2}$$

with

$$\begin{aligned} A &= \sqrt{(k_{\mathrm{B}} + k_{\mathrm{dark}} + k_{\mathrm{T}})^2 - 4 k_{\mathrm{dark}} k_{\mathrm{T}}} \\ B &= \exp(-(k_{\mathrm{B}} + k_{\mathrm{dark}} + k_{\mathrm{T}} - A)\frac{t}{2}) \\ C &= \exp(-(k_{\mathrm{B}} + k_{\mathrm{dark}} + k_{\mathrm{T}} + A)\frac{t}{2}) \\ D &= \frac{B-C}{2A}(k_{\mathrm{B}} + k_{\mathrm{dark}} - k_{\mathrm{T}}) \end{aligned} \tag{A.3}$$

It is assumed that initially, when no excitation light is applied, all molecules are in the ON-state ($P_{\text{ON}}(0) = 1$). The time evolution of the probability of residing in the ON- or the T-state can then be written as:

$$P_{\text{ON}}(t) = \frac{B + C}{2} + D$$
$$P_{\text{T}}(t) = k_{\text{T}} \cdot \frac{B - C}{A} \tag{A.4}$$

Since the molecules either reside in the ON- , T- or OFF-state the population of the OFF-state can be described as

$$
\begin{aligned}
P_{\text{OFF}}(t) &= 1 - P_{\text{ON}}(t) - P_{\text{T}}(t) \\
&= 1 - \frac{C}{2}\left(1 - \frac{(k_{\text{B}} + k_{\text{dark}} + k_{\text{T}})}{A}\right) - \frac{B}{2}\left(1 + \frac{(k_{\text{B}} + k_{\text{dark}} + k_{\text{T}})}{A}\right)
\end{aligned} \tag{A.5}
$$

The factor A can also be written as

$$A = (k_{\text{B}} + k_{\text{dark}} + k_{\text{T}})\sqrt{1 - \frac{4k_{\text{dark}}k_{\text{T}}}{(k_{\text{B}} + k_{\text{dark}} + k_{\text{T}})^2}} \tag{A.6}$$

The fraction inside the square root is small for conditions like $k_{\text{B}} \gg k_{\text{dark}} \cdot k_{\text{T}}$ or $k_{\text{T}} \gg 1$. Under these conditions it is reasonable to approximate the term with the Taylor series $\sqrt{1 - x} \approx 1 - \frac{x}{2}$ [144].

$$
\begin{aligned}
A &\approx (k_{\text{B}} + k_{\text{dark}} + k_{\text{T}})\left(1 - \frac{2k_{\text{dark}}k_{\text{T}}}{(k_{\text{B}} + k_{\text{dark}} + k_{\text{T}})^2}\right) \\
&= k_{\text{B}} + k_{\text{dark}} + k_{\text{T}} - \frac{2k_{\text{dark}}k_{\text{T}}}{k_{\text{B}} + k_{\text{dark}} + k_{\text{T}}}
\end{aligned} \tag{A.7}
$$

This leads to

$$\frac{k_{\text{B}} + k_{\text{dark}} + k_{\text{T}}}{A} \approx \frac{k_{\text{B}} + k_{\text{dark}} + k_{\text{T}}}{k_{\text{B}} + k_{\text{dark}} + k_{\text{T}} - \dfrac{2k_{\text{dark}}k_{\text{T}}}{k_{\text{B}} + k_{\text{dark}} + k_{\text{T}}}} \approx 1 \tag{A.8}$$

because the term $\dfrac{2k_{\text{dark}}k_{\text{T}}}{k_{\text{B}} + k_{\text{dark}} + k_{\text{T}}}$ is very small.

Inserting Equation A.8 into Equation A.5 results in

$$P_{\text{OFF}}(t) \approx 1 - B \quad \text{with} \quad P_{\text{ON}}(t) + P_{\text{T}}(t) \approx B \tag{A.9}$$

Since only the fluorescence is detected and the fluorescent states ON and T are not distinguishable, the experimentally observable off-switching rate can be derived as

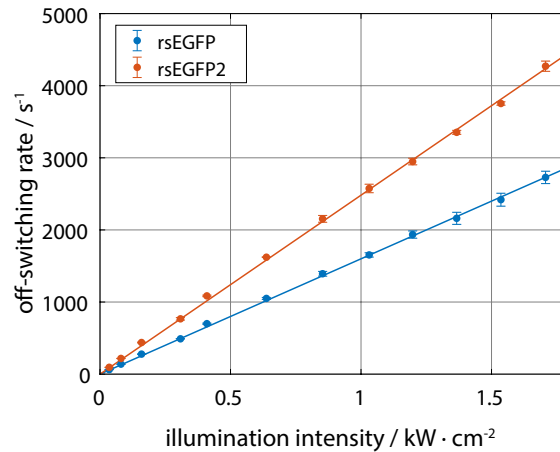$$k(I_{\text{exc}}) = \frac{k_{\text{B}} + k_{\text{dark}} + k_{\text{T}} - A}{2} \tag{A.10}$$

Inserting Equation A.7 into Equation A.10 results in

$$
\begin{aligned}
k(I_{\text{exc}}) &\approx \frac{k_{\text{dark}} k_{\text{T}}}{k_{\text{B}} + k_{\text{dark}} + k_{\text{T}}} = \frac{k_{\text{dark}} \alpha I_{\text{exc}}}{k_{\text{B}} + k_{\text{dark}} + \alpha I_{\text{exc}}} \\[2ex]
&= \frac{\alpha}{k_{\text{B}} + k_{\text{dark}}} \frac{I_{\text{exc}}}{1 + \dfrac{\alpha}{k_{\text{B}} + k_{\text{dark}}} I_{\text{exc}}} k_{\text{dark}} \\[2ex]
&= \frac{I_{\text{exc}}/I_{1/2}}{1 + I_{\text{exc}}/I_{1/2}} k_{\text{dark}} \quad \text{with} \quad I_{1/2} = \frac{k_{\text{B}} + k_{\text{dark}}}{\alpha}.
\end{aligned}
\tag{A.11}
$$

For $k_{\text{B}} \gg k_{\text{dark}}$, it follows $I_{1/2} \approx \dfrac{k_{\text{B}}}{\alpha}$.

A.2 Intensity dependent properties of rsEGFP and rsEGFP2 at low illumination intensities

Figure A.1: Off-switching rate of rsEGFP (blue) and rsEGFP2 (orange) as function of the illumination intensity. Solid lines show a linear fit to the data. All data were recorded in *E. coli* fixed on agarose gel expressing the respective protein in the cytosol. Error bars represent twice the standard deviation.
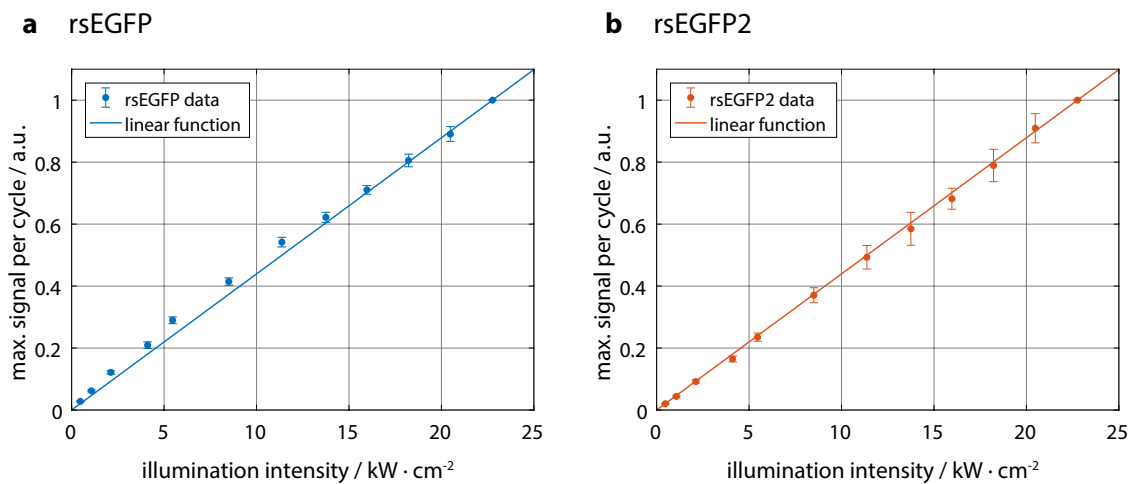

Figure A.2: Maximal fluorescence signal per off-switching cycle depending on the illumination intensity for rsEGFP (**a**) and rsEGFP2 (**b**). Normalized to the maximal value. Data extracted from the same data set as shown in Figure 3.4. All data were recorded in *E. coli* fixed on agarose gel expressing the respective protein in the cytosol. Error bars represent twice the standard deviation.

A.3 RESOLFT imaging with EBT2
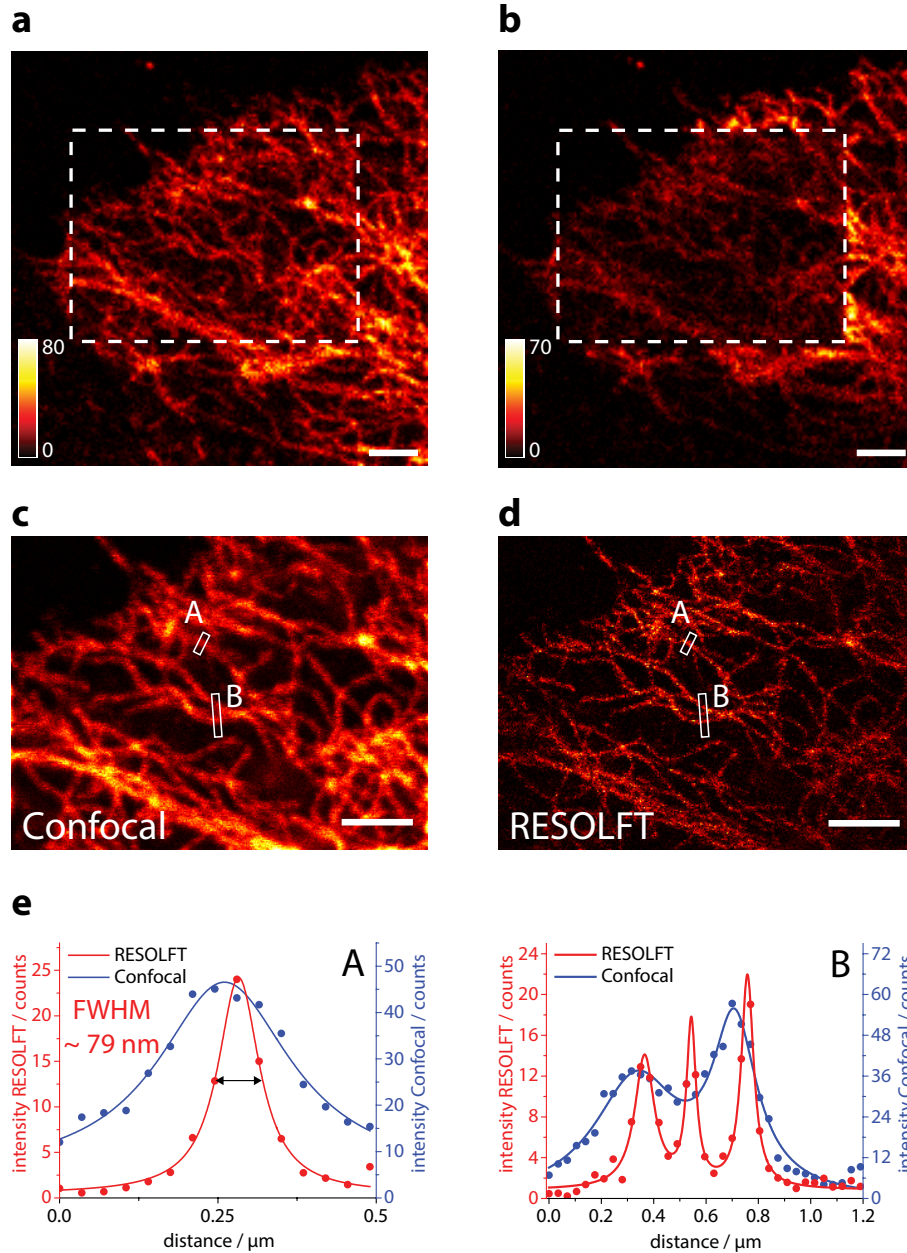
Figure A.3: Confocal overview of fixed Vero cells immunostained with primary antibodies against Vimentin and with EBT2 attached to the secondary antibodies before (**a**) and after (**b**) the high resolution imaging. Confocal (**c**) and RESOLFT (**d**) image of the indicated area in **a** and **b**. The RESOLFT images were recorded before confocal images. Scale bars: 2 µm. All images show raw data and were performed with the settings described in subsection 3.3.4. **e:** Line profiles A and B (averaged over five adjacent lines) display the regions indicated in **c** and **d**. The data (dots) was fitted with a Lorentzian function (solid line) for the RESOLFT (red) and the confocal (blue) images. The FWHM determined on fit A is indicated by the small black arrow.
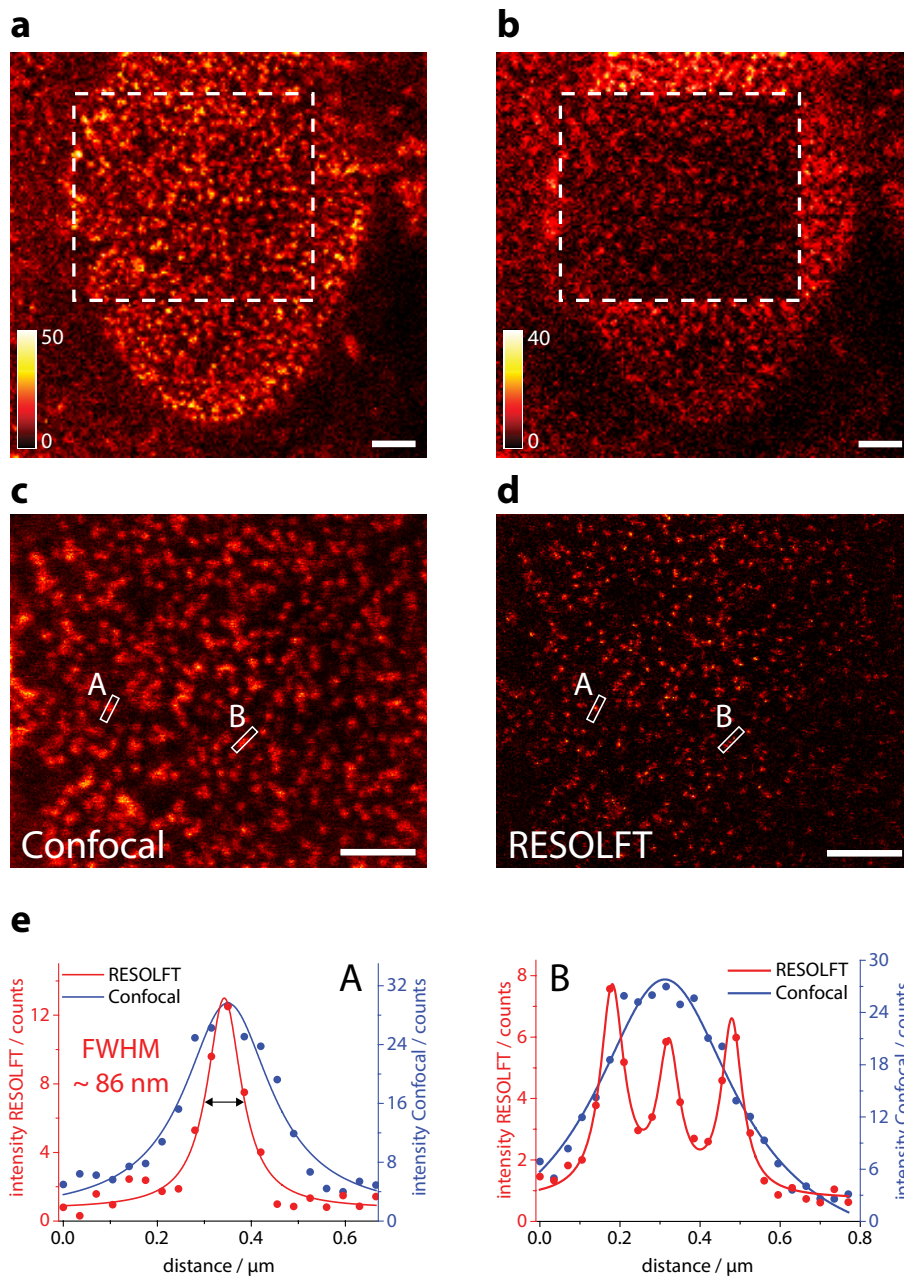
Figure A.4: Confocal overview of fixed Vero cells immunostained with primary antibodies against NUP153 and with EBT2 attached to the secondary antibodies before (**a**) and after (**b**) the high resolution imaging. Confocal (**c**) and RESOLFT (**d**) image of the indicated area in **a** and **b**. The RESOLFT images were recorded before confocal images. Scale bars: 2 µm. All images show raw data and were performed with the settings described in subsection 3.3.4. **e:** Line profiles A and B (averaged over five adjacent lines) display the regions indicated in **c** and **d**. The data (dots) was fitted with a Lorentzian function (solid line) for the RESOLFT (red) and the confocal (blue) images. The FWHM determined on fit A is indicated by the small black arrow.

Line Profile	FWHM / nm
1	72.7
2	79.3
3	75.8
4	78.8
5	74.1
6	74.2
Average	75.8 ± 3
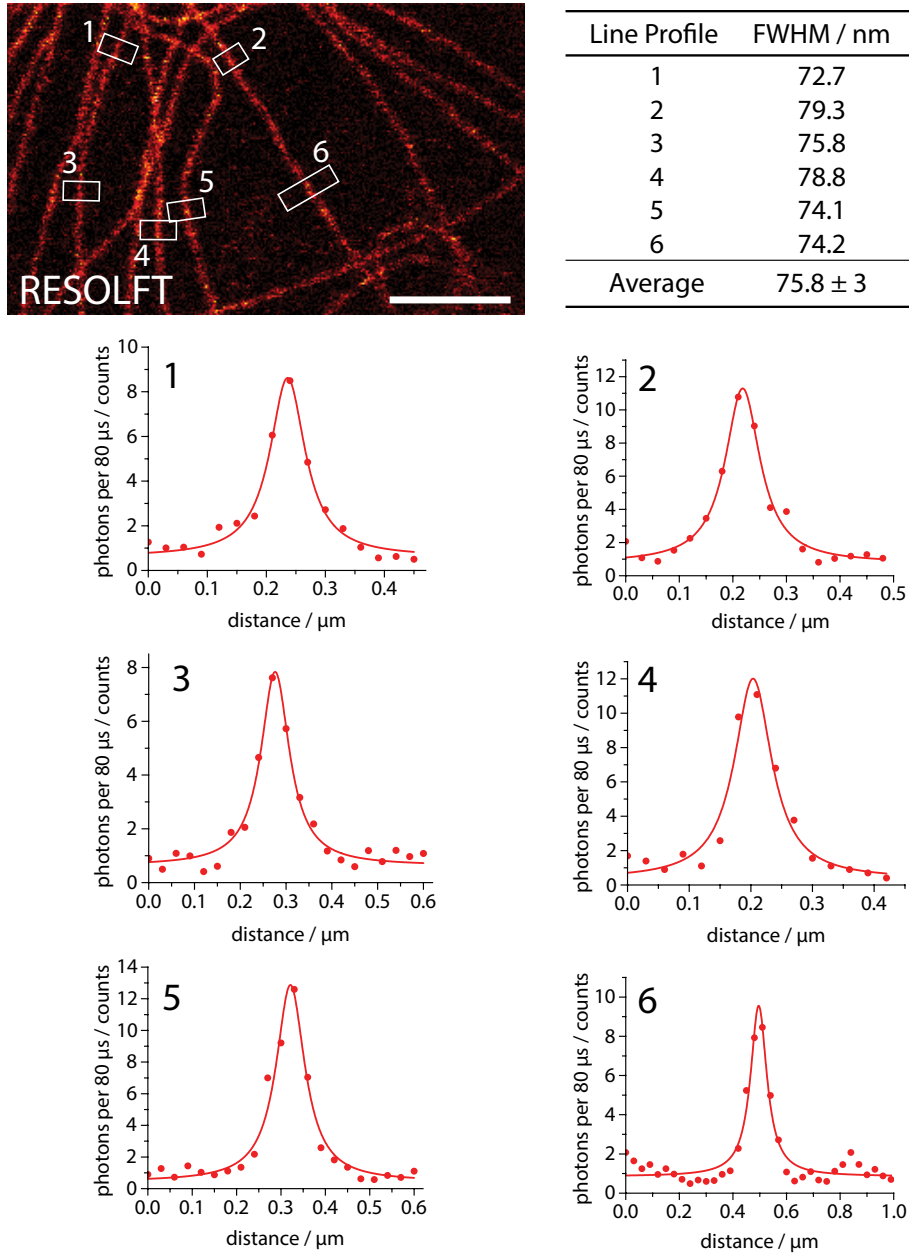
Figure A.5: Determination of achieved lateral image resolution in fixed Vero cells immunostained with primary antibodies against α-Tubulin and with EBT2 attached to the secondary antibodies. Line profiles 1-6 (averaged over ten adjacent lines) display the regions indicated in the RESOLFT image. The data (dots) was fitted with a Lorentzian function (solid line). The FWHM was determined on the fits. Scale bar: 2 μm. Image as shown in Figure 3.20d.

A.4 Molecule sizes in fluorescence microscopy

Figure A.6 shows the size of the target structure Tubulin and different labels used in fluorescence microscopy for a better understanding of the proportions. Tubulin polymerizes to form microtubules, a main part of the cytoskeleton, with an outer diameter of about 24 nm. Most commonly, the α-Tubulin subunit is targeted by immunofluorescence staining or tagging with a fluorescent protein. Immunoglobulin G (IgG), having a size of about 10 nm, is the most frequently used type of antibody to target structures of interest. Fluorescent molecules are conjugated to the antibody causing only a marginal increase in size. These antibodies can be used to directly bind the target molecule (primary) or to bind an unlabeled primary antibody. Thus, immunostained microtubules can have an effective diameter of up to 55 nm, depending on the staining method used. Fluorescent proteins offer the possibility to genetically tag the structures of interest. GFP-based fluorescent proteins all show a similar size of about 2 nm × 2 nm × 4 nm, given by the beta barrel structure consisting of eleven β-strands.
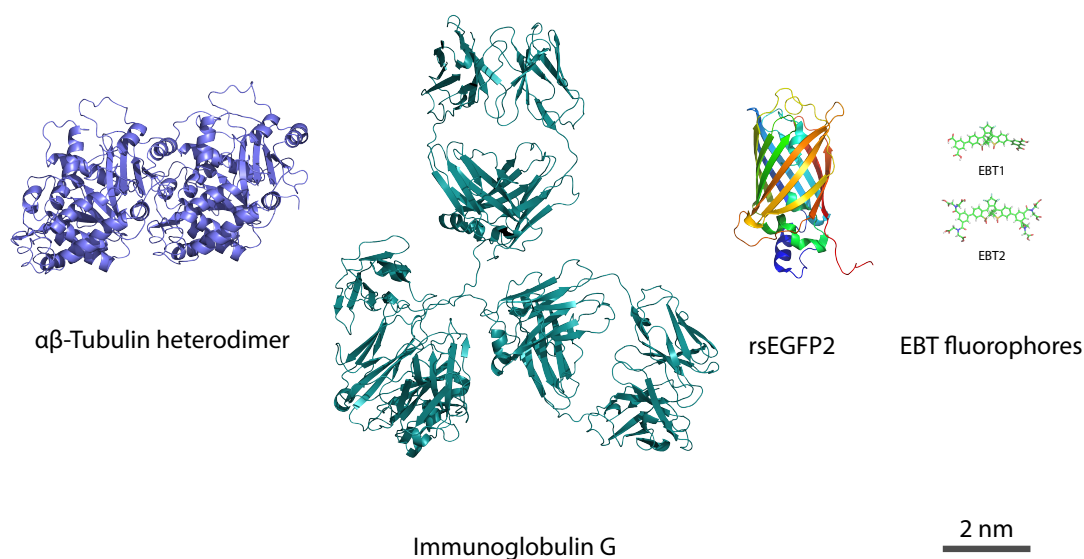
Figure A.6: Illustration of selected proteins and fluorophores involved in fluorescence imaging. From left to right: αβ-Tubulin heterodimer (1TUB)[145], whole immunoglobulin G (IgG) antibody (1IGY)[146], reversible fluorescent protein rsEGFP2 (5DTX)[120] and the fluorophores EBT1 (top) and EBT2 (bottom). The proteins are depicted as ribbon diagrams rendered with PyMOL (Schrödinger, New York, NY, USA) based on the stated crystallographic data taken from the Protein Data Bank (www.pdb.org). Tubulin dimer and IgG are representations of homologs of the actual proteins involved in immunostaining and are given for size comparison only.

Bibliography

[1] P. Mazzarello, A unifying concept: the history of cell theory, *Nature Cell Biology*, **1999**, 1(1), E13–E15.

[2] D. B. Murphy, *Fundamentals of light microscopy and electronic imaging*, John Wiley & Sons, New York, **2002**.

[3] S. H. D. Haddock, M. A. Moline and J. F. Case, Bioluminescence in the Sea, *Annual Review of Marine Science*, **2009**, 2(1), 443–493.

[4] T. Förster, Zwischenmolekulare Energiewanderung und Fluoreszenz, *Annalen der Physik*, **1948**, 437(1-2), 55–75.

[5] D. L. Dexter, A Theory of Sensitized Luminescence in Solids, *The Journal of Chemical Physics*, **1953**, 21(5), 836–850.

[6] G. G. Stokes, On the Change of Refrangibility of Light, *Philosophical Transactions of the Royal Society of London*, **1852**, 142, 463–562.

[7] M. Minsky, Microscopy apparatus, U.S. Patent, US 3013467 A, **1961**.

[8] E. Abbe, Beiträge zur Theorie des Mikroskops und der mikroskopischen Wahrnehmung, *Archiv für mikroskopische Anatomie*, **1873**, 9, 413–468.

[9] G. Airy, On the Diffraction of an Object-glass with Circular Aperture, *Transactions of the Cambridge Philosophical Society*, **1834**, 5, 283.

[10] J. W. Strutt, 3rd Baron Rayleigh, On the theory of optical images, with special reference to the microscope, *Philosophical Magazine Series 5*, **1896**, 42(255), 167–195.

[11] E. J. Ambrose, A Surface Contact Microscope for the study of Cell Movements, *Nature*, **1956**, 178(4543), 1194–1194.

[12] S. W. Hell and E. H. K. Stelzer, Fundamental improvement of resolution with a 4Pi-confocal fluorescence microscope using two-photon excitation, *Optics Communications*, **1992**, 93(5), 277–282.

[13] A. Egner, S. Jakobs and S. W. Hell, Fast 100-nm resolution three-dimensional microscope reveals structural plasticity of mitochondria in live yeast, *Proceedings of the National Academy of Sciences of the United States of America*, **2002**, 99(6), 3370–3375.

[14] S. W. Hell and J. Wichmann, Breaking the diffraction resolution limit by stimulated emission: stimulated-emission-depletion fluorescence microscopy, *Optics Letters*, **1994**, 19(11), 780–782.

[15] S. W. Hell, S. J. Sahl, M. Bates, X. Zhuang, R. Heintzmann, M. J. Booth, J. Bewersdorf, G. Shtengel, H. Hess, P. Tinnefeld, A. Honigmann, S. Jakobs, I. Testa, L. Cognet, B. Lounis, H. Ewers, S. J. Davis, C. Eggeling, D. Klenerman, K. I. Willig, G. Vicidomini, M. Castello, A. Diaspro and T. Cordes, The 2015 super-resolution microscopy roadmap, *Journal of Physics D: Applied Physics*, **2015**, 48(44), 443001.

[16] S. W. Hell, S. Jakobs and L. Kastrup, Imaging and writing at the nanoscale with focused visible light through saturable optical transitions, *Applied Physics A*, **2003**, 77(7), 859–860.

[17] S. W. Hell, Toward fluorescence nanoscopy, *Nature Biotechnology*, **2003**, 21(11), 1347–1355.

[18] M. Hofmann, C. Eggeling, S. Jakobs and S. W. Hell, Breaking the diffraction barrier in fluorescence microscopy at low light intensities by using reversibly photoswitchable proteins, *Proceedings of the National Academy of Sciences of the United States of America*, **2005**, 102(49), 17565–17569.

[19] S. W. Hell and M. Kroug, Ground-state-depletion fluorscence microscopy: A concept for breaking the diffraction resolution limit, *Applied Physics B*, **1995**, 60(5), 495–497.

[20] S. Bretschneider, C. Eggeling and S. W. Hell, Breaking the Diffraction Barrier in Fluorescence Microscopy by Optical Shelving, *Physical Review Letters*, **2007**, 98(21), 218103–218103.

[21] J. Keller, A. Schönle and S. W. Hell, Efficient fluorescence inhibition patterns for RESOLFT microscopy, *Optics Express*, **2007**, 15(6), 3361–3371.

[22] B. Harke, J. Keller, C. K. Ullal, V. Westphal, A. Schönle and S. W. Hell, Resolution scaling in STED microscopy, *Optics Express*, **2008**, 16(6), 4154–4162.

[23] S. W. Hell, M. Dyba and S. Jakobs, Concepts for nanoscale resolution in fluorescence microscopy, *Current Opinion in Neurobiology*, **2004**, 14(5), 599–609.

[24] T. A. Klar and S. W. Hell, Subdiffraction resolution in far-field fluorescence microscopy, *Optics Letters*, **1999**, 24(14), 954–956.

[25] T. A. Klar, S. Jakobs, M. Dyba, A. Egner and S. W. Hell, Fluorescence microscopy with diffraction resolution barrier broken by stimulated emission, *Proceedings of the National Academy of Sciences of the United States of America*, **2000**, 97(15), 8206–8210.

[26] M. Sednev, V. N. Belov and S. W. Hell, Fluorescent dyes with large Stokes shifts for super-resolution optical microscopy of biological objects: a review, *Methods and Applications in Fluorescence*, **2015**, 3(4), 042004.

[27] M. Y. Berezin and S. Achilefu, Fluorescence Lifetime Measurements and Biological Imaging, *Chemical Reviews*, **2010**, 110(5), 2641–2684.

[28] S. W. Hell, Far-Field Optical Nanoscopy, *Science*, **2007**, 316(5828), 1153–1158.

[29] P. Bingen, M. Reuss, J. Engelhardt and S. W. Hell, Parallelized STED fluorescence nanoscopy, *Optics Express*, **2011**, 19(24), 23716–23726.

[30] F. Bergermann, L. Alber, S. J. Sahl, J. Engelhardt and S. W. Hell, 2000-fold parallelized dual-color STED fluorescence nanoscopy, *Optics Express*, **2015**, 23(1), 211–223.

[31] S. T. Hess, T. P. K. Girirajan and M. D. Mason, Ultra-High Resolution Imaging by Fluorescence Photoactivation Localization Microscopy, *Biophysical Journal*, **2006**, 91(11), 4258–4272.

[32] E. Betzig, G. H. Patterson, R. Sougrat, O. W. Lindwasser, S. Olenych, J. S. Bonifacino, M. W. Davidson, J. Lippincott-Schwartz and H. F. Hess, Imaging Intracellular Fluorescent Proteins at Nanometer Resolution, *Science*, **2006**, 313(5793), 1642–1645.

[33] M. J. Rust, M. Bates and X. Zhuang, Sub-diffraction-limit imaging by stochastic optical reconstruction microscopy (STORM), *Nature Methods*, **2006**, 3(10), 793–796.

[34] G. T. Dempsey, J. C. Vaughan, K. H. Chen, M. Bates and X. Zhuang, Evaluation of fluorophores for optimal performance in localization-based super-resolution imaging, *Nature Methods*, **2011**, 8(12), 1027–1036.

[35] S. A. Jones, S.-H. Shim, J. He and X. Zhuang, Fast, three-dimensional super-resolution imaging of live cells, *Nature Methods*, **2011**, 8(6), 499–505.

[36] S.-H. Shim, C. Xia, G. Zhong, H. P. Babcock, J. C. Vaughan, B. Huang, X. Wang, C. Xu, G.-Q. Bi and X. Zhuang, Super-resolution fluorescence imaging of organelles in live cells with photoswitchable membrane probes, *Proceedings of the National Academy of Sciences of the United States of America*, **2012**, 109(35), 13978–13983.

[37] T. Grotjohann, I. Testa, M. Leutenegger, H. Bock, N. T. Urban, F. Lavoie-Cardinal, K. I. Willig, C. Eggeling, S. Jakobs and S. W. Hell, Diffraction-unlimited all-optical imaging and writing with a photochromic GFP, *Nature*, **2011**, 478(7368), 204–208.

[38] T. Brakemann, A. C. Stiel, G. Weber, M. Andresen, I. Testa, T. Grotjohann, M. Leutenegger, U. Plessmann, H. Urlaub, C. Eggeling, M. C. Wahl, S. W. Hell and S. Jakobs, A reversibly photoswitchable GFP-like protein with fluorescence excitation decoupled from switching, *Nature Biotechnology*, **2011**, 29(10), 942–947.

[39] T. Grotjohann, I. Testa, M. Reuss, T. Brakemann, C. Eggeling, S. W. Hell and S. Jakobs, rsEGFP2 enables fast RESOLFT nanoscopy of living cells, *eLife*, **2012**, 1, e00248.

[40] P. Dedecker, J. Hotta, C. Flors, M. Sliwa, H. Uji-i, M. B. J. Roeffaers, R. Ando, H. Mizuno, A. Miyawaki and J. Hofkens, Subdiffraction Imaging through the Selective Donut-Mode Depletion of Thermally Stable Photoswitchable Fluorophores: Numerical Analysis and Application to the Fluorescent Protein Dronpa, *Journal of the American Chemical Society*, **2007**, 129(51), 16132–16141.

[41] S. Wäldchen, J. Lehmann, T. Klein, S. van de Linde and M. Sauer, Light-induced cell damage in live-cell super-resolution microscopy, *Scientific Reports*, **2015**, 5, 15348.

[42] D. M. Shcherbakova, P. Sengupta, J. Lippincott-Schwartz and V. V. Verkhusha, Photocontrollable fluorescent proteins for superresolution imaging, *Annual Review of Biophysics*, **2014**, 43, 303–29.

[43] T. J. Chozinski, L. A. Gagnon and J. C. Vaughan, Twinkle, twinkle little star: Photoswitchable fluorophores for super-resolution imaging, *FEBS Letters*, **2014**, 588(19), 3603–3612.

[44] X. X. Zhou and M. Z. Lin, Photoswitchable fluorescent proteins: ten years of colorful chemistry and exciting applications, *Current Opinion in Chemical Biology*, **2013**, 17(4), 682–690.

[45] D. Bourgeois and V. Adam, Reversible photoswitching in fluorescent proteins: A mechanistic view, *IUBMB Life*, **2012**, 64(6), 482–491.

[46] W. Vandenberg, M. Leutenegger, T. Lasser, J. Hofkens and P. Dedecker, Diffraction-unlimited imaging: from pretty pictures to hard numbers, *Cell and Tissue Research*, **2015**, 360(1), 151–178.

[47] S. A. Hilderbrand, in *Live Cell Imaging: Methods and Protocols*, Ed. D. B. Papkovsky, Labels and Probes for Live Cell Imaging: Overview and Selection Guide, Humana Press, Totowa, NJ, **2010**; pp. 17–45.

[48] O. Shimomura, F. H. Johnson and Y. Saiga, Extraction, Purification and Properties of Aequorin, a Bioluminescent Protein from the Luminous Hydromedusan, Aequorea, *Journal of Cellular and Comparative Physiology*, **1962**, 59(3), 223–239.

[49] M. Chalfie, Y. Tu, G. Euskirchen, W. Ward and D. Prasher, Green fluorescent protein as a marker for gene expression, *Science*, **1994**, 263(5148), 802–805.

[50] S. Inouye and F. I. Tsuji, Aequorea green fluorescent protein, *FEBS Letters*, **1994**, 341(2-3), 277–280.

[51] H. Niwa, S. Inouye, T. Hirano, T. Matsuno, S. Kojima, M. Kubota, M. Ohashi and F. Tsuji, Chemical nature of the light emitter of the Aequorea green fluorescent protein, *Proceedings of the National Academy of Sciences of the United States of America*, **1996**, 93(24), 13617–13622.

[52] G. H. Patterson, S. M. Knobel, W. D. Sharif, S. R. Kain and D. W. Piston, Use of the green fluorescent protein and its mutants in quantitative fluorescence microscopy, *Biophysical Journal*, **1997**, 73(5), 2782–2790.

[53] N. C. Shaner, R. E. Campbell, P. A. Steinbach, B. N. G. Giepmans, A. E. Palmer and R. Y. Tsien, Improved monomeric red, orange and yellow fluorescent proteins derived from Discosoma sp. red fluorescent protein, *Nature Biotechnology*, **2004**, 22(12), 1567–1572.

[54] G. H. Patterson and J. Lippincott-Schwartz, A Photoactivatable GFP for Selective Photolabeling of Proteins and Cells, *Science*, **2002**, 297(5588), 1873–1877.

[55] R. Ando, H. Hama, M. Yamamoto-Hino, H. Mizuno and A. Miyawaki, An optical marker based on the UV-induced green-to-red photoconversion of a fluorescent protein, *Proceedings of the National Academy of Sciences of the United States of America*, **2002**, 99(20), 12651–12656.

[56] K. Nienhaus and G. Ulrich Nienhaus, Fluorescent proteins for live-cell imaging with super-resolution, *Chemical Society Reviews*, **2014**, 43(4), 1088–1106.

[57] M. Andresen, M. C. Wahl, A. C. Stiel, F. Gräter, L. V. Schäfer, S. Trowitzsch, G. Weber, C. Eggeling, H. Grubmüller, S. W. Hell and S. Jakobs, Structure and mechanism of the reversible photoswitch of a fluorescent protein, *Proceedings of the National Academy of Sciences of the United States of America*, **2005**, 102(37), 13070–13074.

[58] M. Andresen, A. C. Stiel, S. Trowitzsch, G. Weber, C. Eggeling, M. C. Wahl, S. W. Hell and S. Jakobs, Structural basis for reversible photoswitching in Dronpa, *Proceedings of the National Academy of Sciences of the United States of America*, **2007**, 104(32), 13005–13009.

[59] K. A. Lukyanov, A. F. Fradkov, N. G. Gurskaya, M. V. Matz, Y. A. Labas, A. P. Savitsky, M. L. Markelov, A. G. Zaraisky, X. Zhao, Y. Fang, W. Tan and S. A. Lukyanov, Natural Animal Coloration Can Be Determined by a Nonfluorescent Green Fluorescent Protein Homolog, *Journal of Biological Chemistry*, **2000**, 275(34), 25879–25882.

[60] R. Ando, H. Mizuno and A. Miyawaki, Regulated Fast Nucleocytoplasmic Shuttling Observed by Reversible Protein Highlighting, *Science*, **2004**, 306(5700), 1370–1373.

[61] M. A. Schwentker, H. Bock, M. Hofmann, S. Jakobs, J. Bewersdorf, C. Eggeling and S. W. Hell, Wide-field subdiffraction RESOLFT microscopy using fluorescent protein photoswitching, *Microscopy Research and Technique*, **2007**, 70(3), 269–280.

[62] I. Testa, E. D'Este, N. T. Urban, F. Balzarotti and S. W. Hell, Dual Channel RESOLFT Nanoscopy by Using Fluorescent State Kinetics, *Nano Letters*, **2015**, 15(1), 103–106.

[63] F. Lavoie-Cardinal, N. A. Jensen, V. Westphal, A. C. Stiel, A. Chmyrov, J. Bierwagen, I. Testa, S. Jakobs and S. W. Hell, Two-Color RESOLFT Nanoscopy with Green and Red Fluorescent Photochromic Proteins, *ChemPhysChem*, **2014**, 15(4), 655–663.

[64] M. Ratz, I. Testa, S. W. Hell and S. Jakobs, CRISPR/Cas9-mediated endogenous protein tagging for RESOLFT super-resolution microscopy of living human cells, *Scientific Reports*, **2015**, 5, 9592.

[65] S. Schnorrenberg, T. Grotjohann, G. Vorbrüggen, A. Herzig, S. W. Hell and S. Jakobs, In vivo super-resolution RESOLFT microscopy of Drosophila melanogaster, *eLife*, **2016**, 5, e15567.

[66] A. H. Coons, The Beginnings of Immunofluorescence, *The Journal of Immunology*, **1961**, 87(5), 499.

[67] M. Fernandez-Suarez and A. Y. Ting, Fluorescent probes for super-resolution imaging in living cells, *Nature Reviews Molecular Cell Biology*, **2008**, 9(12), 929–943.

[68] A. Keppler, S. Gendreizig, T. Gronemeyer, H. Pick, H. Vogel and K. Johnsson, A general method for the covalent labeling of fusion proteins with small molecules in vivo, *Nature Biotechnology*, **2003**, 21(1), 86–89.

[69] A. Gautier, A. Juillerat, C. Heinis, I. R. Corrêa, M. Kindermann, F. Beaufils and K. Johnsson, An Engineered Protein Tag for Multiprotein Labeling in Living Cells, *Chemistry & Biology*, **2008**, 15(2), 128–136.

[70] G. V. Los, L. P. Encell, M. G. McDougall, D. D. Hartzell, N. Karassina, C. Zimprich, M. G. Wood, R. Learish, R. F. Ohana, M. Urh, D. Simpson, J. Mendez, K. Zimmerman, P. Otto, G. Vidugiris, J. Zhu, A. Darzins, D. H. Klaubert, R. F. Bulleit and K. V. Wood, HaloTag: A Novel Protein Labeling Technology for Cell Imaging and Protein Analysis, *ACS Chemical Biology*, **2008**, 3(6), 373–382.

[71] M. J. Hinner and K. Johnsson, How to obtain labeled proteins and what to do with them, *Current Opinion in Biotechnology*, **2010**, 21(6), 766–776.

[72] M. Bossi, J. Fölling, M. Dyba, V. Westphal and S. W. Hell, Breaking the diffraction resolution barrier in far-field microscopy by molecular optical bistability, *New Journal of Physics*, **2006**, 8(11), 275.

[73] J. Fölling, S. Polyakova, V. Belov, A. van Blaaderen, M. L. Bossi and S. W. Hell, Synthesis and Characterization of Photoswitchable Fluorescent Silica Nanoparticles, *Small*, **2008**, 4(1), 134–142.

[74] J. Kwon, J. Hwang, J. Park, G. R. Han, K. Y. Han and S. K. Kim, RESOLFT nanoscopy with photoswitchable organic fluorophores, *Scientific Reports*, **2015**, 5, 17804–17804.

[75] M. Irie, T. Fukaminato, K. Matsuda and S. Kobatake, Photochromism of Diarylethene Molecules and Crystals: Memories, Switches, and Actuators, *Chemical Reviews*, **2014**, 114(24), 12174–12277.

[76] M. Irie and M. Mohri, Thermally irreversible photochromic systems. Reversible photocyclization of diarylethene derivatives, *The Journal of Organic Chemistry*, **1988**, 53(4), 803–808.

[77] K. Uchida, Y. Nakayama and M. Irie, Thermally Irreversible Photochromic Systems. Reversible Photocyclization of 1,2-Bis(benzo[b]thiophen-3-yl)ethene Derivatives, *Bulletin of the Chemical Society of Japan*, **1990**, 63(5), 1311–1315.

[78] G. Berkovic, V. Krongauz and V. Weiss, Spiropyrans and Spirooxazines for Memories and Switches, *Chemical Reviews*, **2000**, 100(5), 1741–1754.

[79] G. S. Kumar and D. Neckers, Photochemistry of azobenzene-containing polymers, *Chemical Reviews*, **1989**, 89(8), 1915–1925.

[80] D. Guillaumont, T. Kobayashi, K. Kanda, H. Miyasaka, K. Uchida, S. Kobatake, K. Shibata, S. Nakamura and M. Irie, An ab Initio MO Study of the Photochromic Reaction of Dithienylethenes, *The Journal of Physical Chemistry A*, **2002**, 106(31), 7222–7227.

[81] M. Boggio-Pasqua, M. Ravaglia, M. J. Bearpark, M. Garavelli and M. A. Robb, Can Diarylethene Photochromism Be Explained by a Reaction Path Alone? A CASSCF Study with Model MMVB Dynamics, *The Journal of Physical Chemistry A*, **2003**, 107(50), 11139–11152.

[82] K. Kosma, S. A. Trushin, Fu and W. E. Schmid, Cyclohexadiene ring opening observed with 13 fs resolution: coherent oscillations confirm the reaction path, *Physical Chemistry Chemical Physics*, **2009**, 11(1), 172–181.

[83] R. B. Woodward and R. Hoffmann, The Conservation of Orbital Symmetry, *Angewandte Chemie International Edition*, **1969**, 8(11), 781–853.

[84] M. Irie, K. Sakemura, M. Okinaka and K. Uchida, Photochromism of Dithienylethenes with Electron-Donating Substituents, *The Journal of Organic Chemistry*, **1995**, 60(25), 8305–8309.

[85] M. Hanazawa, R. Sumiya, Y. Horikawa and M. Irie, Thermally irreversible photochromic systems. Reversible photocyclization of 1,2-bis (2-methylbenzo[b]thiophen-3-yl)perfluorocyclocoalkene derivatives, *Journal of the Chemical Society, Chemical Communications*, **1992**, (3), 206–207.

[86] Y.-C. Jeong, S. I. Yang, K.-H. Ahn and E. Kim, Highly fluorescent photochromic diarylethene in the closed-ring form, *Chemical Communications*, **2005**, (19), 2503–2505.

[87] Y.-C. Jeong, D. G. Park, I. S. Lee, S. I. Yang and K.-H. Ahn, Highly fluorescent photochromic diarylethene with an excellent fatigue property, *Journal of Materials Chemistry*, **2009**, 19(1), 97–103.

[88] J. M. Endtner, F. Effenberger, A. Hartschuh and H. Port, Optical ON/OFF Switching of Intramolecular Photoinduced Charge Separation in a Donor-Bridge-Acceptor System Containing Dithienylethene, *Journal of the American Chemical Society*, **2000**, 122(13), 3037–3046.

[89] L. Giordano, T. M. Jovin, M. Irie and E. A. Jares-Erijman, Diheteroarylethenes as Thermally Stable Photoswitchable Acceptors in Photochromic Fluorescence Resonance Energy Transfer (pcFRET), *Journal of the American Chemical Society*, **2002**, 124(25), 7481–7489.

[90] T. Fukaminato, T. Sasaki, T. Kawai, N. Tamai and M. Irie, Digital Photoswitching of Fluorescence Based on the Photochromism of Diarylethene Derivatives at a Single-Molecule Level, *Journal of the American Chemical Society*, **2004**, 126(45), 14843–14849.

[91] M. Frigoli and G. Mehl, Room Temperature Nematic Photoswitchable Liquid Crystals — Molecular Modularisation of Functional Elements, *European Journal of Organic Chemistry*, **2004**, 2004(3), 636–642.

[92] T. Fukaminato, T. Doi, N. Tamaoki, K. Okuno, Y. Ishibashi, H. Miyasaka and M. Irie, Single-Molecule Fluorescence Photoswitching of a Diarylethene-Perylenebisimide Dyad: Non-destructive Fluorescence Readout, *Journal of the American Chemical Society*, **2011**, 133(13), 4984–4990.

[93] K. Liu, Y. Wen, T. Shi, Y. Li, F. Li, Y.-l. Zhao, C. Huang and T. Yi, DNA gated photochromism and fluorescent switch in a thiazole orange modified diarylethene, *Chemical Communications*, **2014**, 50(65), 9141–9144.

[94] G. Lv, B. Cui, H. Lan, Y. Wen, A. Sun and T. Yi, Diarylethene based fluorescent switchable probes for the detection of amyloid-[small beta] pathology in Alzheimer's disease, *Chemical Communications*, **2015**, 51(1), 125–128.

[95] K. Uno, H. Niikura, M. Morimoto, Y. Ishibashi, H. Miyasaka and M. Irie, In Situ Preparation of Highly Fluorescent Dyes upon Photoirradiation, *Journal of the American Chemical Society*, **2011**, 133(34), 13558–13564.

[96] Y. Shoji, A. Yagi, M. Horiuchi, M. Morimoto and M. Irie, Photochromic Diarylethene Derivatives Bearing Hydrophilic Substituents, *Israel Journal of Chemistry*, **2013**, 53(5), 303–311.

[97] M. Takeshita, N. Kato, S. Kawauchi, T. Imase, J. Watanabe and M. Irie, Photochromism of Dithienylethenes Included in Cyclodextrins, *The Journal of Organic Chemistry*, **1998**, 63(25), 9306–9313.

[98] T. Hirose, K. Matsuda and M. Irie, Self-Assembly of Photochromic Diarylethenes with Amphiphilic Side Chains: Reversible Thermal and Photochemical Control, *The Journal of Organic Chemistry*, **2006**, 71(20), 7499–7508.

[99] T. Hirose, M. Irie and K. Matsuda, Temperature-Light Dual Control of Clouding Behavior of an Oligo(ethylene glycol)-Diarylethene Hybrid System, *Advanced Materials*, **2008**, 20(11), 2137–2141.

[100] Y. Zou, T. Yi, S. Xiao, F. Li, C. Li, X. Gao, J. Wu, M. Yu and C. Huang, Amphiphilic Diarylethene as a Photoswitchable Probe for Imaging Living Cells, *Journal of the American Chemical Society*, **2008**, 130(47), 15750–15751.

[101] S.-C. Pang, H. Hyun, S. Lee, D. Jang, M. J. Lee, S. H. Kang and K.-H. Ahn, Photoswitchable fluorescent diarylethene in a turn-on mode for live cell imaging, *Chemical Communications*, **2012**, 48(31), 3745–3747.

[102] T. Wu, B. Johnsen, Z. Qin, M. Morimoto, D. Baillie, M. Irie and N. R. Branda, Two-colour fluorescent imaging in organisms using self-assembled nanosystems of upconverting nanoparticles and molecular switches, *Nanoscale*, **2015**, 7(26), 11263–11266.

[103] S. M. Polyakova, V. N. Belov, M. L. Bossi and S. W. Hell, Synthesis of Photochromic Compounds for Aqueous Solutions and Focusable Light, *European Journal of Organic Chemistry*, **2011**, 2011(18), 3301–3312.

[104] N. Soh, K. Yoshida, H. Nakajima, K. Nakano, T. Imato, T. Fukaminato and M. Irie, A fluorescent photochromic compound for labeling biomolecules, *Chemical Communications*, **2007**, (48), 5206–5208.

[105] F. Görlitz, P. Hoyer, H. Falk, L. Kastrup, J. Engelhardt and S. W. Hell, A STED microscope designed for routine biomedical applications, *Progress In Electromagnetics Research*, **2014**, 147, 57–68.

[106] J. Schindelin, I. Arganda-Carreras, E. Frise, V. Kaynig, M. Longair, T. Pietzsch, S. Preibisch, C. Rueden, S. Saalfeld, B. Schmid, J.-Y. Tinevez, D. J. White, V. Hartenstein, K. Eliceiri, P. Tomancak and A. Cardona, Fiji: an open-source platform for biological-image analysis, *Nature Methods*, **2012**, 9(7), 676–682.

[107] J. Enderlein and R. Erdmann, Fast fitting of multi-exponential decay curves, *Optics Communications*, **1997**, 134(1-6), 371–378.

[108] A. Akbarzadeh, R. Rezaei-Sadabady, S. Davaran, S. W. Joo, N. Zarghami, Y. Hanifehpour, M. Samiei, M. Kouhi and K. Nejati-Koshki, Liposome: classification, preparation, and applications, *Nanoscale Research Letters*, **2013**, 8(1), 102–102.

[109] R. Zondervan, F. Kulzer, M. A. Kol'chenk and M. Orrit, Photobleaching of Rhodamine 6G in Poly(vinyl alcohol) at the Ensemble and Single-Molecule Levels, *The Journal of Physical Chemistry A*, **2004**, 108(10), 1657–1665.

[110] H. Bock, C. Geisler, C. Wurm, C. von Middendorff, S. Jakobs, A. Schönle, A. Egner, S. W. Hell and C. Eggeling, Two-color far-field fluorescence nanoscopy based on photoswitchable emitters, *Applied Physics B*, **2007**, 88(2), 161–165.

[111] H. Tokiwa, M. Irie, K. Ikeda and T. Otsubo, Water-soluble photochromic molecule, European Patent, EP 2902402 A1, **2015**.

[112] Y. Takagi, T. Kunishi, T. Katayama, Y. Ishibashi, H. Miyasaka, M. Morimoto and M. Irie, Photoswitchable fluorescent diarylethene derivatives with short alkyl chain substituents, *Photochemical & Photobiological Sciences*, **2012**, 11(11), 1661–1665.

[113] B. Roubinet, M. L. Bossi, P. Alt, M. Leutenegger, H. Shojaei, S. Schnorrenberg, S. Nizamov, M. Irie, V. N. Belov and S. W. Hell, Carboxylated Photoswitchable Diarylethenes for Biolabeling and Super-Resolution RESOLFT Microscopy, *Angewandte Chemie International Edition*, **2016**, 55(49), 15429–15433.

[114] M. Brinkley, A brief survey of methods for preparing protein conjugates with dyes, haptens and crosslinking reagents, *Bioconjugate Chemistry*, **1992**, 3(1), 2–13.

[115] S. Vira, E. Mekhedov, G. Humphrey and P. S. Blank, Fluorescent labeled antibodies - balancing functionality and degree of labeling, *Analytical Biochemistry*, **2010**, 402(2), 146–150.

[116] L. Frahm, *Stochastic modeling of photoswitchable fluorophores for quantitative superresolution microscopy*, Doctoral thesis, University of Göttingen, Göttingen, **2017**.

[117] H. Mizuno, P. Dedecker, R. Ando, T. Fukano, J. Hofkens and A. Miyawaki, Higher resolution in localization microscopy by slower switching of a photochromic protein, *Photochemical & Photobiological Sciences*, **2010**, 9(2), 239–248.

[118] T. Roebroek, S. Duwé, W. Vandenberg and P. Dedecker, Reduced Fluorescent Protein Switching Fatigue by Binding-Induced Emissive State Stabilization, *International Journal of Molecular Sciences*, **2017**, 18(9).

[119] J. W. Borst, M. A. Hink, A. van Hoek and A. J. Visser, Effects of refractive index and viscosity on fluorescence and anisotropy decays of enhanced cyan and yellow fluorescent proteins, *Journal of Fluorescence*, **2005**, 15(2), 153–60.

[120] M. El Khatib, A. Martins, D. Bourgeois, J.-P. Colletier and V. Adam, Rational design of ultrastable and reversibly photoswitchable fluorescent proteins for super-resolution imaging of the bacterial periplasm, *Scientific Reports*, **2016**, 6, 18459.

[121] S. Duwé, E. De Zitter, V. Gielen, B. Moeyaert, W. Vandenberg, T. Grotjohann, K. Clays, S. Jakobs, L. Van Meervelt and P. Dedecker, Expression-Enhanced Fluorescent Proteins Based on Enhanced Green Fluorescent Protein for Super-resolution Microscopy, *ACS Nano*, **2015**, 9(10), 9528–9541.

[122] X. Piao, Y. Zou, J. Wu, C. Li and T. Yi, Multiresponsive Switchable Diarylethene and Its Application in Bioimaging, *Organic Letters*, **2009**, 11(17), 3818–3821.

[123] Z. Tong, S. Pu, Q. Xiao, G. Liu and S. Cui, Synthesis and photochromism of a novel water-soluble diarylethene with glucosyltriazolyl groups, *Tetrahedron Letters*, **2013**, 54(6), 474–477.

[124] S. Pu, H. Liu, G. Liu, B. Chen and Z. Tong, The effects of phenyl-bridged glucosyltriazolyl groups on the properties of water-soluble diarylethene derivatives, *Tetrahedron*, **2014**, 70(4), 852–858.

[125] Y.-C. Jeong, S. I. Yang, E. Kim and K.-H. Ahn, Development of highly fluorescent photochromic material with high fatigue resistance, *Tetrahedron*, **2006**, 62(25), 5855–5861.

[126] S. Fredrich, R. Gostl, M. Herder, L. Grubert and S. Hecht, Switching Diarylethenes Reliably in Both Directions with Visible Light, *Angewandte Chemie International Edition*, **2016**, 55(3), 1208–12.

[127] F. Gillanders, L. Giordano, S. A. Diaz, T. M. Jovin and E. A. Jares-Erijman, Photoswitchable fluorescent diheteroarylethenes: substituent effects on photochromic and solvatochromic properties, *Photochemical & Photobiological Sciences*, **2014**, 13(3), 603–612.

[128] L. D. Hughes, R. J. Rawle and S. G. Boxer, Choose Your Label Wisely: Water-Soluble Fluorophores Often Interact with Lipid Bilayers, *PLoS ONE*, **2014**, 9(2), e87649.

[129] S. Habuchi, R. Ando, P. Dedecker, W. Verheijen, H. Mizuno, A. Miyawaki and J. Hofkens, Reversible single-molecule photoswitching in the GFP-like fluorescent protein Dronpa, *Proceedings of the National Academy of Sciences of the United States of America*, **2005**, 102(27), 9511–9516.

[130] S. van de Linde and M. Sauer, How to switch a fluorophore: from undesired blinking to controlled photoswitching, *Chemical Society Reviews*, **2014**, 43(4), 1076–1087.

[131] T. Ha and P. Tinnefeld, Photophysics of Fluorescence Probes for Single Molecule Biophysics and Super-Resolution Imaging, *Annual Review of Physical Chemistry*, **2012**, 63, 595–617.

[132] S. V. Gudkov, O. E. Karp, S. A. Garmash, V. E. Ivanov, A. V. Chernikov, A. A. Manokhin, M. E. Astashev, L. S. Yaguzhinsky and V. I. Bruskov, Generation of reactive oxygen species in water under exposure to visible or infrared irradiation at absorption bands of molecular oxygen, *Biophysics*, **2012**, 57(1), 1–8.

[133] C. Eggeling, J. Widengren, R. Rigler and C. A. M. Seidel, Photobleaching of Fluorescent Dyes under Conditions Used for Single-Molecule Detection: Evidence of Two-Step Photolysis, *Analytical Chemistry*, **1998**, 70(13), 2651–2659.

[134] C. Duan, V. Adam, M. Byrdin, J. Ridard, S. Kieffer-Jaquinod, C. Morlot, D. Arcizet, I. Demachy and D. Bourgeois, Structural Evidence for a Two-Regime Photobleaching Mechanism in a Reversibly Switchable Fluorescent Protein, *Journal of the American Chemical Society*, **2013**, 135(42), 15841–15850.

[135] Y. Ishibashi, M. Mukaida, M. Falkenstrom, H. Miyasaka, S. Kobatake and M. Irie, One- and multi-photon cycloreversion reaction dynamics of diarylethene derivative with asymmetrical structure, as revealed by ultrafast laser spectroscopy, *Physical Chemistry Chemical Physics*, **2009**, 11(15), 2640–2648.

[136] M. Murakami, H. Miyasaka, T. Okada, S. Kobatake and M. Irie, Dynamics and Mechanisms of the Multiphoton Gated Photochromic Reaction of Diarylethene Derivatives, *Journal of the American Chemical Society*, **2004**, 126(45), 14764–14772.

[137] T. M. Jeitner and D. A. Lawrence, Mechanisms for the Cytotoxicity of Cysteamine, *Toxicological Sciences*, **2001**, 63(1), 57–64.

[138] A. Chmyrov, J. Keller, T. Grotjohann, M. Ratz, E. D'Este, S. Jakobs, C. Eggeling and S. W. Hell, Nanoscopy with more than 100,000 'doughnuts', *Nature Methods*, **2013**, 10(8), 737–740.

[139] J. G. Danzl, S. C. Sidenstein, C. Gregor, N. T. Urban, P. Ilgen, S. Jakobs and S. W. Hell, Coordinate-targeted fluorescence nanoscopy with multiple off states, *Nature Photonics*, **2016**, 10(2), 122–128.

[140] O. Nevskyi, D. Sysoiev, A. Oppermann, T. Huhn and D. Wöll, Nanoscopic Visualization of Soft Matter Using Fluorescent Diarylethene Photoswitches, *Angewandte Chemie International Edition*, **2016**, 55(41), 12698–12702.

[141] Y. Arai, S. Ito, H. Fujita, Y. Yoneda, T. Kaji, S. Takei, R. Kashihara, M. Morimoto, M. Irie and H. Miyasaka, One-colour control of activation, excitation and deactivation of a fluorescent diarylethene derivative in super-resolution microscopy, *Chemical Communications*, **2017**, 53(29), 4066–4069.

[142] B. Roubinet, M. Weber, H. Shojaei, M. Bates, M. L. Bossi, V. N. Belov, M. Irie and S. W. Hell, Fluorescent Photoswitchable Diarylethenes for Biolabeling and Single Molecule Localization Microscopies with Optical Superresolution, *Journal of the American Chemical Society*, **2017**, 139(19), 6611–6620.

[143] Y. Takagi, M. Morimoto, R. Kashihara, S. Fujinami, S. Ito, H. Miyasaka and M. Irie, Turn-on mode fluorescent diarylethenes: Control of the cycloreversion quantum yield, *Tetrahedron*, **2017**, 73(33), 4918–4924.

[144] I. N. Bronshtein, K. A. Semendyayev, G. Musiol and H. Mühlig, *Handbook of Mathematics*, 6th Ed., Springer Berlin Heidelberg, Berlin, Heidelberg, **2015**.

[145] E. Nogales, S. G. Wolf and K. H. Downing, Structure of the $\alpha\beta$ tubulin dimer by electron crystallography, *Nature*, **1998**, 391(6663), 199–203.

[146] L. J. Harris, E. Skaletsky and A. McPherson, Crystallographic structure of an intact IgG1 monoclonal antibody1, *Journal of Molecular Biology*, **1998**, 275(5), 861–872.

List of Figures

Publications resulting from this thesis

Parts of this thesis have been published in the following publication:

B. Roubinet, M. L. Bossi, P. Alt, M. Leutenegger, H. Shojaei, S. Schnorrenberg, S. Nizamov, M. Irie, V. N. Belov, S. W. Hell, Carboxylated Photoswitchable Diaryl-ethenes for Biolabeling and Super-Resolution RESOLFT Microscopy, *Angewandte Chemie International Edition*, **2016**, 55(49), 15429-15433.

Acknowledgments

At this point I would like to thank all who have supported me in the recent years and without whom this work would not have been possible.

First and foremost, I would like to thank Prof. Stefan Hell for giving me the opportunity to work on this interesting topic in such an inspiring environment, for his motivation and for sharing his knowledge.

Moreover, I thank Prof. Jürgen Troe and Dr. Thomas Burg for fruitful discussions and giving a different perspective on my work. Additionally, I am indebted to Dr. Melina Schuh, Dr. Alexander Egner and Prof. Tim Salditt for being members of the examination board.

I am especially grateful to Marcel Leutenegger for his inspiring supervision, critical discussions and encouraging words when the experiments did not run very smoothly.

Many thanks go to Benoît Roubinet and Heydar Shojaei for their excellent work in the synthesis of the *me*DAE and EBT fluorophores used in this thesis, Mariano Bossi for his contribution to the characterization of the fluorophores, the antibody coupling and many inspiring discussions and Prof. Masahiro Irie for providing the *myo*-inositol substituted diarylethenes. Furthermore, I thank Prof. Stefan Jakobs for the possibility to work on the Abberior microscope and Dr. Vladimir Belov for valuable discussions on fluorophore chemistry.

Great thanks go to Ellen Rothermel, Tanja Gilat and Sylvia Löbermann for exceptional technical assistance and many perfect samples.

Thanks are also due to Jan Keller-Findeisen and Lars Frahm who always found the right comment on my MATLAB code and how it could be improved.

I am grateful to Jaydev Jethwa for all kind of technical advice and lessons on how to solder properly.

I thank the optical, mechanical and electrical workshops at the institute for outstanding consulting, all kind of custom-made parts and last minute fabrications.

Curriculum vitae

Name	Philipp Johannes Alt
Date of birth	11.03.1990
Place of birth	Trier
Nationality	German

Education

2013 - present	**PhD in Physics** Georg-August-Universität Göttingen and Max Planck Institute for Biophysical Chemistry, Germany Thesis: *RESOLFT nanoscopy with water-soluble synthetic fluorophores* Supervisor: Prof. Dr. Stefan W. Hell
2009 - 2013	**Studies in Biophysics** University of Kaiserslautern, Germany Diploma Thesis: *Ultraschnelle Dynamik von Wassermolekülen in Bacteriorhodopsin nach Photoanregung* Supervisor: Prof. Dr. Rolf Diller

Publications

B. Roubinet, M. L. Bossi, P. Alt, M. Leutenegger, H. Shojaei, S. Schnorrenberg, S. Nizamov, M. Irie, V. N. Belov, S. W. Hell, Carboxylated Photoswitchable Diarylethenes for Biolabeling and Super-Resolution RESOLFT Microscopy, *Angewandte Chemie International Edition*, **2016**, 55(49), 15429-15433.

Contributions to Conferences

1. **Third Infinity**
   Göttingen, 2015
   Oral presentation: Characterizing photoswitchable proteins for high resolution microscopy

2. **Labeling and Nanoscopy**
   Heidelberg, 2016
   Poster presentation: Photoswitchable diarylethenes for biolabeling and RESOLFT nanoscopy

3. **4th GGNB Science Day**
   Göttingen, 2016
   Oral presentation: New photoswitchable labels for high resolution microscopy